MODULATION OF LYMPHOCYTE DEVELOPMENT AND FUNCTION VIA SNAIL FAMILY TRANSCRIPTIONAL REGULATORS

by

Peter Dion Pioli

A dissertation submitted to the faculty of
The University of Utah
in partial fulfillment of the requirements for the degree of

Doctor of Philosophy

in

Microbiology and Immunology

Department of Pathology

The University of Utah

May 2015

The University of Utah Graduate School

STATEMENT OF DISSERTATION APPROVAL

The dissertation of **Peter Dion Pioli**

has been approved by the following supervisory committee members:

John Weis	, Chair	**03/02/2015** Date Approved
Srividya Bhaskara	, Member	**03/02/2015** Date Approved
Xinjian Chen	, Member	**03/02/2015** Date Approved
Gerald Spangrude	, Member	**03/02/2015** Date Approved
Roland D. Tantin	, Member	**03/02/2015** Date Approved

and by **Peter Jensen** , Chair/Dean of the Department/College/School of **Pathology**

and by David B. Kieda, Dean of The Graduate School.

ABSTRACT

Antigen receptor-encoding lymphocytes (i.e., B and T cells) are key mediators of the adaptive immune response. Hence, the developmental and functional programs of these cells are crucial to the sustained viability of metazoans such as mouse and man. One strategy to ensure these cellular programs is through the use of tightly orchestrated networks of gene expression. To preserve these networks, a myriad of proteins function to activate or repress particular sets of genes.

The Snail family of transcription factors consists of three members: *Snai1* (*Snail*), *Snai2* (*Slug*), and *Snai3* (*Smuc*). These proteins are conserved throughout evolution and share a high degree of protein sequence homology. While best known for roles in developmental biology and malignancy, members of the family (i.e., *Snai2*) have been shown to function in hematopoietic progenitor biology. Additionally, the overlapping expression of Snail genes is evident in a multitude of hematopoietic cell types. To test whether *Snai2* and *Snai3* functioned redundantly in hematopoiesis, germline double knockout animals were generated.

Analysis of *Snai2/Snai3* germline double knockouts demonstrated imbalances in the development of lymphoid and myeloid lineages, which absolutely required the deletion of both *Snai2* and *Snai3*. These animals were

also affected nonhematopoietically as evidenced by the almost complete absence of female double knockout progeny and accelerated thymic atrophy. Furthermore, one allele of either *Snai2* or *Snai3* rescued all phenotypes to a similar degree suggesting that both gene products were haplo sufficient in the ability to compensate for the loss of the other three alleles.

Snai2/3 conditional double knockout mice were generated in an effort to better ascertain the hematopoietic cell intrinsic roles of *Snai2* and *Snai3*. *Snai2/3* conditional double knockout animals expired at approximately one month of age due to rampant autoimmunity inclusive of both IgM and IgG autoantibodies. Adoptive transfer of wildtype regulatory T cells halted autoimmune pathology, autoantibody production, and rescued animals from death. Importantly, autoimmunity was generated in *Snai2* sufficient *Rag2*$^{-/-}$ animals receiving double knockout bone marrow. These data supported a cell intrinsic role for *Snai2* and *Snai3* in regulating immune tolerance.

To my wife, KimAnh…with you by my side, I am invincible.

TABLE OF CONTENTS

ACKNOWLEDGMENTS

I've always found "acknowledgments" to be somewhat difficult as it is not necessarily easy to strike the right balance between showing genuine appreciation and coming off as a bit of a "chimney sweep". As such, I will try and be short and sweet. First of all, I want to thank the pathology department as a whole. It has been a privilege to be a part of such an open and collaborative group of individuals. From top to bottom, there is a genuine concern for and desire to see only the best for all colleagues involved.

Thank you to my committee members: Vidya Bhaskara, Xinjian Chen, Jerry Spangrude, and Dean Tantin. You have all contributed to my scientific growth in unique ways whether it has been prelims, teaching new techniques or just "shootin' the sh*t" about science. Additionally, I would also like to recognize Janis Weis and her lab for their support throughout the years.

I want to thank John Weis, my mentor. He fostered my growth and enthusiasm for the field of immunology. More importantly, he gave me an "opportunity" and at the end of the day, that is all one can every really ask for. For that, I will always be appreciative and my only regret is that I wasn't able to accomplish more as a way to repay that debt.

And finally, thank you to my wife, KimAnh. She is without a doubt, the most important person in my life…my soul mate. She is the source of my

determination and fire. Hun, I can never thank you enough except to say…I love you, Kitten.

CHAPTER 1

INTRODUCTION

Snail Family Overview

The Snail family of transcriptional regulators is composed of three members: *Snai1* (*Snail*), *Snai2* (*Slug*), and *Snai3* (*Smuc)* (1, 2). *Snai1* was first discovered in *Drosophila melanogaster* (3). The other two family members (i.e., *Snai2* and *Snai3*) are thought to have arisen in metazoan evolution via gene duplication events (4, 5). As a result, all three family members are present in the genomes of mouse and man.

Snail proteins consist of two main functional domains. The N-terminus of all three proteins contains a SNAG (Snail and Gfi-1) domain, which is essential in the recruitment of chromatin modifiers such as histone deacetylases (HDACs) and histone methyl transferases (HMTs) (6-8). In the C-terminus, each protein contains a variable number of C_2H_2 zinc finger DNA-binding domains (DBDs) (four for Snai1, five for Snai2 and Snai3) (2). These DBDs recognize and bind to canonical E-box motifs (CANNTG). In particular, Snail proteins bind to E-box motifs enriched for G/C-rich central dinucleotides suggesting at least some level of binding site specificity (9, 10). Through these domains, Snail proteins act to modulate target genes, most notably in a repressive fashion (11).

The Snail Family in Development and Cancer

Although not the focus of this dissertation, it is important to provide an overview of how Snail proteins play a role not only in development, but also cancer progression. Over the years, these proteins have been studied in a wide variety of invertebrate and vertebrate systems. For the sake of brevity, only work that utilized models of mouse and man will be discussed in detail.

Snail proteins are best known for their roles in a multitude of developmental processes. The function of this family in mouse development begins at the pre-implantation stage of embryonic development. Both Snai1 and Snai2 proteins are expressed at the one-cell (zygote), two-cell, four-cell, eight-cell, compacted, and blastocyst stages (12). Examination of these stages, in particular at the earliest cleavage events, demonstrated an almost random pattern of protein distributed among daughter cells perhaps suggesting a stochastic inheritance of pre-existing protein among cellular progeny. Interestingly, Galvagni et al. has since shown that embryonic stem cells (ESCs) (derived from the inner cell mass) can be induced to express *Snai1* via retinoic acid (normally derived from the trophectoderm) (13). This was specific to *Snai1* as *Snai2*, *Snai3*, and other epithelial-to-mesenchymal transition (EMT) factors such as *Twist* were unaffected. Furthermore, forced overexpression of *Snai1* led to the premature differentiation of ESCs into all three germ layers. Mechanistically, Snai1 repressed a multitude of target genes previously characterized as promoters of self-renewal. Some of these targets included *Nanog*, *Klf4* and *Essrb* (a direct Nanog target) (13, 14). It has been known for some time that *Snai1* germline knockout mice die by embryonic day 8.5 (E8.5) due to gastrulation defects. This has mainly been attributed to defective mesoderm migration as a result of continued *Cdh1* (E-cadherin) expression (15). Perhaps less appreciated was the dysregulated expression of various germ layer "markers" such as *Otx2*, normally expressed in the visceral endoderm and epiblast. These studies suggested a role for the initiation and perhaps

maintenance of proper germ layer differentiation independent of a cellular migration context. As a continuum of this work, the laboratory of Thomas Gridley conditionally deleted *Snai1* in the embryo using a *Meox2*-driven *Cre* (16, 17). Similar to the germline deletion of *Snai1*, these animals were also embryonic lethal. However, mortality was seen at E9.5 due to the inability to form complex vascular networks in accord with enhanced formation of endothelial cell aggregates (16). Additionally, left-right asymmetry and neural crest migration were also examined in these mice (17). Similar to its role in avian species, *Snai1* was required for proper left-right asymmetry in mice (18, 19). Both model systems demonstrated similar phenotypes including aberrant heart looping and the upregulation of *Nodal* and *Pitx2* on the right side of the body. This demonstrated that similar to the role of *Snai1* in gastrulation, the function of *Snai1* in left-right asymmetry had also been evolutionarily conserved. In contrasting fashion, *Snai1* and *Snai2* were both dispensable for proper neural crest formation in these mice (17). This diverged from results in both *Xenopus laevis* and avian model systems. This may suggest a redundant role for *Snai3* or possibly a Snail-independent program of neural crest formation in mice (20, 21).

Snai2 is widely expressed in the organs of the developing embryo (22). However, Snai2 germline knockout animals display relatively minor phenotypes. One of the tissues with the highest expression of *Snai2* is the skin (23, 24). Detection of Snai2 expression can be found in the mouse epidermis as soon as E11 and in the hair pegs by E14 (24). Accordingly, *Snai2* knockout neonates

show retarded kinetics in hair growth; however, they are undistinguishable from wildtype animals by adulthood. Of more interest, *Snai2* has been shown to be a critical mediator of keratinocyte re-epithelialization following cutaneous wounding suggestive of a more critical role for *Snai2* in stress related responses (23). As might be expected, this was due to the repression of cell-cell junctions by *Snai2,* a well known mediator of EMT (25). Switching focus slightly, it has been observed that *Snai2*$^{-/-}$ animals demonstrate a slight growth deficiency within the pre-weaning period. In accordance with this phenotype, *Snai2* deficient mice also displayed a significant loss of white adipose tissue (WAT) (26). This phenotype was not due to activity differences between wildtype and knockout strains. Rather reduction of WAT was attributed to the loss of *Pparg2* expression, a key driver of adipogenesis (27). Perhaps most noteworthy, *in vitro* analysis showed that Snai2 synergized with C/EBPα, and to a lesser extent C/EBPβ, in promoting *Pparg2* expression. Currently unknown is whether these factors directly interact. In rare instances of direct gene induction, Snai1 has been shown to interact with partners such as EGR-1, SP-1, and Nanog (28, 29). In total, this work points to much more dynamic roles for Snai1 and Snai2 proteins beyond that of “obligate gene repressors.” Perhaps the most profound phenotypes of *Snai2*$^{-/-}$ deficient mice revolve around reproduction, a hormonally driven process like adipogenesis. *Snai2*$^{-/-}$ female mice display reduced mammary gland formation due to a combination of decreased proliferation and increased differentiation of mammary basal epithelial cells (30). This compartment, inclusive of mammary stem/progenitor cells, is normally enriched

for *Snai2* expression in comparison to luminal epithelial cells (i.e., differentiated epithelium). Using CommaDβ cells, a breast cancer cell line, it was found that enforced overexpression of *Snai2* increased mammosphere growth (a measure of stemness) via increased cell proliferation ($Ki67^+$ cells) and decreased apoptosis ($Caspase\text{-}3^+$ cells) (30). From the male perspective, mice deficient in *Snai2* have diminished fertility due to testicular defects that include a reduction in seminiferous tubules and Leydig cells, both of which are critical for spermatogenesis (31). The reason for these defects is currently unknown. Both the male and female reproductive phenotypes are relatively modest in magnitude (i.e., mammary glands and sperm still ultimately developed). In $Snai2^{-/-}$ mammary glands, *Snai3* is upregulated approximately five fold at five weeks and eight fold by ten weeks postbirth suggestive of potential compensation among Snail members (30). Surprisingly, this was specific to *Snai3*, as *Snai1* expression was not enhanced in $Snai2^{-/-}$ mammary glands. This may be indicative of unique regulatory mechanisms for the control of *Snai3* expression. This is not completely unheard of as Snai1 and Snai2 can be differentially regulated via TGFβ and Notch in certain cellular contexts (32).

Currently, the literature regarding the developmental roles of *Snai3* is quite limited. In fact, *Snai3* germline knockouts have no apparent developmental phenotypes (33-35). However, use of the *in vitro* C2C12 myoblast differentiation system has demonstrated the potential for Snai3 to repress muscle differentiation. Using an electromobility shift assay (EMSA), Snai3 was shown to directly compete with MyoD for E-box binding (9). Similar to Snai3, both Snai1

and Snai2 are also capable of blocking MyoD-driven differentiation of muscle (10). Collectively, this work provides a potential explanation for the lack of *Snai3*$^{-/-}$ phenotypes: Snail family redundancy.

As summarized above, the Snail family plays significant roles in development. As such, it is not surprising that this family also contributes to the progression of various malignancies inclusive of processes such as EMT and de-differentiation (36). Snai1 and Snai2 have been studied extensively in cancer. However, only recently has Snai3 gained attention in this regard (37). Gras et al. demonstrated that *Snai3* was overexpressed in samples from multiple breast cancer subsets. Overexpression of the Snail proteins in breast cancer cell lines suggested that Snai3 was a relatively inefficient driver of EMT when compared to both Snai1 and Snai2. Interestingly, Snail proteins were able to repress a largely overlapping gene set; however, Snai3 did this at a lower magnitude (37). Why Snai3 was as ineffective as Snai1 and Snai2 is unknown. Perhaps Snai3 recruits a differential set of chromatin modifiers that were poorly expressed in these particular cell lines. Alternatively Snai3 may not bind E-boxes with the same affinity as Snai1 and Snai2. Snail-driven EMT is crucial for cancer progression; however, the activity of Snail proteins is not limited to this process (11). Perhaps the most therapeutically relevant is the ability of Snail proteins to block apoptosis in response to external stress. Kim et al. showed that Snai2 promoted the survival of breast cancer cells during lung metastasis through the direct repression of *Puma* (38). Additionally, *Snai2* overexpression was protective from Doxorubicin-induced cell death. Conversely, breast cancer cells depleted of

Snai2 were sensitized to cell death; however, this effect was reversed upon the concomitant knockdown of *Puma* (38). In a separate report, Snai2 decreased radiosensitivity of melanoma cells also through the repression of *Puma* (39). Clearly, this contribution of Snail members to cancer biology requires further investigation. Overall, Snail proteins are key mediators of cancer progression/metastasis but may also be essential in determining therapeutic resistance.

The Snail Family in Hematopoiesis

At this time, there are no data addressing the role of *Snai1* within the hematopoietic system. Recently, we have generated a hematopoietic-specific deletion of *Snai1* via utilization of the *Vav-Cre* deleter strain and a strain possessing a conditionally targeted *Snai1* gene. Unlike the case in embryogenesis, *Snai1* is not required for hematopoiesis since these conditional *Snai1*-deleted mice are viable, outwardly healthy, and present no obvious hematopoietic deficiencies (Pioli et al. unpublished data).

While the importance of *Snai1* in hematopoiesis may be a nascent field, *Snai2* has been studied in this context for over a decade. An initial report by Inukai et al. demonstrated overexpression of *Snai2* in several human B cell leukemia cell lines. Upregulation of *Snai2* was dependent upon the E2A-HLF oncoprotein generated from a t(17;19) chromosomal translocation. Usage of the murine IL-3 dependent Baf3 Pro-B cell line demonstrated that overexpression of *Snai2* was sufficient to confer resistance to apoptosis induced by growth factor withdrawal which was accompanied by exit from the cell cycle (40). In regards to

cancer progression, *Snai2* and *Snai1* are most commonly identified for their ability to augment solid tumor phenotypes. This result suggested a potential role for these proteins in regards to hematological cancers. Interestingly, Perez-Losada et al. demonstrated the ability of c-Kit signaling to induce *Snai2* expression. *In vitro* studies utilized both Baf3 and LAMA-84 cells overexpressing c-Kit. Of note, LAMA-84 cells were originally derived from a chronic myeloid leukemia (CML) patient undergoing blast crisis (41). The mechanism of *Snai2* upregulation becomes relevant when one considers that c-Kit is highly expressed on the surface of acute myeloid leukemia (AML) cells (42, 43). A later study by Mancini et al. demonstrated enhanced levels of Snai2 in CML patients. Depletion of *Snai2* via siRNA increased sample sensitivity to apoptosis as these cells lost expression of Bcl-xL (anti-apoptotic) and increased levels of Puma (pro-apoptotic) (44). In this instance, *Snai2* expression appeared to be driven by BCR-ABL signaling as Imatinib treatment decreased *Snai2* levels. These data formally demonstrated an important function for Snail proteins in hematopoietic oncology.

Moving forward, the point of emphasis shifts towards the role of *Snai2* in more physiologic hematopoietic settings. Included within the Perez-Losada et al. report was an initial description of hematopoiesis in the *Snai2* knockout mouse. They observed multiple defects, which mainly focused on erythropoiesis (31). Complete blood counts showed a trend towards lower erythroid “output.” Using *in vivo* models of phenylhydrazine (PHZ)- and pregnancy-induced anemia, a lower percentage of $Ter119^{+}$ cells was observed in the spleen. This pointed to a

role for *Snai2* in hematopoietic stress responses and its requirement in reconstituting the erythroid lineage. Intriguingly, *Snai2*$^{+/-}$ animals showed similar defects as the *Snai2*$^{-/-}$ suggesting a gene dosage component. Examination of steady state hematopoiesis did not show any deviation from normal myeloid and B cell generation. However, a decreased ratio of developing CD4 and CD8 double positive thymocytes was observed in *Snai2* knockout animals. This was apparently a result of increased apoptosis as indicated by terminal deoxynucleotidyl transferase dUTP nick end labeling (TUNEL) staining of thymic cross-sections. Almost immediately following this publication, a separate study from the Look lab showed the expression of *Snai2* in multiple bone marrow progenitor lineages including the hematopoietic stem cell (HSC) (long-term (HSC-LT) and short-term (HSC-ST)), common lymphoid (CLP), and common myeloid (CMP) progenitors among others. Colony forming assays were performed to evaluate differentiation potential of progenitors in the bone marrow and spleen. While the *Snai2*$^{-/-}$ progenitors trended towards an increase in colony forming units (CFUs) for various lineages, no clear-cut enhancement over wildtype (WT) was observed. Expanding on this, they assayed the ability of *Snai2*$^{-/-}$ animals to reconstitute the hematopoietic compartment following an LD_{50} dose of total body irradiation (TBI), also a stress response (45). By thirteen days post-irradiation, all *Snai2*$^{-/-}$ animals had died due to pancytopenia. This was in stark contrast to both WT and *Snai2*$^{+/-}$ animals in which approximately fifty percent survival was achieved when followed out to twenty-nine days. Closer examination of these animals demonstrated increased apoptosis within the

Snai2$^{-/-}$ lineage negative (Lin^{-}) bone marrow leading to the pancytopenia. As such, administration of a thrombopoietin analog rescued irradiation-induced lethality of *Snai2*$^{-/-}$ animals. Using bone marrow chimeras, a follow up study demonstrated that loss of *Snai2* in the hematopoietic compartment was sufficient to propagate the irradiation phenotype described above (46). Importantly, WT bone marrow administered to irradiated *Snai2*$^{-/-}$ hosts completely prevented any lethality providing further evidence for a cell intrinsic role for *Snai2* in hematopoiesis. Using a well-designed combination of knockout and transgenic animals, it was shown that Snai2 functioned downstream of p53 to block the activation of *Puma*. This was accomplished via a direct E-box interaction within intron one of the *Puma* gene. Similar to previously discussed data, this effect was specific to *Puma* as *Snai2*$^{-/-}$ *Puma*$^{-/-}$ compound knockout animals were completely radio-resistant (46). If other apoptotic mediators were playing a role, an intermediate phenotype would have been expected. Finally, a group led by Wen-Shu Wu examined the self-renewal capacity of hematopoietic stem cells with and without *Snai2* (47). Using limiting dilution bone marrow chimera transplants, it was determined that *Snai2*$^{-/-}$ marrow possessed an approximately eight-fold higher repopulation efficiency as compared to *Snai2*$^{+/-}$. Competitive serial transplantation, a gold standard for assessing hematopoietic stem cell (HSC) fidelity, further demonstrated the enhanced ability of the *Snai2*$^{-/-}$ HSC to reconstitute the entire hematopoietic system. Incorporation of 5-ethynyl-2'-deoxyuridine (Edu) combined with Annexin V cell surface staining demonstrated that this result was a consequence of higher proliferative capacity rather than

augmented apoptosis within the *Snai2*$^{-/-}$ Lin^{-} Sca1^{+} compartment. This result coalesces with the previously identified ability of *Snai2* overexpression to induce cell cycle exit by Baf3 cells (40). While the molecular targets of Snai2 were not identified, they may be similar to what has been previously observed for Snai1. In a nontumorigenic context, Snai1 is able to inhibit the cell cycle of MDCK cells by repressing cyclin D2 at the transcriptional level (48). In a noncanonical role for the Snail family, it was also reported that Snai1 co-associated with EGR-1 and SP-1 to upregulate *p15INK4b*, leading to the arrest of HepG2 cells (29).

The function of the Snai3 transcriptional regulator in the hematopoietic system was first analyzed in an indirect investigation, the analysis of proteins binding to negative regulator elements of the murine *Itgb2l* (Pactolus) gene (49). Using a combination of EMSA and supershift assays, it was shown that Snai3 was capable of binding to these transcriptional regulatory sites. The most intriguing aspect of this work was the hypothesis that in scenarios where diverse cell types, such as B cells and neutrophils, express a common transcriptional activator (e.g., PU.1), differential expression of a negative regulator may potentially augment lineage specific expression of downstream genes. Thinking more globally, Dahlem et al. asked whether retroviral-induced overexpression of *Snai3* in a bone marrow chimera model was capable of augmenting hematopoiesis. Using c-Kit and Sca-1 based analysis of lineage depleted marrow, it was determined that overexpression of *Snai3* did not alter ratios of various subsets of hematopoietic progenitors (50). However, inspection of peripheral blood demonstrated a clear loss of B and T cell lineages in cells that

were infected with the *Snai3*-expressing retrovirus (as assayed by GFP expression). This effect was dose dependent as B and T cell populations were present when Snai3 overexpression was at a modest amount (GFP low). Importantly, B and T cells were present when the empty vector was expressed at both low and high levels, arguing against any retroviral-induced artifacts. These data suggested that Snai3 was either capable of saturating endogenous E-boxes necessary for the proper bifurcation of lymphoid and myeloid lineages or directly repressing gene expression by the recruitment of transcriptional control complexes. These data also alluded to a requirement for precise regulation of *Snai3* within the hematopoietic system.

Redundancy Among Snail Family Members

There is plenty of evidence to suggest that Snail family members are capable of compensating for the absence of one another. This includes a limited number of single knockout phenotypes, overlapping patterns of gene expression, upregulation of one family member when another is removed, and the regulation of overlapping gene sets when each member is singly overexpressed (see above). However, the best evidence is derived through genetic models of multi-gene knockouts (35, 51, 52). Murray et al. were the first to provide genetic evidence of a functional redundancy between Snail family members (52). Analysis of *Snai2*$^{-/-}$ neonates demonstrated an approximately fifty percent penetrance of cleft palate. However, *Snai1*$^{+/-}$ *Snai2*$^{-/-}$ presented with a one-hundred percent penetrance of this disorder. While *Snai1* was able to compensate for *Snai2*, this relationship was susceptible to gene dosage. Not

surprisingly, wildtype animals showed overlapping expression of *Snai1* and *Snai2* in the palatal mesenchyme at E14.5. Furthermore, the use of a *Snai2*^{lacZ} reporter demonstrated enhanced expression of *Snai2* in a *Snai1*$^{+/-}$ background. In another report from the Gridley lab, *Snai1* and *Snai2* functioned in a compensatory manner to preserve chondrogenesis and long bone development (51). Conditional deletion of *Snai1* via *Prrx1-Cre* combined with a *Snai2* germline deficiency resulted in shortening of the long bones. This was attributed to not only the loss of proper chondrocyte organization during development, but also decreased chondrocyte proliferation due to aberrant expression of cell cycle inhibitors (i.e., *Cdkn1a*). Not only was *Snai1* overexpressed in the absence of *Snai2* and vice versa, but these genes were also expressed in cell types normally dormant for their expression. This was later attributed to the ability of Snai1 and Snai2 to directly antagonize the expression of one another (53). As an extension of this, we asked whether *Snai2* and *Snai3* might function redundantly to augment hematopoiesis. The reasons we focused on these two family members are as follows: overlapping expression in various hematopoietic lineages, published hematopoietic phenotypes, and *Snai1* was difficult to work with given the issue of embryonic lethality of the germline deleted animal.

Chapter two describes the generation and analysis of a *Snai2/Snai3* germline double knockout animal (35). *Snai2/Snai3* germline double knockouts possessed multiple hematopoietic and nonhematopoietic phenotypes, all of them greater than that found in the single *Snai2*$^{-/-}$ or *Snai3*$^{-/-}$ animals. These animals were runted in physical stature and progeny were significantly skewed

towards the generation of the male sex. Additionally, lymphoid organs such as spleens and thymi were significantly reduced in size and possessed distorted cellular organization/localization. The most striking hematopoietic phenotype of the double knockouts was the enhanced ratio of myeloid lineage-derived cells in the bone marrow. This was met with a concomitant reduction of B cell percentages. In the thymus of *Snai2*$^{-/-}$ *Snai3*$^{-/-}$ mice, double positive thymocytes were reduced in favor of enhanced percentages of CD4 single positive thymocytes. Unlike in the marrow, skewing of thymocyte populations displayed variable penetrance perhaps due to the presence of intact *Snai1* alleles. Analysis of compound heterozygotes suggested that on a per allele basis, one allele of either *Snai2* or *Snai3* equivalently compensated for the loss of the other three alleles.

Due to the nonhematopoietic phenotypes evident in the germline double knockout, it was necessary to evaluate the roles of *Snai2* and *Snai3* in a more hematopoietically-restricted context. Chapter three details the generation and analysis of a “conditional” *Snai2/Snai3* double knockout. These animals displayed severe lymphopenia, alopecia, and dermatitis as well as profound autoimmunity manifested by the production of high levels of autoantibodies as early as three weeks of age. This led to death by thirty days after birth. Autoantibodies included both IgM and IgG isotypes and were reactive against cytoplasmic and membranous components. A regulatory T cell defect contributed to the autoimmune response in that adoptive transfer of wildtype regulatory T cells alleviated symptoms of autoimmunity. Additionally,

transplantation of *Snai2/Snai3* double knockout bone marrow into *Snai2* sufficient *Rag2*$^{-/-}$ recipients resulted in autoantibody generation. The results demonstrated that appropriate expression of *Snai2* and *Snai3* in cells of hematopoietic derivation plays an important role in development and maintenance of immune tolerance.

References

1. Manzanares, M., A. Locascio, and M. A. Nieto. 2001. The increasing complexity of the Snail gene superfamily in metazoan evolution. *Trends in Genetics: TIG* 17: 178-181.

2. Nieto, M. A. 2002. The snail superfamily of zinc-finger transcription factors. *Nature Reviews. Molecular Cell Biology* 3: 155-166.

3. Boulay, J. L., C. Dennefeld, and A. Alberga. 1987. The *Drosophila* developmental gene *Snail* encodes a protein with nucleic acid binding fingers. *Nature* 330: 395-398.

4. Barrallo-Gimeno, A., and M. A. Nieto. 2009. Evolutionary history of the Snail/Scratch superfamily. *Trends in Genetics: TIG* 25: 248-252.

5. Manzanares, M., M. J. Blanco, and M. A. Nieto. 2004. Snail3 orthologues in vertebrates: divergent members of the Snail zinc-finger gene family. *Development Genes and Evolution* 214: 47-53.

6. Peinado, H., E. Ballestar, M. Esteller, and A. Cano. 2004. Snail mediates E-cadherin repression by the recruitment of the Sin3A/histone deacetylase 1 (HDAC1)/HDAC2 complex. *Molecular and Cellular Biology* 24: 306-319.

7. Tong, Z. T., M. Y. Cai, X. G. Wang, L. L. Kong, S. J. Mai, Y. H. Liu, H. B. Zhang, Y. J. Liao, F. Zheng, W. Zhu, T. H. Liu, X. W. Bian, X. Y. Guan, M. C. Lin, M. S. Zeng, Y. X. Zeng, H. F. Kung, and D. Xie. 2012. EZH2 supports nasopharyngeal carcinoma cell aggressiveness by forming a co-repressor complex with HDAC1/HDAC2 and Snail to inhibit E-cadherin. *Oncogene* 31: 583-594.

8. Tien, C. L., A. Jones, H. Wang, M. Gerigk, S. Nozell, and C. Chang. 2015. Snail2/Slug cooperates with Polycomb repressive complex 2 (PRC2) to regulate neural crest development. *Development*.

9. Kataoka, H., T. Murayama, M. Yokode, S. Mori, H. Sano, H. Ozaki, Y. Yokota, S. Nishikawa, and T. Kita. 2000. A novel snail-related transcription factor Smuc regulates basic helix-loop-helix transcription factor activities via specific E-box motifs. *Nucleic Acids Research* 28: 626-633.

10. Soleimani, V. D., H. Yin, A. Jahani-Asl, H. Ming, C. E. Kockx, W. F. van Ijcken, F. Grosveld, and M. A. Rudnicki. 2012. Snail regulates MyoD binding-site occupancy to direct enhancer switching and differentiation-specific transcription in myogenesis. *Molecular Cell* 47: 457-468.

11. Hemavathy, K., S. I. Ashraf, and Y. T. Ip. 2000. Snail/slug family of repressors: slowly going into the fast lane of development and cancer. *Gene* 257: 1-12.

12. Bell, C. E., and A. J. Watson. 2009. SNAI1 and SNAI2 are asymmetrically expressed at the 2-cell stage and become segregated to the TE in the mouse blastocyst. *PloS One* 4: e8530.

13. Galvagni, F., C. Lentucci, F. Neri, D. Dettori, C. DeClemente, M. Orlandini, F. Anselmi, S. Rapelli, M. Grillo, S. Borghi, and S. Oliviero. 2014. Snai1 promotes ESC exit from the pluripotency by direct repression of self-renewal genes. *Stem Cells*.

14. Festuccia, N., R. Osorno, F. Halbritter, V. Karwacki-Neisius, P. Navarro, D. Colby, F. Wong, A. Yates, S. R. Tomlinson, and I. Chambers. 2012. Esrrb is a direct Nanog target gene that can substitute for Nanog function in pluripotent cells. *Cell Stem Cell* 11: 477-490.

15. Carver, E. A., R. Jiang, Y. Lan, K. F. Oram, and T. Gridley. 2001. The mouse snail gene encodes a key regulator of the epithelial-mesenchymal transition. *Molecular and Cellular Biology* 21: 8184-8188.

16. Lomeli, H., C. Starling, and T. Gridley. 2009. Epiblast-specific Snai1 deletion results in embryonic lethality due to multiple vascular defects. *BMC Research Notes* 2: 22.

17. Murray, S. A., and T. Gridley. 2006. Snail family genes are required for left-right asymmetry determination, but not neural crest formation, in mice. *Proceedings of the National Academy of Sciences of the United States of America* 103: 10300-10304.

18. Isaac, A., M. G. Sargent, and J. Cooke. 1997. Control of vertebrate left-right asymmetry by a snail-related zinc finger gene. *Science* 275: 1301-1304.

19. Patel, K., A. Isaac, and J. Cooke. 1999. Nodal signalling and the roles of the transcription factors SnR and Pitx2 in vertebrate left-right asymmetry. *Current Biology: CB* 9: 609-612.

20. Aybar, M. J., M. A. Nieto, and R. Mayor. 2003. Snail precedes slug in the genetic cascade required for the specification and migration of the *Xenopus* neural crest. *Development* 130: 483-494.

21. Nieto, M. A., M. G. Sargent, D. G. Wilkinson, and J. Cooke. 1994. Control of cell behavior during vertebrate development by Slug, a zinc finger gene. *Science* 264: 835-839.

22. Oram, K. F., E. A. Carver, and T. Gridley. 2003. Slug expression during organogenesis in mice. *The Anatomical Record. Part A, Discoveries in Molecular, Cellular, and Evolutionary Biology* 271: 189-191.

23. Savagner, P., D. F. Kusewitt, E. A. Carver, F. Magnino, C. Choi, T. Gridley, and L. G. Hudson. 2005. Developmental transcription factor slug is required for effective re-epithelialization by adult keratinocytes. *Journal of Cellular Physiology* 202: 858-866.

24. Parent, A. E., K. M. Newkirk, and D. F. Kusewitt. 2010. Slug (Snai2) expression during skin and hair follicle development. *The Journal of Investigative Dermatology* 130: 1737-1739.

25. Bolos, V., H. Peinado, M. A. Perez-Moreno, M. F. Fraga, M. Esteller, and A. Cano. 2003. The transcription factor Slug represses E-cadherin expression and induces epithelial to mesenchymal transitions: a comparison with Snail and E47 repressors. *Journal of Cell Science* 116: 499-511.

26. Perez-Mancera, P. A., C. Bermejo-Rodriguez, I. Gonzalez-Herrero, M. Herranz, T. Flores, R. Jimenez, and I. Sanchez-Garcia. 2007. Adipose tissue mass is modulated by SLUG (SNAI2). *Human Molecular Genetics* 16: 2972-2986.

27. Janani, C., and B. D. Ranjitha Kumari. 2015. PPAR gamma gene - A review. *Diabetes & Metabolic Syndrome* 9: 46-50.

28. Gingold, J. A., M. Fidalgo, D. Guallar, Z. Lau, Z. Sun, H. Zhou, F. Faiola, X. Huang, D. F. Lee, A. Waghray, C. Schaniel, D. P. Felsenfeld, I. R. Lemischka, and J. Wang. 2014. A genome-wide RNAi screen identifies opposing functions of Snai1 and Snai2 on the Nanog dependency in reprogramming. *Molecular Cell* 56: 140-152.

29. Hu, C. T., T. Y. Chang, C. C. Cheng, C. S. Liu, J. R. Wu, M. C. Li, and W. S. Wu. 2010. Snail associates with EGR-1 and SP-1 to upregulate transcriptional activation of p15INK4b. *The FEBS Journal* 277: 1202-1218.

30. Nassour, M., Y. Idoux-Gillet, A. Selmi, C. Come, M. L. Faraldo, M. A. Deugnier, and P. Savagner. 2012. Slug controls stem/progenitor cell growth dynamics during mammary gland morphogenesis. *PloS One* 7: e53498.

31. Perez-Losada, J., M. Sanchez-Martin, A. Rodriguez-Garcia, M. L. Sanchez, A. Orfao, T. Flores, and I. Sanchez-Garcia. 2002. Zinc-finger transcription factor Slug contributes to the function of the stem cell factor c-kit signaling pathway. *Blood* 100: 1274-1286.

32. Niessen, K., Y. Fu, L. Chang, P. A. Hoodless, D. McFadden, and A. Karsan. 2008. Slug is a direct Notch target required for initiation of cardiac cushion cellularization. *The Journal of Cell Biology* 182: 315-325.

33. Bradley, C. K., C. R. Norton, Y. Chen, X. Han, C. J. Booth, J. K. Yoon, L. T. Krebs, and T. Gridley. 2013. The snail family gene *Snai3* is not essential for embryogenesis in mice. *PloS One* 8: e65344.

34. Norton, C. R., Y. Chen, X. H. Han, C. K. Bradley, L. T. Krebs, J. K. Yoon, and T. Gridley. 2013. Absence of a major role for the *Snai1* and *Snai3* genes in regulating skeletal muscle regeneration in mice. *PLoS Currents* 5.

35. Pioli, P. D., T. J. Dahlem, J. J. Weis, and J. H. Weis. 2013. Deletion of Snai2 and Snai3 results in impaired physical development compounded by lymphocyte deficiency. *PloS One* 8: e69216.

36. Tania, M., M. A. Khan, and J. Fu. 2014. Epithelial to mesenchymal transition inducing transcription factors and metastatic cancer. *Tumour Biology: The Journal of the International Society for Oncodevelopmental Biology and Medicine* 35: 7335-7342.

37. Gras, B., L. Jacqueroud, A. Wierinckx, C. Lamblot, F. Fauvet, J. Lachuer, A. Puisieux, and S. Ansieau. 2014. Snail family members unequally trigger EMT and thereby differ in their ability to promote the neoplastic transformation of mammary epithelial cells. *PloS One* 9: e92254.

38. Kim, S., J. Yao, K. Suyama, X. Qian, B. Z. Qian, S. Bandyopadhyay, O. Loudig, C. De Leon-Rodriguez, Z. N. Zhou, J. Segall, F. Macian, L. Norton, and R. B. Hazan. 2014. Slug promotes survival during metastasis through suppression of Puma-mediated apoptosis. *Cancer Research* 74: 3695-3706.

39. Arienti, C., A. Tesei, S. Carloni, P. Ulivi, A. Romeo, G. Ghigi, E. Menghi, A. Sarnelli, E. Parisi, R. Silvestrini, and W. Zoli. 2013. SLUG silencing increases radiosensitivity of melanoma cells in vitro. *Cellular Oncology* 36: 131-139.

40. Inukai, T., A. Inoue, H. Kurosawa, K. Goi, T. Shinjyo, K. Ozawa, M. Mao, T. Inaba, and A. T. Look. 1999. SLUG, a ces-1-related zinc finger transcription factor gene with antiapoptotic activity, is a downstream target of the E2A-HLF oncoprotein. *Molecular Cell* 4: 343-352.

41. Seigneurin, D., P. Champelovier, G. Mouchiroud, R. Berthier, D. Leroux, M. Prenant, J. McGregor, J. Starck, F. Morle, C. Micouin, and et al. 1987. Human chronic myeloid leukemic cell line with positive Philadelphia chromosome exhibits megakaryocytic and erythroid characteristics. *Experimental Hematology* 15: 822-832.

42. Cascavilla, N., P. Musto, G. D'Arena, L. Melillo, A. M. Carella, M. P. Petrilli, G. Sanpaolo, and M. Carotenuto. 1998. CD117 (c-kit) is a restricted antigen of acute myeloid leukemia and characterizes early differentiative levels of M5 FAB subtype. *Haematologica* 83: 392-397.

43. Wakita, S., H. Yamaguchi, K. Miyake, Y. Mitamura, F. Kosaka, K. Dan, and K. Inokuchi. 2011. Importance of c-kit mutation detection method sensitivity in prognostic analyses of t(8;21)(q22;q22) acute myeloid leukemia. *Leukemia* 25: 1423-1432.

44. Mancini, M., S. Petta, I. Iacobucci, V. Salvestrini, E. Barbieri, and M. A. Santucci. 2010. Zinc-finger transcription factor slug contributes to the survival advantage of chronic myeloid leukemia cells. *Cellular Signalling* 22: 1247-1253.

45. Inoue, A., M. G. Seidel, W. Wu, S. Kamizono, A. A. Ferrando, R. T. Bronson, H. Iwasaki, K. Akashi, A. Morimoto, J. K. Hitzler, T. I. Pestina, C. W. Jackson, R. Tanaka, M. J. Chong, P. J. McKinnon, T. Inukai, G. C. Grosveld, and A. T. Look. 2002. Slug, a highly conserved zinc finger transcriptional repressor, protects hematopoietic progenitor cells from radiation-induced apoptosis in vivo. *Cancer Cell* 2: 279-288.

46. Wu, W. S., S. Heinrichs, D. Xu, S. P. Garrison, G. P. Zambetti, J. M. Adams, and A. T. Look. 2005. Slug antagonizes p53-mediated apoptosis of hematopoietic progenitors by repressing puma. *Cell* 123: 641-653.

47. Sun, Y., L. Shao, H. Bai, Z. Z. Wang, and W. S. Wu. 2010. Slug deficiency enhances self-renewal of hematopoietic stem cells during hematopoietic regeneration. *Blood* 115: 1709-1717.

48. Vega, S., A. V. Morales, O. H. Ocana, F. Valdes, I. Fabregat, and M. A. Nieto. 2004. Snail blocks the cell cycle and confers resistance to cell death. *Genes & Development* 18: 1131-1143.

49. Hale, J. S., T. J. Dahlem, R. L. Margraf, I. Debnath, J. J. Weis, and J. H. Weis. 2006. Transcriptional control of Pactolus: evidence of a negative control region and comparison with its evolutionary paralogue, CD18 (beta2 integrin). *Journal of Leukocyte Biology* 80: 383-398.

50. Dahlem, T., S. Cho, G. J. Spangrude, J. J. Weis, and J. H. Weis. 2012. Overexpression of Snai3 suppresses lymphoid- and enhances myeloid-cell differentiation. *European Journal of Immunology* 42: 1038-1043.

51. Chen, Y., and T. Gridley. 2013. Compensatory regulation of the *Snai1* and *Snai2* genes during chondrogenesis. *Journal of Bone and Mineral Research: The Official Journal of the American Society for Bone and Mineral Research* 28: 1412-1421.

52. Murray, S. A., K. F. Oram, and T. Gridley. 2007. Multiple functions of Snail family genes during palate development in mice. *Development* 134: 1789-1797.

53. Chen, Y., and T. Gridley. 2013. The SNAI1 and SNAI2 proteins occupy their own and each other's promoter during chondrogenesis. *Biochemical and Biophysical Research Communications* 435: 356-360.

CHAPTER 2

DELETION OF *SNAI2* AND *SNAI3* RESULTS IN IMPAIRED PHYSICAL DEVELOPMENT COMPOUNDED BY LYMPHOCYTE DEFICIENCY

Reprinted from Deletion of *Snai2* and *Snai3* Results in Impaired Physical Development Compounded by Lymphocyte Deficiency. PLoS ONE 8(7):e69216. Peter D. Pioli, Timothy J. Dahlem, Janis J. Weis, and John H. Weis.

OPEN ACCESS Freely available online

PLOS ONE

Deletion of *Snai2* and *Snai3* Results in Impaired Physical Development Compounded by Lymphocyte Deficiency

Peter D. Pioli, Timothy J. Dahlem, Janis J. Weis, John H. Weis*

The Division of Cell Biology and Immunology, Department of Pathology, University of Utah School of Medicine, Salt Lake City, Utah, United States of America

Abstract

The Snail family of transcriptional regulators consists of three highly conserved members. These proteins regulate (repress) transcription via the recruitment of histone deacetylases to target gene promoters that possess the appropriate E-box binding sequences. Murine *Snai1* is required for mouse development while *Snai2* deficient animals survive with some anomalies. Less is known about the third member of the family, *Snai3*. To investigate the function of *Snai3*, we generated a conditional knockin mouse. Utilizing *Cre*-mediated deletion to facilitate the ablation of *Snai3* in T cells or the entire animal, we found little to no effect of the loss of *Snai3* in the entire animal or in T cell lineages. This finding provided the hypothesis that absence of Snai3 was mitigated, in part, by the presence of Snai2. To test this hypothesis we created *Snai2/Snai3* double deficient mice. The developmental consequences of lacking both of these proteins was manifested in stunted growth, a paucity of offspring including a dramatic deficiency of female mice, and impaired immune cell development within the lymphoid lineages.

Citation: Pioli PD, Dahlem TJ, Weis JJ, Weis JH (2013) Deletion of *Snai2* and *Snai3* Results in Impaired Physical Development Compounded by Lymphocyte Deficiency. PLoS ONE 8(7): e69216. doi:10.1371/journal.pone.0069216

Editor: Rafael Aldabe, Centro de Investigación en Medicina Aplicada (CIMA), Spain

Received November 7, 2012; **Accepted** June 5, 2013; **Published** July 16, 2013

Funding: This work was supported by grants from the NIH (JHW: AI24158 and AI AI088451)(JJW: AI-32223 and AR-43521). The funders had no role in study design, data collection and analysis, decision to publish, or preparation of the manuscript.

Competing interests: The authors have declared that no competing interests exist.

* E-mail: john.weis@path.utah.edu

Introduction

Snail transcription factors (TF) comprise a highly conserved family consisting of three members: *Snai1* (*Snail*), *Snai2* (*Slug*), and *Snai3* (*Smuc*) [1,2]. *Snai1* was first discovered in *Drosophila melanogaster* [3] and all 3 members have been identified in organisms ranging from *D. melanogaster* and *Caenorhabditis elegans* to *Mus musculus* and *Homo sapiens* [4]. The encoded proteins share high sequence homology and range from 30–37 kilodaltons (kD) in size. All members share two characteristic features: an amino terminal SNAG (Snail and Gfi-1) domain and zinc finger DNA-binding domains (DBDs) (five DBD domains for Snai2 and Snai3 and four for Snai1) in the carboxy terminus [4]. These transcription factors recognize the consensus E-box sequence, CANNTG [5] preferentially binding to E-boxes that possess GC-rich central di-nucleotides as opposed to, for example, MyoD that prefers to bind to E-box sites enriched for AT central di-nucleotides [5]. While the DBDs determine binding specificity, it is the SNAG domain that imparts functionality to these proteins. Through this domain, Snail TFs interact with various histone deacetylases (HDACs) resulting in the silencing of target gene expression [6,7].

Previously, the roles of Snail members in embryonic and muscle development have been defined. Germline deletion of *Snai1* is an embryonic lethal due to gastrulation defects [8,9]. All three Snail members have been shown to negatively regulate muscle differentiation by competing for E-box binding with other myogenic regulatory factors (MRFs) [5,10]. Additionally the members of the Snail family have been linked to epithelial-mesenchymal transition, the migration of neural crest cells and generation of neural tubes, the regulation of E-cadherin which is linked to the progression of cancer metastasis, and controlling the response to apoptosis initiators (for reviews, see 11,12). For example, *Snai2* deficient animals are more sensitive to total body γ irradiation than WT [13], and *Snai2* deficient hematopoietic progenitor cells demonstrate enhanced levels of apoptosis following radiation-induced DNA damage than WT cells [13,14]. A later study described the role of Snai2 in antagonizing p53-mediated apoptosis in hematopoietic precursor cells by inhibiting Puma (Bbc3) [15]. Snai2 also has a variety of functions in skin development, response to skin insults (sunburn, wound healing, skin cancer) and hair growth [16,17].

The role of the Snail proteins in immune cell development is less defined. A report by Inukai et al. demonstrated that *Snai2* over-expression in IL-3-dependent Baf cells (pro-B cell line) overcame the apoptotic stimuli induced by IL-3 withdrawal [18]. Perez-Losada et al. reported that germline deletion of *Snai2* resulted in diminished $CD4^+CD8^+$ double positive (DP) T cell cells in the thymus which skewed the population to enhanced

numbers of $CD4^+$ single positive (SP) thymocytes, similar to that found in animals with deficient c-kit signaling [19]. This report further linked *Snai2* expression to c-kit pathways, demonstrating erythroid development defects and pigmentation anomalies in the *Snai2* deficient animals, but normal B cell and myeloid cell development. Bone marrow chimera models demonstrated that such defects were intrinsic to the stem cell [19]. Others have also reported that the numbers of T and B cells, the mitogenic responses of splenic and thymic lymphocytes and circulating blood cell counts in *Snai2KO* animals were equivalent to WT [13]. Snai2 does appear to have fundamental functions in early steps of hematopoiesis. The expression of the gene is apparent in both long term and short tem repopulating hematopoietic stems cells, in common lymphoid and myeloid precursor populations and precursors in the granulocyte, megakaryocyte and erythrocyte lineages [13]. Interestingly hematopoietic stem cell precursors that lack Snai2 show a heightened ability to repopulate the animal following 5-FU treatment, compared to WT, suggesting that Snai2 functions to negatively regulate the self-renewal division of such cells [20].

We have shown that the over-expression of *Snai3* in hematopoietic stem cell lineages resulted in the loss of mature lymphocytes and the enhanced development of cells of the myeloid lineage [21] suggesting that lymphoid/myeloid fate decisions are controlled, in part, by E-box binding proteins with a predilection for GC-rich central di-nucleotides. In this study, we took the opposite approach and attempted to define the phenotypes of mice lacking *Snai3* in T cell lineages (due to the high level of expression of *Snai3* in developing T cells) and the entire animal, and subsequently the phenotype of mice lacking functional *Snai2* and *Snai3* genes. *Snai3* is highly expressed in T cell lineages (both DP cells of the thymus and $CD8^+$ cells in the periphery) however deletion of this gene in either T cell lineages or the entire animal had little effect upon animal development or T cell lineages/functions. Since *Snai2* had previously been shown to alter thymocyte development, we generated *Snai2/Snai3* double KO (DKO) animals to test for functional complementation of the two gene products. Mice lacking both of these genes demonstrated much greater physical anomalies than single *Snai2KO* or *Snai3KO* animals including severe running and the dramatic lack of female offspring. Effects to cells of the immune system upon *Snai2/Snai3* deletion included the altered development of double positive ($CD4^+CD8^+$) thymocytes and a significant impairment of B cell development in the bone marrow. Overall, our data demonstrate a significant physiological role for *Snai2* and *Snai3* within cells of the immune system.

Results

Snai3 is not required for thymocyte development

The gene encoding the mouse Snai3 transcription factor is highly expressed in three tissue samples of the animal: skeletal muscle, cardiac muscle and the thymus (Figure S1 in File S1) [10,22]. Expression was also noted in the kidney, liver and spleen, all organs with significant numbers of blood cells. These data suggested that germline deletion of *Snai3* might result in an embryonic lethality (similar to that of a *Snai1* deletion) due to defects in skeletal or cardiac muscle development. Since we were primarily interested in the role of Snai3 in the development of bone marrow lineages, including T cells, we generated a *Snai3* knockout (*Snai3KO*) construct amenable to *Cre*-mediated deletion (Figure 1). This construct resulted in the placement of LoxP recombination sites 5' and 3' of the first exon containing the initiating ATG and encoding the SNAG domain.

Once obtained, the *Snai3KO* mouse was bred to the *Lck-Cre* animal, which would delete *Snai3* specifically in T cells at the double negative stage in thymocyte development [23,24]. Successful deletion of the *Snai3* gene in T cell but not B cell lineages was confirmed by RT-PCR of *Snai3* transcripts (Figure S2 in File S1). FACS analysis of samples obtained from the *Snai3* conditional deletion animals indicated there were no alterations in steady state T cell populations in the thymus, spleen or blood (Figure S3 in File S1) suggesting that if Snai3 was essential for the development of T cells, its action was prior to the expression of *Lck*. To test this possibility, we bred the *Snai3KO* mouse with a *Hprt-Cre* deleter strain which resulted in the germline deletion of *Snai3* [25]. *Snai3* homozygous deleted mice were viable and displayed no apparent developmental defects when compared to WT mice. This included growth rates, offspring sex ratios and fertility. Analysis of transcript (Figure S4 in File S1) and protein production (Figure S5 in File S1) demonstrated a loss of the *Snai3* gene products in the germline *Snai3KO* animals. Analysis of T cells in the thymus, and T and B cells in the periphery was also the same as WT (data not shown) suggesting that Snai3 alone is not essential for the development of such cells.

Differential expression of *Snai1*, *Snai2* and *Snai3*

The absence of any demonstrable phenotype in mice lacking Snai3 suggested that its function may be irrelevant to the animal, or that its absence may be complemented by that of the other Snail family members. The *Snai3* coding sequence has been highly conserved over vertebrate evolution suggesting it does serve a defined function(s) [26]. Alternatively many instances of transcription factor functional redundancy have been demonstrated. MEF2 family members have been shown to display partially overlapping functions in neuronal development [27]. More relevantly, both Snai1 and Snai2 have exhibited migratory and anti-apoptotic functions when studied in cancer models [11,28–30]. Additionally, all three Snail family members have been shown to inhibit myoblast differentiation *in vitro* [5,10] and all three possess very conserved SNAG and DNA binding protein domains [26]. Animals require the Snai1 protein in that the loss of *Snai1* results in an embryonic lethality [8,9]. Animals lacking *Snai2* are born viable but demonstrate decreased growth rate, skewing of immature T cell populations, eyelid defects and deficiencies in erythropoiesis and fertility [13,19,31].

To determine if either Snai1 or Snai2 could potentially complement Snai3, we first evaluated their expression in defined tissue and cell types using quantitative RT-PCR (Figure 2). We confirmed the specificity of the oligonucleotide

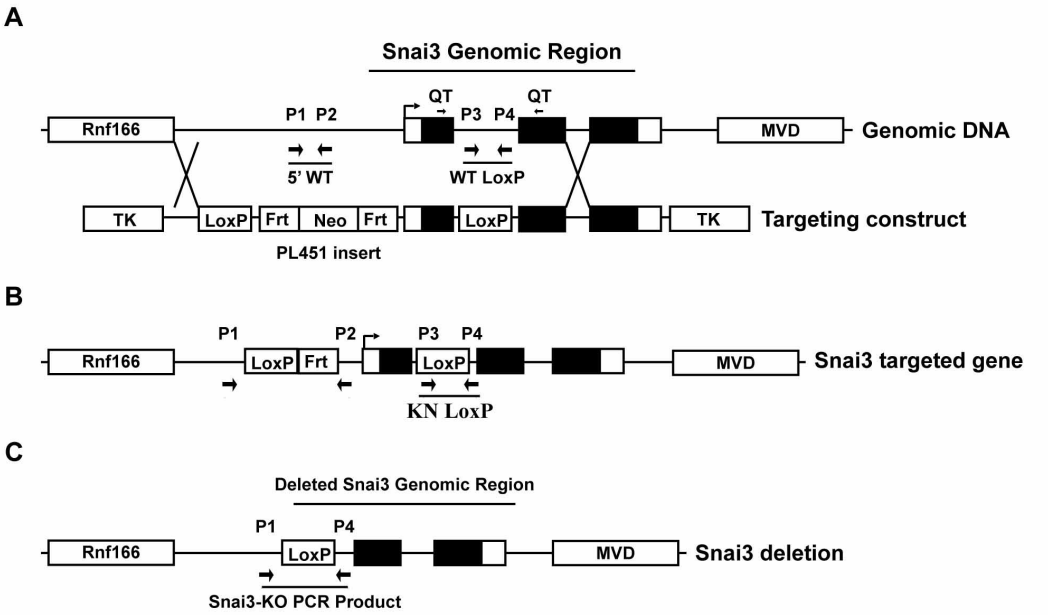

Figure 1. Conditional *Snai3* deletion strategy. (A) The *Snai3* WT genomic DNA region contains the *Rnf166* gene 5 kb upstream and the *MVD* gene 10 kb downstream. The *Snai3* gene consists of 5' and 3' untranslated regions (white boxes), three exons (black boxes), and two introns. Arrow marks the transcriptional start site (TSS). Primers used for genotyping mice and for QT-PCR of *Snai3* transcript are labeled as P1-P4 and QT, respectfully, and listed in Supplemental Table 1. The Targeting Construct had a LoxP site inserted into the PacI site of intron one and the PL451 cassette inserted into the SalI site 2kb upstream of the TSS. (B) Homologous recombination created the *Snai3* targeted genome containing unique 5' PL451 and Knockin LoxP PCR products. The Neomycin (Neo) cassette was deleted via FLP-mediated recombination of Frt sites. (C) Cre recombinase activity deleted the *Snai3* genomic region and created a new PCR product by bringing together primers P1 and P4, which are normally 6kb apart and unable to make a PCR product. Figure is not to scale.

doi: 10.1371/journal.pone.0069216.g001

sets using testes mRNA which is highly enriched for transcripts from all three Snail family members (Figure 2A). Whole tissues (thymus, spleen and total marrow cells) were also analyzed for *Snai1*, *Snai2* and *Snai3* expression (Figure 2B). Due to differences in amplification efficiencies it is not possible to directly compare the absolute numbers of gene specific transcripts to each other but clearly *Snai3* is expressed in thymus, spleen and marrow samples as is *Snai1* while *Snai2* is most highly expressed in marrow cells. RNA was then obtained from FACS sorted thymus, spleen and marrow cell populations (see *Materials*) and analyzed. While *Snai1* was expressed in all populations analyzed (Figure 2C), there was a clear enrichment of transcripts in the DP thymocyte population relative to all other thymic cell types examined. Additionally, *Snai*1 expression was evident in mature T cells, B cells and myeloid cells of the spleen and in immature B cell and myeloid lineages of the bone marrow. The expression of *Snai2* was detectable in the most immature of T cell subsets of the thymus (thymus double negative, DN, populations) and $CD4^+$ T cells in the spleen but was most evident in immature precursor and stromal cells of the marrow ($B220^-$ or $CD11b^-$ cells) (Figure 2D). Cells in these populations include uncommitted and committed progenitor cells with the potential to generate myeloid and lymphoid cell lineages.

Snai3 expression was apparent in the DN and DP thymocyte populations, and maintained in the $CD8^+$ SP cells of the thymus and spleen (Figure 2E). The loss of *Snai3* in T cells after commitment to the $CD4^+$ SP lineage is evident in both maturing cells in the thymus and mature peripheral cells in the spleen, potentially suggesting a role for Snai3 in defining the $CD4^+$ versus $CD8^+$ fate decision [32,33]. However, as described above, total deletion of *Snai3* had no effect on $CD4^+$ or $CD8^+$ SP populations of the thymus or spleen. In bone marrow, *Snai3* was expressed at increased levels in the B cell lineage relative to myeloid cells (Figure 2E).

To confirm whether protein expression paralleled transcript data, whole cell lysates were generated from total thymus, spleen, bone marrow, and testes as a positive control. Lysates were electrophoresed and blotted (Western blot: see *Materials*). As shown in Figure 3A, Snai1 (~30 kD) protein

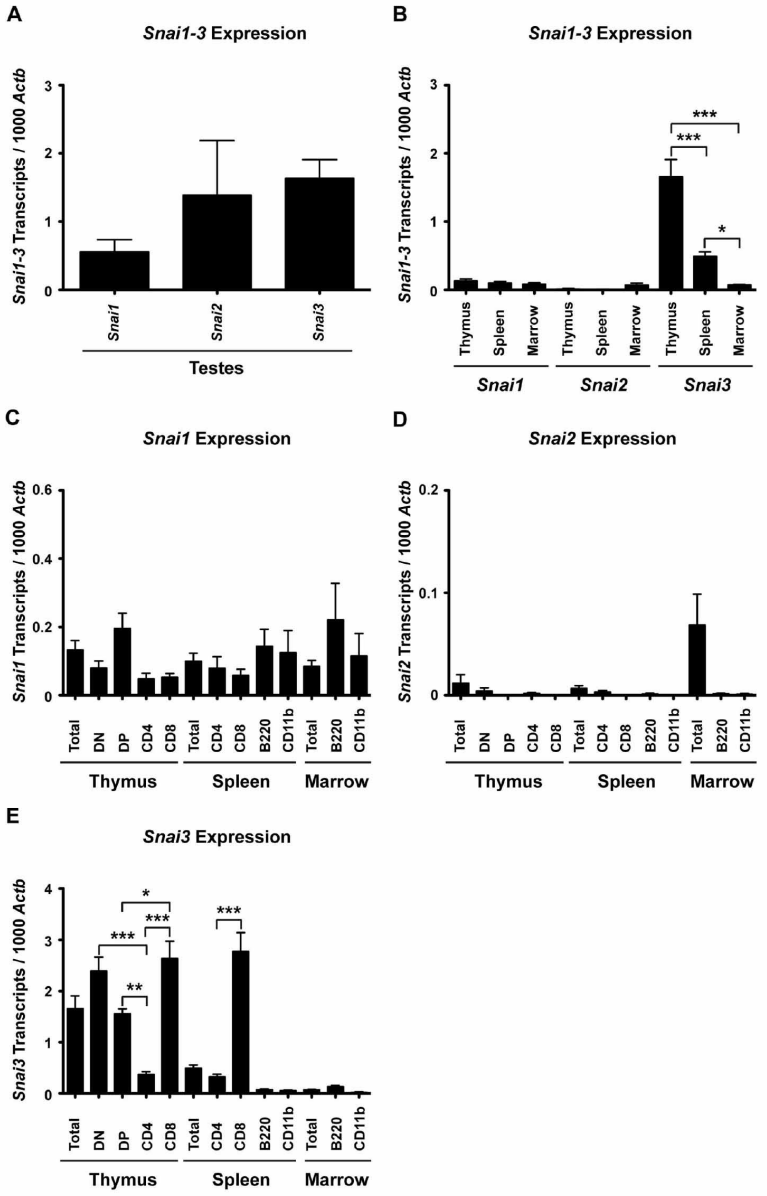

Figure 2. *Snai1-3* transcripts are differentially expressed in primary and secondary lymphoid organs of wild type mice. RNA was isolated and cDNA synthesized as described in the *Materials*. Quantitative real-time RT-PCR was performed via LightCycler as described in the *Materials*. (A) cDNA from testes served as a positive control for all RT-PCR analysis. (B) *Snai1-3* transcript analysis of cDNA generated from total thymus, spleen, and bone marrow. (C–E) RT-PCR of specific cell subsets demonstrating the distribution patterns of *Snai1* (C), *Snai2* (D), and *Snai3* (E) expression. Three mice were analyzed for the testes. At least 4 mice were analyzed per immune cell type. Levels of *Snai1-3* transcripts are relative to 1000 *Actb* transcripts per each individual sample. Data are represented by the mean ± SEM. One-way ANOVA with Bonferroni post hoc test: * $p < 0.05$, ** $p < 0.01$, *** $p < 0.001$.

doi: 10.1371/journal.pone.0069216.g002

levels were highest in the thymus, lower in the spleen and undetectable in the bone marrow although transcript levels would have predicted that thymus and marrow would have provided nearly equivalent protein quantities. Snai2 (~34 kD) protein was detectable in bone marrow and spleen but not thymus (Figure 3B). [The specificity of the anti-Snai2 antibody was confirmed by comparing the presence of the protein in testes obtained from WT and animals lacking both Snai2 and Snai3 (Figure S6A,B in File S1)]. Post-transcriptional/ translational regulation may be controlling Snai1 and/or Snai2 protein levels. For example, both Snai1 and Snai2 are targeted for degradation via GSK3β and MDM2 dependent mechanisms, respectively [34,35]. Additionally *Snai2* transcripts were recently described as targets of miR-206 [5] and *Snai1* transcripts as targets of miR-30a [36] the result of which can destabilize the gene transcripts and block translation.

The Snai3 protein (~36 kD) was detectable in the testes and less so in the marrow but not found in either spleen or thymus samples (Figure 3C). These data are also in contrast to the transcript data in that thymus showed much higher levels of *Snai3* transcripts than either spleen (primarily from $CD8^+$ SP T cells) or marrow. The specificity of the anti-Snai3 antibody was confirmed by comparing the presence of the protein in bone marrow obtained from WT and *Snai3KO* animals (Figure S5 in File S1). The production of Snai3 protein may also be affected by miRNA functions in that the mouse *Snai3* transcript also possesses a seed sequence for binding to miR-182-3p (data not shown).

Animals lacking Snai2 and Snai3 demonstrate more profound anatomical deficiencies than singe KO animals

The expression data described above suggested that the expression of *Snai1*, *Snai2* and *Snai3* may overlap in specific cell types/tissues and that a different family member may functionally complement the deficiency of the Snai3 protein in the *Snai3KO* mouse. To test for this possibility, we created a double KO animal lacking both *Snai2* and *Snai3* (DKO). As mentioned above, germline deletion of *Snai1* results in embryonic lethality. In contrast, single germline deletions of either *Snai2* [13,31] or *Snai3* are viable although *Snai2* deficient males are described as having decreased fertility due to testicular atrophy [19].

In order to create a *Snai2/3DKO* we first bred the *Snai2KO* back onto the C57BL/6 lineage for five generations. To circumvent any potential problems of fertility due to the lack of Snai2 [19] we utilized breeding pairs in which both parents were $Snai2^{+/-}$ $Snai3^{-/-}$ since we had observed no loss of fertility in the *Snai3KO* animals. This mating scheme was convenient for Mendelian analysis as 1 out of 4 progeny were predicted to be homozygous DKO. PCR amplification was performed on genomic DNA to detect the presence of WT and KO alleles for *Snai2* and *Snai3* (Figure 4A). Of the 129 progeny, 80 mice were $Snai2^{+/-}$ $Snai3^{-/-}$, 34 animals $Snai2^{+/+}$ $Snai2^{-/-}$ and 15 mice of the DKO phenotype, $Snai2^{-/-}$ $Snai3^{-/-}$ (Figure 4B). Based upon normal Mendelian ratios we would have expected about 32 DKO animals from this breeding scheme, half of which

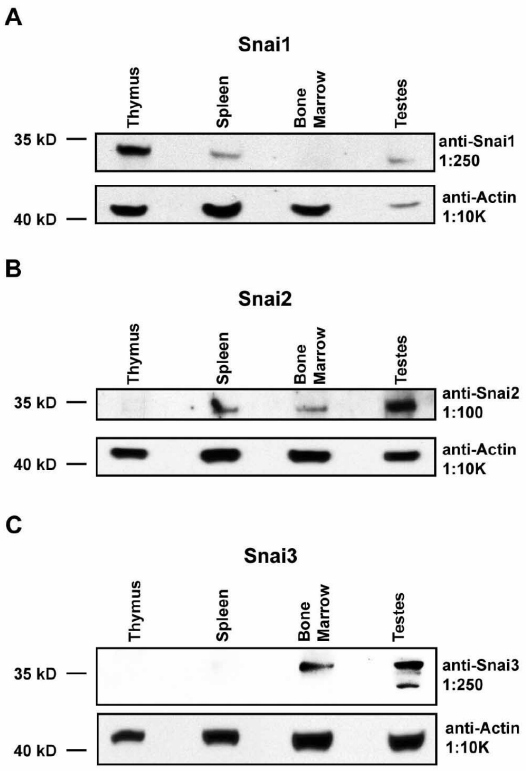

Figure 3. Snai1-3 protein expression suggests post-translational regulation. Whole cell lysates were generated from total thymus, spleen, bone marrow, and testes. Samples were subjected to immunoblot analysis as described in the *Materials*. (A–C) Samples were probed with primary antibodies specific for Snai1 (A), Snai2 (B), and Snai3 (C). Blots were probed for β-actin to verify equal protein loading. Representative blots are shown but similar results were generated for two independent mice.

doi: 10.1371/journal.pone.0069216.g003

should have been female. The sex ratio of the DKO animals also suggested a bias for male animals in that of the 15 DKO mice, 14 were males and only 1 was female (Figure 4C,D). No such sex distinctions in progeny from the *Snai2* deficient lines were previously noted nor had we observed such a gender polarization in the *Snai3KO* progeny. Neither *Snai2* (chromosome 16) nor *Snai3* (chromosome 8) are on sex chromosomes.

To confirm that the DKO animals were truly deficient in the Snai2 and Snai3 proteins, testes were harvested from the DKO animals and analyzed for *Snai2* and *Snai3* transcripts (Supplemental Figure S6A) and Snai2 and Snai3 proteins (Figure S6B in File S1) (The expression of Snai1 by transcript and protein production was not altered in the testes of the DKO

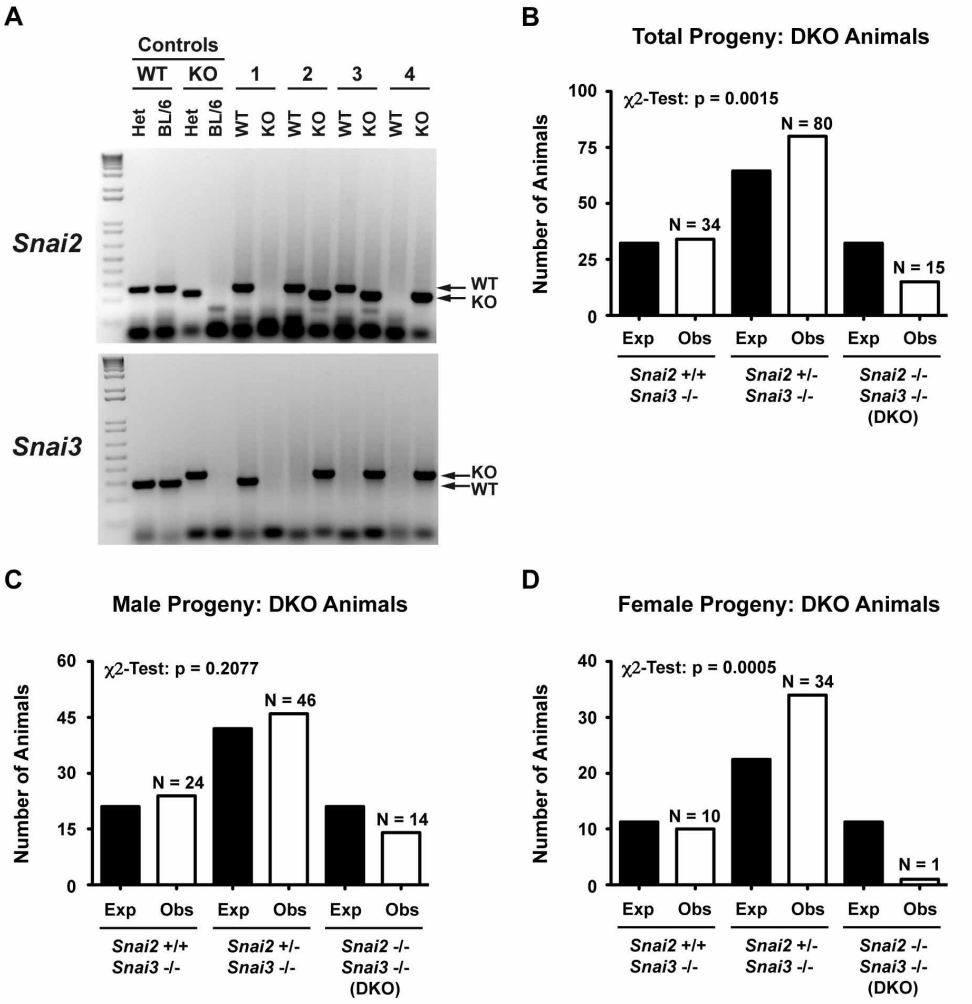

Figure 4. Generation and Mendelian analysis of *Snai2* and *Snai3* double knockout (DKO) mice. (A) Representative 2% agarose gels demonstrating genotyping of *Snai2* and *Snai3*. WT and KO refer to primer sets specific for the wild type or knocked out allele. 1-4 refer to 4 separate experimental mice. Het = heterozygous control DNA, BL/6 = wild type control DNA (B) Analysis of all progeny derived from mating *Snai2*$^{+/-}$ *Snai3*$^{-/-}$ parents. Black bars indicate expected numbers while the open bars indicate actual progeny obtained per genotype. (C–D) Distribution of male (C) and female (D) DKO animals generated from *Snai2*$^{+/-}$ *Snai3*$^{-/-}$ parents. Animal numbers per group are represented by the "N" values (open bars) while predicted numbers based upon the numbers of males and females generated in the DKO colony are shown in the black bars. More total males of all three genotypes (about 2:1) were generated in this mouse mating scheme compared to females with all of the combined genotypes. χ^2-test analysis for panels B, C, D demonstrates significance between predicted progeny genotypes and those obtained.

doi: 10.1371/journal.pone.0069216.g004

animals: Figure S6C,D in File S1). The DKO animals clearly lack these two Snail family gene products.

The physical characterization of DKO mice revealed a stunted growth phenotype. When compared with age and sex matched WT mice, DKO animals were approximately half size (Figure 5A). These animals were in general sickly, rarely survived longer than 15 weeks in the animal facility and when provided WT female mice, never generated offspring (unlike

male *Snai2KO* animals which did). The DKO animals also demonstrated the eyelid anomalies previously seen in the *Snai2KO* animals [31] which was exacerbated into the loss of the eyes, presumably due to infections, in the single DKO animal that we could maintain (alone) for 6 months of age (Figure 5B). Previously the *Snai2KO* animal (on an outbred background) demonstrated a slow growth rate for the first three weeks but in later weeks grew at the same rate as WT [31]. While the *Snai2*$^{+/-}$ *Snai3*$^{-/-}$ and WT animals displayed similar body mass, Snai2$^{-/-}$ Snai3$^{+/-}$ animals displayed a phenotype corresponding to that previously published for the *Snai2KO* (DNS). However, the difference in body mass between WT and the DKO was obvious in animals maintained for 13 weeks (Figure 5C) and longer (the 6 month DKO shown in Figure 5B), and much more dramatic than that previously reported for the *Snai2* deficient line.

Next we examined various lymphoid organs for gross morphology. The thymus, spleen and bone structure from DKO mice had a normal outward appearance (Figure 6A) although the sizes of the lymphoid organs were smaller in the DKO animal. When normalized to body weight, the DKO thymus was significantly smaller compared to WT (Figure 6B). No significant changes were seen in splenic mass between WT and DKO animals (Figure 6C). Additionally, Snai2$^{+/-}$ Snai3$^{-/-}$ and Snai2$^{-/-}$ Snai3$^{+/-}$ mice had organ masses comparable to WT mice.

Histological analysis of the 4wk DKO animal's spleen (Figure 7A) demonstrated a relatively normal splenic germinal center organization even though the spleen itself was about a third the size of the age matched *Snai2*$^{+/-}$ *Snai3*$^{+/-}$ spleen. A previous report showing splenic cross sections of *Snai2* deficient animals had similarly shown normal follicle structure [19]. The follicles in the DKO were ringed with a lighter, cell deficient zone that was not evident in the *Snai2*$^{+/-}$ *Snai3*$^{+/-}$ spleen. The thymus of the 4wk DKO animal demonstrated an unusual morphology with a decreased quantity of the densely staining, lymphocyte rich cortex region compared to the lighter staining medulla region (Figure 7B). This is in contrast to the age matched *Snai2*$^{+/-}$ *Snai3*$^{+/-}$ thymus sample which demonstrated normal morphology.

Histological analysis of the 6 month old DKO spleen and thymus (Figure 8) continued to show alterations in structure. As shown in Figure 8A, the spleens of the WT, *Snai2*$^{+/-}$ *Snai3*$^{-/-}$, *Snai2*$^{-/-}$ *Snai3*$^{+/-}$ and DKO animals all possessed germinal centers, however, there was a progressive lack of organization of the follicles in the compound heterozygotes culminating in the DKO which demonstrated the greatest degree of follicle disorganization. The DKO spleens had fewer follicles interspersed in a dense staining cellular matrix. Analysis of the thymus from the DKO and compound heterozygote animals also demonstrated an altered medulla and cortex organization (compared to WT) (Figure 8B). The DKO thymus morphology was the most dramatic in which the thymus was largely involuted and fibrotic. A small section of relatively normal thymus tissue in the DKO sample is marked in the figure (yellow asterisk) and appears to contain both medulla and cortex like thymic cellular populations.

Animals lacking *Snai2* and *Snai3* demonstrate more profound immune cell deficiencies than singe KO animals

DKO animals (along with controls) were analyzed for T, B and myeloid cells in the appropriate anatomic compartments. Previously the *Snai2KO* animals had been described as possessing normal numbers of B and T cells along with normal circulating blood cell counts compared to WT [13], and, as noted above, we did not observe any alterations in such cell populations in the *Snai3KO* animal. We first analyzed the DKO animals for T cell populations. FACS analysis of a single DKO animal (compared to a WT animal) for T cells in the thymus, peripheral blood and spleen is shown in Figure S7 in File S1. These analyses were expanded with additional animals possessing more diverse genotypes for quantification of cell lineages (Figure 9). These analyses revealed a significant reduction of thymic CD4^{+}CD8^{+} DP cells in the DKO along with a significant increase in CD4^{+} SP cells (Figure 9A). The observed trend for increased CD8^{+} T cells did not rise to the level of statistical significance. Interestingly, there was no difference in thymic T cell populations between WT mice and mice lacking the Snai2 protein, contrary to the previous analysis of *Snai2KO* animals on a mixed genetic background [19]. Further analysis of T cells in the peripheral blood (Figure 9B) and spleen (Figure 9C) of the DKO demonstrated normal distributions of both CD4^{+} and CD8^{+} SP cells. These data suggest that any alterations in T cell phenotypes in the thymus of the DKO animal are not perpetuated in the periphery with mature CD4^{+} and CD8^{+} T cells.

Similar protocols were employed to analyze B cell constituents in the bone marrow, peripheral blood and spleen of the DKO animals. A representative FACS analysis of a WT and DKO animal is shown in Figure S8 in File S1 using the co-expression of B220 and CD19 to quantify immature and mature B cells, and B220^{+}CD19^{-} staining in the marrow for the identification of immature but committed B cell precursors. These analyses are quantified in Figure 10. The DKO animals possess fewer B220^{+}CD19^{-} and significantly less B220^{+}CD19^{+} bone marrow B cells than the WT controls while the heterozygous controls show intermediate levels of B220^{+}CD19^{+} B cells in the marrow (Figure 10A). Reduced percentages of B cells in the DKO are maintained in the blood as is the intermediate phenotype of the heterozygote animals (Figure 10B). Of these, the *Snai2*$^{-/-}$ *Snai3*$^{+/-}$ animals show a greater B cell deficiency than the *Snai2*$^{+/-}$ *Snai3*$^{-/-}$ animals. In the spleen, the percentages of B cells are only significantly reduced in the DKO animal compared to WT or the heterozygote animals (Figure 10C).

The other major cell lineage that develops in the marrow is the myeloid lineage that gives rise to macrophages (defined as CD11b^{+}Gr1^{Int}), neutrophils (CD11b^{+}Gr1^{Hi}) and other cells types. Representative FACS plots for WT and DKO mice are provided in Figure S9 in File S1, and the quantitative analysis of these data, along with heterozygotes, is shown in Figure 11. In the bone marrow, the apparent loss of maturing B cells resulted in significant increases in both macrophage and neutrophil populations (Figure 11A). When peripheral blood was examined, PMN were significantly enhanced in the DKO

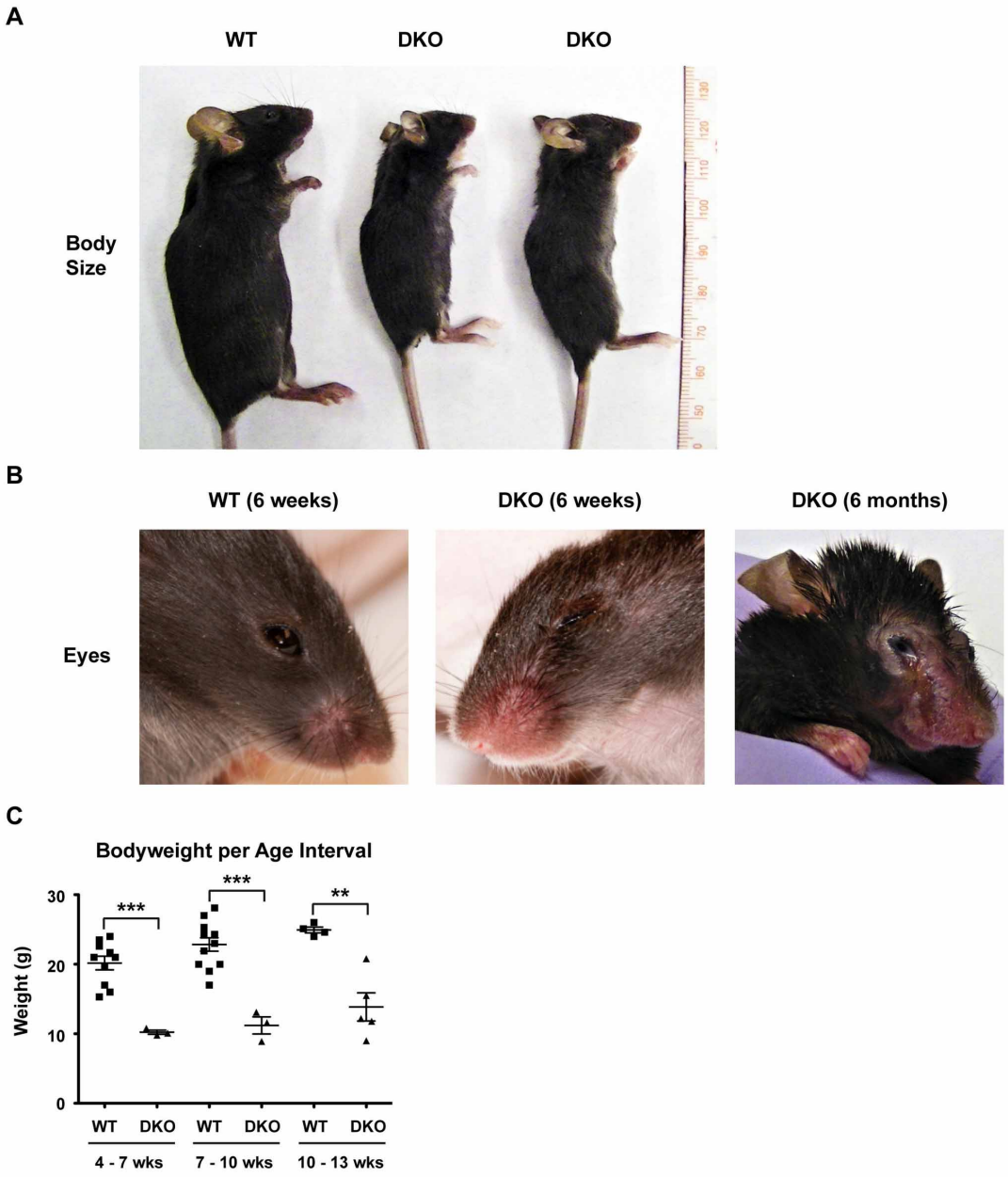

Figure 5. *Snai2* and *Snai3* DKO mice are developmentally stunted with ocular deformities. (A) Representative photo of age and sex matched (males) WT and DKO mice. Animals are approximately 6 weeks of age and presented alongside a ruler for reference. (B) Representative photo of WT and DKO male facial ocular area. (C) Graphical representation comparing ages (weeks, wks) and weights (grams, g) of WT and DKO animals over 3 week intervals. One-way ANOVA with Bonferroni post hoc test: ** $p < 0.01$, *** $p < 0.001$.

doi: 10.1371/journal.pone.0069216.g005

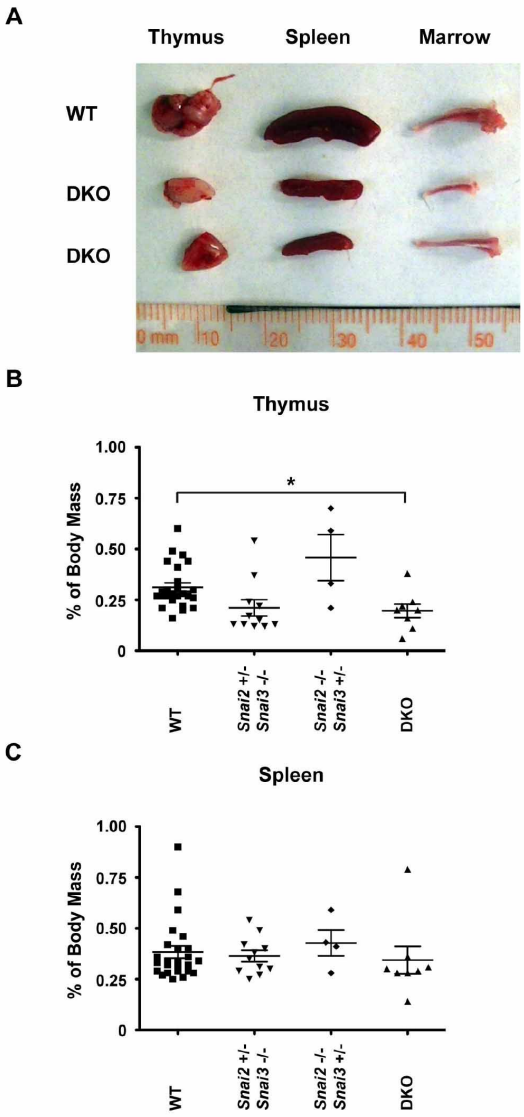

Figure 6. *Snai2* and *Snai3* DKO lymphoid organs are reduced in size but present a healthy appearance. (A) Representative photo of thymus, spleen, and bone marrow dissected from age and sex matched WT and DKO animals. Organs are presented with a ruler for reference. (B–C) Quantification of thymic (B) and splenic (C) mass among different iterations of *Snai2* and *Snai3* knockouts. % of Body Mass = (Organ Weight (mg) / Body Weight (mg)) X 100, One-way ANOVA with Bonferroni post hoc test: * $p < 0.05$.

doi: 10.1371/journal.pone.0069216.g006

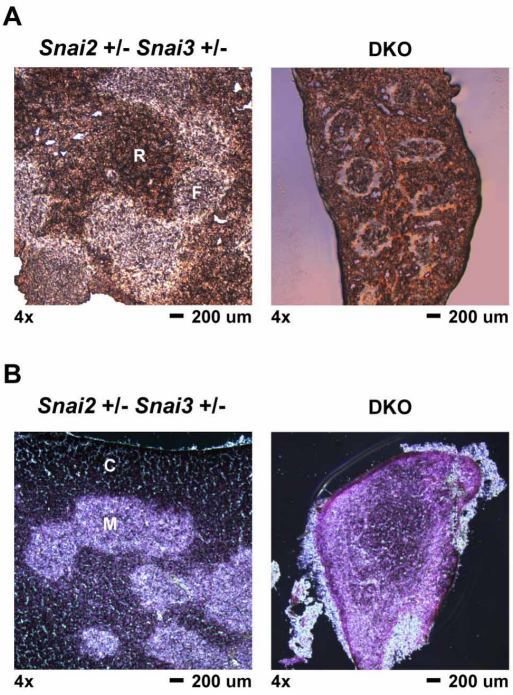

Figure 7. Histological analysis of 4 week old DKO spleen and thymus. Spleen and thymus were dissected from 4 week old Snai2$^{+/-}$ Snai3$^{+/-}$ and DKO animals. Organs were processed for histological analysis as described in the *Materials*. Tissue sections were cut to an approximate thickness of 10 µm. Representative images are shown for all genotypes and tissues assayed. (A) Splenic sections were left unstained and viewed by brightfield microscopy. 4x magnification of spleen sections from the Snai2$^{+/-}$ Snai3$^{+/-}$ and DKO. F = lymphoid follicle; R = red pulp. The DKO spleen is reduced in size compared to the Snai2$^{+/-}$ Snai3$^{+/-}$ spleen. (B) Thymus sections were stained with hematoxylin and eosin to differentiate between thymic cortex (darker stain in Snai2$^{+/-}$ Snai3$^{+/-}$) and thymic medulla (lighter stain in Snai2$^{+/-}$ Snai3$^{+/-}$): Snai2$^{+/-}$ Snai3$^{+/-}$ (left panel) and DKO (right panel). C = cortex; M = medulla. The DKO thymus is reduced in size compared to the Snai2$^{+/-}$ Snai3$^{+/-}$ thymus.

doi: 10.1371/journal.pone.0069216.g007

(Figure 11B). WT animals analyzed ranged from ~2–10% circulating neutrophils, however, the DKO animals averaged ~20% neutrophils in the blood. While infections can cause the increased mobilization of neutrophils into the bloodstream, no infections were noted in the DKO animals at the time of analysis suggesting the elevated levels of neutrophils in the bloodstream were due to enhanced production of this cell type. Macrophages in the blood were also enhanced albeit not to a significant level. This may in part be a reflection of the propensity of macrophages to migrate and establish tissue

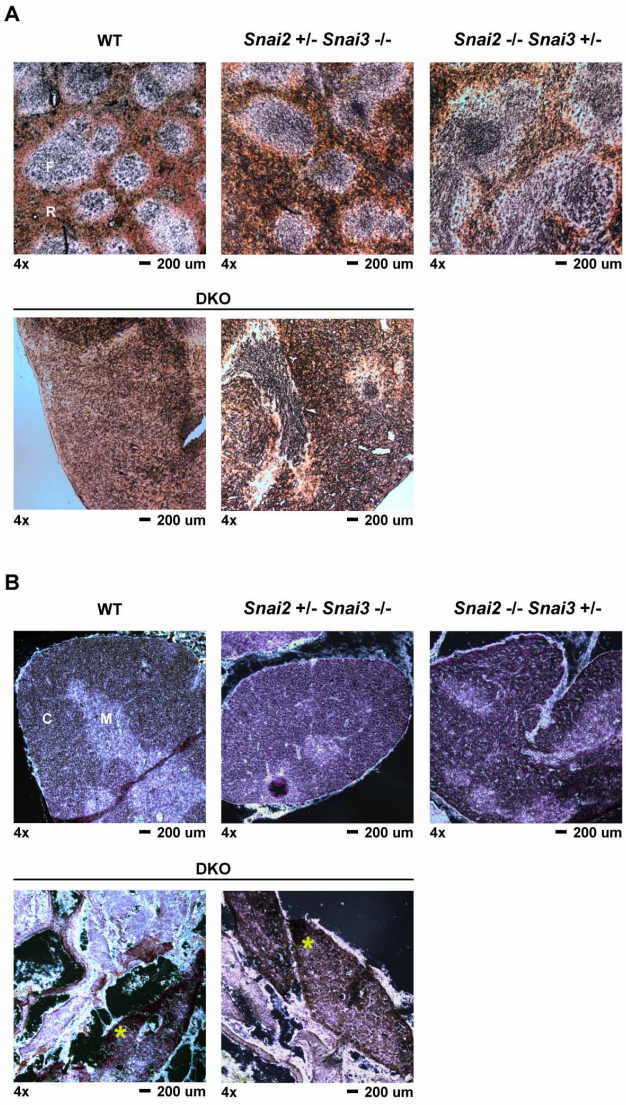

Figure 8. Histological analysis of six month DKO spleen and thymus tissues. Spleen and thymus tissues were harvested from six month old mice and processed as described in the *Materials*. Tissue sections were cut to an approximate thickness of 10 µm. All images were captured at 4x magnification. Representative images are shown for all genotypes and tissues assayed with two different sections shown for the DKO samples. (A) Spleen samples from the animals as marked. Sections were kept unstained and viewed via light microscopy for easier assessment of follicular versus red pulp areas of the spleen. F = lymphoid follicle; R = red pulp (B) Thymus sections were stained with hematoxylin and eosin to differentiate between thymic cortex (darker stain) and thymic medulla (lighter stain). C = cortex; M = medulla. An * is shown in the DKO sample to highlight the localization of thymus-like epithelial tissue.

doi: 10.1371/journal.pone.0069216.g008

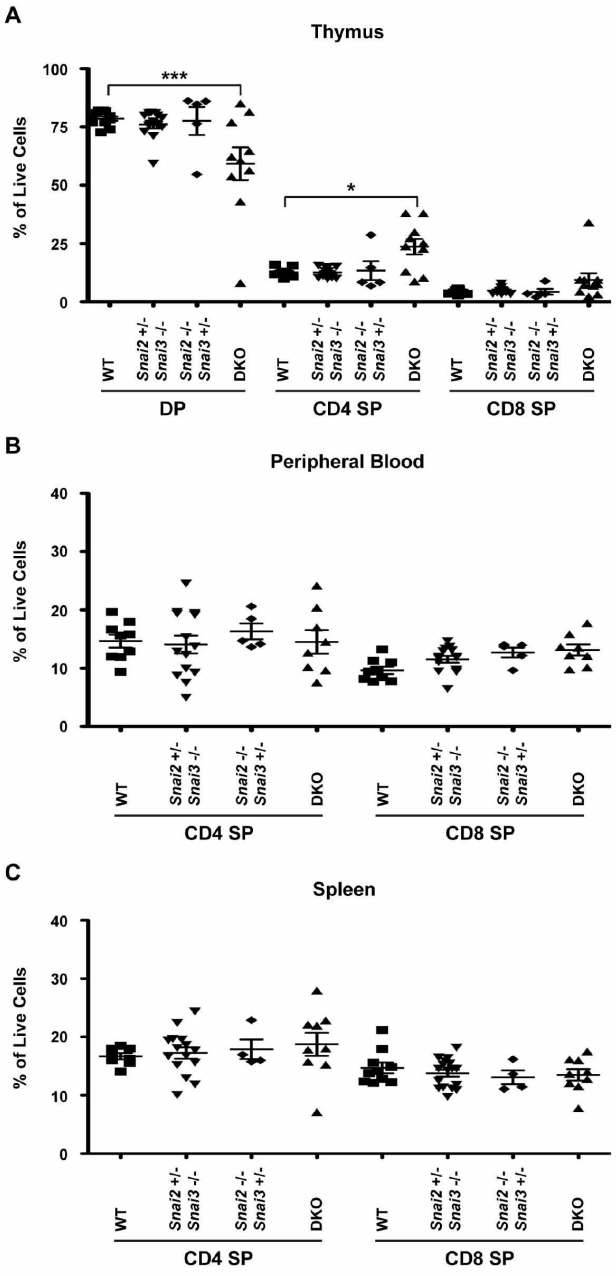

Figure 9. Double positive thymocytes are reduced in favor of an increased CD4⁺ single positive population in the *Snai2* and *Snai3* DKO. FACS analysis was performed to assess T cell populations in the thymus (A), peripheral blood (B), and spleen (C). Cells were assayed for CD4 and CD8 cell surface staining. DP = $CD4^+CD8^+$ double positive cells, CD4 = $CD4^+$ single positive, CD8 = $CD8^+$ single positive, Results are presented as a percentage of total cells analyzed. One-way ANOVA with Bonferroni post hoc test: * $p < 0.05$, *** $p < 0.001$.

doi: 10.1371/journal.pone.0069216.g009

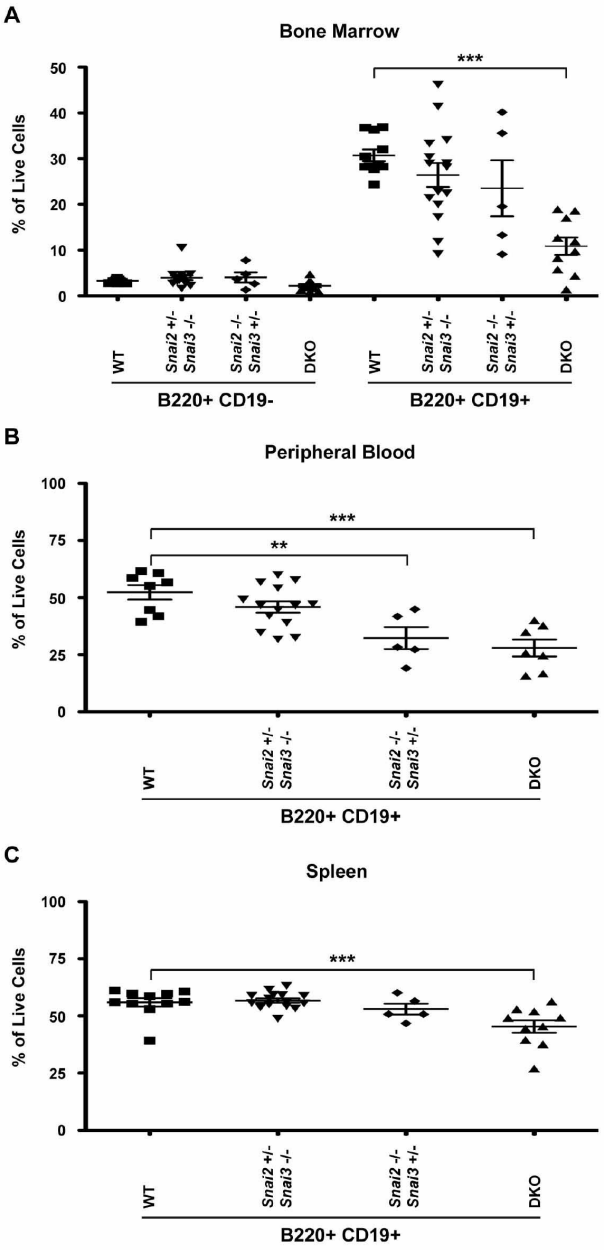

Figure 10. *Snai2* and *Snai3* DKO mice demonstrate a severe impairment in B cell development. FACS analysis was performed to assess B cell populations in the bone marrow (A), peripheral blood (B), and spleen (C). B cell populations were assessed using surface staining for B220 and CD19. In the bone marrow (A), $B220^{+}CD19^{-}$ (pre-pro-) and $B220^{+}CD19^{+}$ (pro-, pre-, immature, and mature re-circulating) cells were assayed. In the peripheral blood (B) and spleen (C), B cells were defined as $B220^{+}CD19^{+}$. Results are presented as a percentage of total cells analyzed. One-way ANOVA with Bonferroni post hoc test: ** $p < 0.01$, *** $p < 0.001$.

doi: 10.1371/journal.pone.0069216.g010

residence. In the spleen, macrophages and neutrophils showed a significant enrichment in the DKO (Figure 11C).

The analysis of cell types in the blood of the DKO animals was further investigated using older (6 months) WT and compound heterozygote animals and the single DKO animal that survived to 6 months. Blood samples from such mice were analyzed for both percentages of cell types (Figure 12A), total numbers of cells per 1µl of blood (Figure 12B) and analyzed by cytospin (Figure 12C). The percentages of blood cells in these animals showed a skewing towards greater percentage of T cells and PMN in the animals lacking both *Snai2* alleles. Total numbers of cells in the blood of the Snai2$^{-/-}$ Snai3$^{+/-}$ animals were also increased, compared to WT and the Snai2$^{+/-}$ Snai3$^{-/-}$ mice via the expansion of PMN, macrophage and T cell numbers. The elevated numbers of cells in the blood of the DKO and Snai2$^{-/-}$ Snai3$^{+/-}$ mice were also evident in the cytospins in which greater numbers of myeloid and lymphoid cells were visible when compared to the WT or Snai2$^{+/-}$ Snai3$^{-/-}$ animals.

Discussion

In this study we have examined the roles of the transcriptional repressor proteins Snai2 and Snai3 on the development of the mouse and immune cell lineages. The high level of expression of *Snai3* in skeletal and cardiac muscle tissue and thymus suggested that deletion of the gene might be an embryonic lethality and lead to T cell development anomalies. Instead we found that deletion of *Snai3*, either only in T cell lineages via *Lck-Cre* or in the entire animal had no effect upon viability, reproduction, physical appearance or immune cell derivation. Therefore, unlike *Snai1*, *Snai3* is not an essential gene.

The absence of phenotype associated with the lack of the Snai3 protein either suggested that the protein has only minimal function or that another member of the family functionally complements its absence. While *Snai1* expression is demonstrable in many bone marrow lineages (Figure 2C) animals lacking the factor do not survive. Alternatively *Snai2* expression is confined to the more immature cell types of the marrow and thymus (Figure 2D); a previous report documented the expression of *Snai2* in early lymphoid and myeloid precursors as well as hematopoietic stem cells [13]. *Snai2* deficient animals are viable but do demonstrate a number of deficiencies. *Snai2* deficient animals were described as possessing swollen eyelids that enhanced infections of the eye and displayed moderate postnatal growth retardation that was most evident in animals prior to weaning [31]. The numbers of T and B cells and their mitogenic responses were not altered in the *Snai2* deficient animals nor were there differences in blood counts between WT and *Snai2* deficient animals [13]. There were, however, increased numbers of hematopoietic colony forming units in the marrow and spleen of such animals [13,20]. A previous analysis of *Snai2* expression in the thymus and spleen using a Snai2-LacZ fusion protein had identified only a small subset of scattered cells of unknown identity expressing the protein: no report of marrow cell expression of the Snai2-LacZ fusion protein was noted [37]. Although *Snai2* deficient animals were described as having normal T and B cell numbers [13], a different report did document the skewing of immature T cell populations in the thymus of a *Snai2* deficient animal, the same populations that we observed high levels of *Snai3* expression [19]. Therefore we chose to create a double knockout animal of both Snai2 and Snai3 proteins to determine if T cell populations (and those of other bone marrow lineage cells) had enhanced developmental anomalies compared to those found for the *Snai2* deficiency alone.

The *Snai2/Snai3* deficient, DKO animals demonstrated a number of phenotypes enhanced over the single KO lines. At the most superficial layer, the DKO animals were dramatically reduced in size at birth compared to WT and maintained the runted phenotype for the life of the animal (Figure 5). This size differential was much greater than that previously described for the *Snai2KO* animals. There was also a sex specific skewing of the DKO progeny (Figure 4). While males were generated at near Mendelian levels, the number of female progeny was well below expectations. Indeed of the 15 DKO animals analyzed for this study only one was female. A similar gender skewing was not reported for the *Snai2* deficient animals and we did not observe this with the *Snai3KO* line. Most instances of sex specific lethality map to the X-chromosome yet neither *Snai2* or *Snai3* are on that chromosome. The *Snai2/3* gene products, however, may influence the expression of other genes on the sex chromosomes. For example, deletion of components essential in initiating and maintaining X-chromosome inactivation (XCI) consistently results in a female-specific block in embryonic development [38,39] and their expression could be modulated by Snai2/Snai3. Long non-coding RNAs (lncRNAs) such as *Xist* function to initiate XCI. In contrast, additional effectors such as *Tsix* act to directly inhibit the function of *Xist* [40]. Thus Snai2/Snai3 may modulate the expression of these components via the recruitment of HDACs. An alternative explanation for the sex skewing of the DKO offspring may be by complementation via Snai1 in male offspring that is not readily available to females *in utero*. All three Snail family members are expressed in the testes (Figure 3) such that altered expression of *Snai1* in the sperm of the DKO animals may negatively influence the ability of the XX fertilized egg to survive. We have not identified at what point in gestation female DKO animals are lost.

The analysis of the hematopoietic system of the DKO indicated that gene dosage of Snail family members can influence the development of bone marrow derived cells and the structure and organization of lymphoid tissues. For example, the thymus architecture of the DKO is different than WT or the compound heterozygotes (Figures 7, 8). Maturing T cells lacking both Snai2 and Snai3 proteins showed a lower CD4^{+}CD8^{+} DP population than either of the compound heterozygotes or WT as well as an elevated CD4^{+} population (Figure 9). CD8^{+} cells demonstrate much higher expression of *Snai3* than CD4^{+} cells (Figure 2) thus the lack of the two transcriptional repressors Snai2 and Snai3 in CD8^{+} cells may promote the development of the CD4^{+} lineage. If this is the case, then negative and positive selection of such cells may have been compromised in the thymus leaving such animals vulnerable to autoimmune traits that would be evident in older

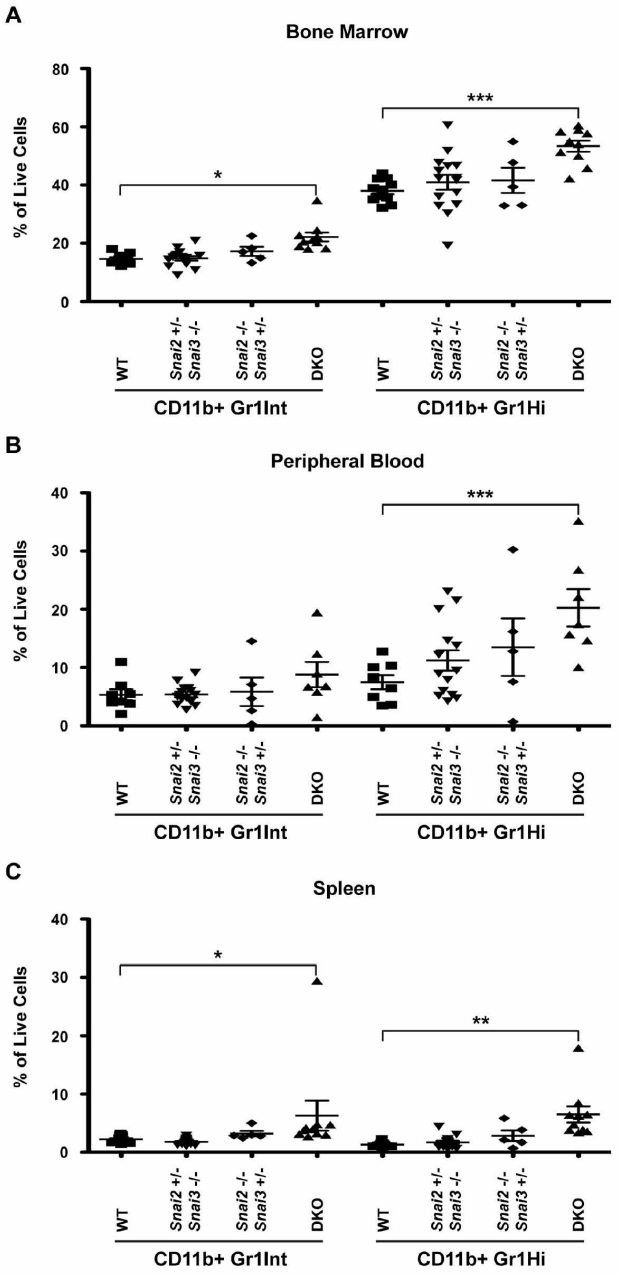

Figure 11. Myeloid populations are enhanced in the *Snai2* and *Snai3* DKO. FACS analysis was performed to assess myeloid cell populations in the bone marrow (A), peripheral blood (B), and spleen (C). Cells were stained for CD11b and Gr1. Macrophages are identified by $CD11b^{+}$ $Gr1^{Int}$ staining. Neutrophils (representative of granulocytes) are distinguished by $CD11b^{+}$ $Gr1^{Hi}$ staining. Results are presented as a percentage of total cells analyzed. One-way ANOVA with Bonferroni post hoc test: * $p < 0.05$, ** $p < 0.01$, *** $p < 0.001$.

doi: 10.1371/journal.pone.0069216.g011

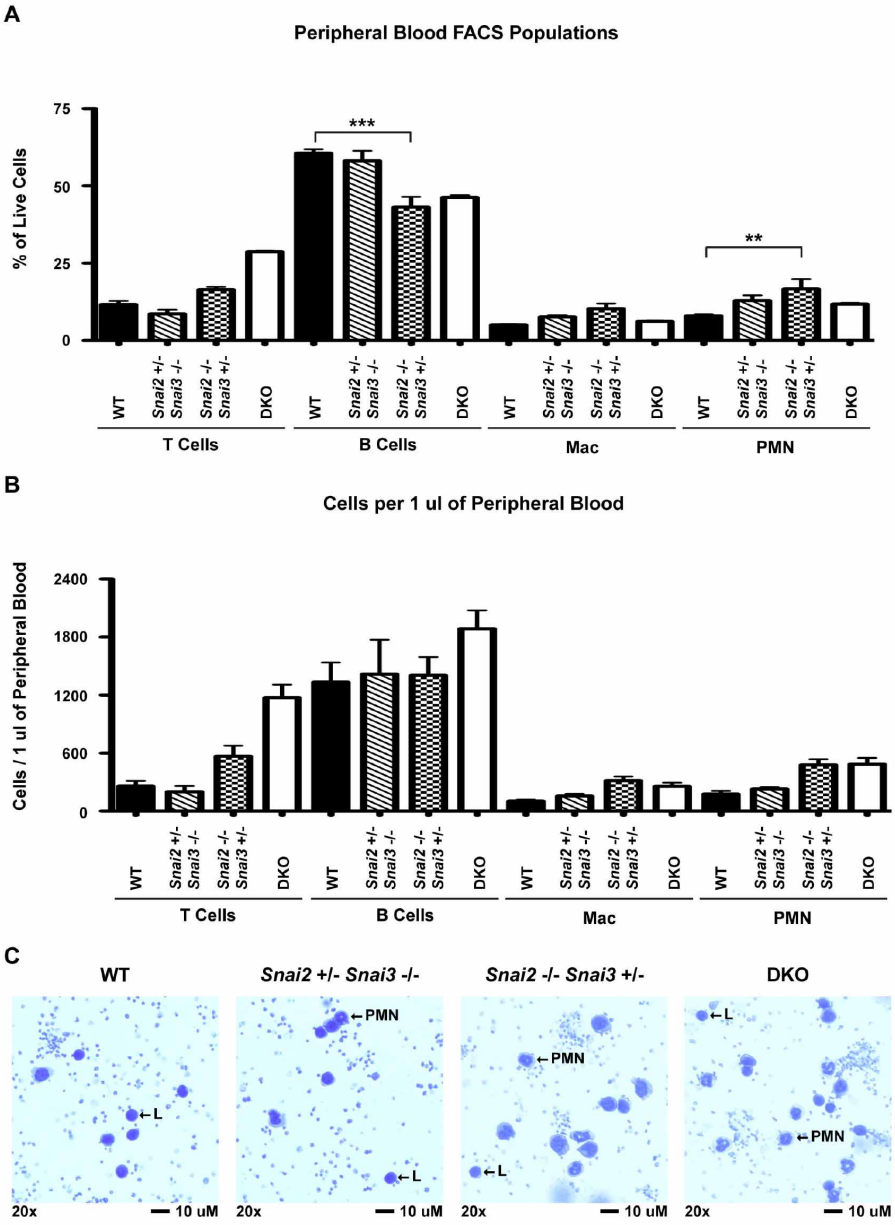

Figure 12. Circulating hematopoietic profile of six month old mice. Retro-orbital bleeds were performed three times for each animal assayed. Three mice were analyzed for WT, Snai2$^{+/-}$ Snai3$^{-/-}$, and Snai2$^{-/-}$ Snai3$^{+/-}$ genotypes. Only one DKO animal survived to six months of age. FACS was used to assess overall percentages (A) and absolute numbers of each lineage (B) within the peripheral blood. Significance was tested using one-way ANOVA followed by the Bonferroni post hoc test. ** $p < 0.01$, *** $p < 0.001$ (C) Snai2$^{-/-}$ Snai3$^{+/-}$ and DKO animals display increased lymphocytes and neutrophils in circulating blood. Cytospins were performed with 30 µl of peripheral blood. Slides were stained with Wright-Giemsa to differentiate between blood cell types. 20x images were photographed and representatives for each genotype are shown.

doi: 10.1371/journal.pone.0069216.g012

mice [41–43]. Unfortunately the severe running of the DKO animals precludes such long-term analyses but they can be addressed in the future using T cell specific deletion of the Snai2/Snai3 proteins. A previous report [20] detailed the role of Snai2 in controlling the generation of the stem cell precursors that feed into the T, B and myeloid lineages analyzed in this paper. That report did not describe deficiencies in such precursors and actually demonstrated an enhanced ability of stem cell expansion following insult in the *absence* of Snai2. Therefore it is unlikely that the alterations in T, B and myeloid precursors observed in this report of the DKO animals is due to compromised stem cell development, and is instead due to alterations in gene expression in more committed lineages.

Similar to the analysis of the thymic precursors, the development of the B cell and myeloid lineages in the bone marrow suggests that the Snail family of proteins is important for the early development of these lineages. Examination of B cell populations in the DKO animals showed a striking reduction that was initiated in the bone marrow (Figure 10A). Percentages of the earliest forms of committed B cells ($B220^+CD19^-$: pre-pro-) were reduced by approximately 30 percent. This difference was further amplified in the more mature bone marrow subsets ($B220^+CD19^+$) (~65% reduction) suggesting an initial deficiency in cells committing to the B cell lineage in the DKO animals. The loss of only Snai2 also negatively impacts the development of marrow B cells and peripheral blood levels of the cells however, only the DKO animal shows significant loss of B cells in the splenic populations again suggesting that the combined loss of both Snai2 and Snai3 in these cell lineages has a greater developmental impact than the loss of only a single family member. The loss of B cells in the DKO may be related to the anti-apoptotic responses associated with the Snail proteins [13,18,44,45]. V(D)J recombination of B (and T) cells primes lymphocytes to undergo apoptosis in the event that the recombinations are non-productive [46–48]. The DKO animals may have heightened sensitivity to such apoptotic signals reducing the production of marrow and bloodstream B cells yet allowing for the eventual colonization of the peripheral lymphatic organs such as the spleen. Indeed the survival of the DKO B cells in the spleen may be enhanced by the actions of BAFF that leads to the expression of anti-apoptotic control proteins [49,50].

The enhanced development of myeloid cells in the DKO animal may be due directly to the absence of the Snai2/Snai3 proteins, or indirectly, to the relative absence of the B cell precursors. Future analysis of progenitor populations such as the granulocyte-monocyte (GMP), common myeloid (CMP) and common lymphoid (CLP) progenitors may begin to shed light onto this question.

The data presented in this manuscript offer a glimpse into the possible functions of the Snail family of proteins in bone marrow cell derivation. Previously we had shown that over-expression of *Snai3* in the earliest of stem cell precursors (via stable *Snai3*-encoding retrovirus infection of stem cells in bone marrow chimera animals) blocked lymphocyte development and shunted bone marrow development into the myeloid lineage [21]. Since Snai3 binds to the canonical E-box motif with an internal GC rich di-nucleotide, the over-expression of the protein would have blocked the binding of other E-box proteins that recognize such sites. The Id proteins are helix-loop-helix proteins that dimerize with E-box binding proteins and block their transcriptional activation potential [51,52]. Ectopic expression of Id in a bone marrow chimera model also blocked the development of lymphocytes, instead shunting cells into the myeloid lineages [53]. These data suggest that expression of an undefined E-box protein is critical for the derivation of the lymphoid lineage: inhibition of this E-box protein (or multiple proteins) by the over-expression of Id or Snai3 thus blocks its function and blocks lymphocyte development. The identification of such an E-box transcriptional activator and the genes it targets would enhance our understanding of myeloid versus lymphoid development. We would predict that such target genes would possess GC-rich di-nucleotide E-box sites.

The removal of Snai2 and Snai3 in the DKO, however, demonstrates their functions in hematopoiesis at stages past the lymphoid versus myeloid differentiation decision. The stages of T and B cell development are altered and perhaps retarded from their normal time line of differentiation, yet mature, end stage T and B cells are still obtained in the DKO animals. The E2A gene encodes two proteins, E12 and E47, that bind to GC-rich di-nucleotide E-boxes (the same sequences favored by the Snail family of proteins). E12 and E47 proteins are critical for the early stages of B cell and T cell development [54,55]. Animals lacking E2A gene products show enhanced $CD4^+$ SP cells in the thymus and decreased $CD4^+CD8^+$ DP cells, similar to our observations with the *Snai2/Snai3* DKO animals. In animals lacking the E2A proteins, the impact on B cell development is dramatic with very few splenic B cells, and marrow B cells blocked at the first stages of immunoglobulin rearrangement. Interestingly the over-expression of E47 leads to the enhanced expression of *Snai3* [54] (and Snail family and E47 proteins directly interact [5]) suggesting that the expression and functions of the E2 and Snail family products are coordinated in the maturation of bone marrow derived cells.

In summary we have shown that the sum of eliminating both *Snai2* and *Snai3* provides for a more profound phenotype than seen with animals deficient in only *Snai2* or *Snai3*. The absence of both proteins is tolerated by male offspring, but only rarely by females, however all DKO animals are runted and fail to thrive. The development of T and B cells is not blocked, but is inhibited and may give rise to cells with impaired functions. These data suggest that the development of the mouse and of bone marrow lineages requires the actions of the Snail family of proteins to inhibit E-box activating proteins and that the loss of both of the Snai2 and Snai3 proteins can lead to phenotypes that are not evident in the animals lacking only one such protein.

Materials and Methods

Animal strains and care

Animals were housed in the Animal Resource Center (University of Utah Health Science Center, Salt Lake City, UT)

according to the guidelines of the National Institute of Health for the care and use of laboratory animals. All animal protocols were reviewed and approved by the University of Utah Institutional Animal Use and Care Committee. C57BL/6 mice (Stock #000664) and B6.SJL-Ptprc Pepc/BoyJ (Stock #002014) were obtained from The Jackson Laboratories. B6; 129S1-Snai2^{tm2Grid}/J mice (Stock #010617) were obtained from The Jackson Laboratories and backcrossed to C57BL/6 for five additional generations. Mice of at least 4 weeks of age were used for all experiments.

Snai3 knockout construct and gene targeting

A 12kb fragment encompassing the entire *Snai3* genomic region (NCBI 30927) was screened out of an 129 lambda phage library using probes specific to *Snai3* coding sequence (NM_013914) and cloned into the NotI and XbaI sites of pSK creating pSK-*Snai3*. The XbaI site of pSK-*Snai3* was changed to NotI and the 12kb *Snai3* fragment was digested by NotI and cloned into ΔSalpSK plasmid creating ΔSalpSK-*Snai3*. LoxP oligos were ligated together and cloned into the PacI site (first intron) of ΔSalpSK-*Snai3*. The NotI site was changed to SalI in the PL451 neo cassette construct and the entire neo cassette (LoxP-Frt-neo gene-Frt) was excised by SalI digest and cloned into the SalI site of ΔSalpSK-*Snai3* creating a complete pSK-*Snai3*-KN targeting construct, see Figure 1. The entire *Snai3*-KN targeting construct was excised by NotI digest and cloned into the TK1-TK2 vector. The TK1-TK2 vector was linearized by FseI digest and used to make targeted ES cells for blastocytes injection by standard transgenic mouse techniques at the University of Utah Knockout/Transgenic Mouse Core.

RNA preparation, cDNA synthesis and RT-PCR

Total RNA was isolated from cells using Illustra RNAspin Mini kit (GE Healthcare) according to the manufacturer's instructions. cDNA was synthesized using SuperScript III First-Strand Synthesis System (Invitrogen) and purified with the GeneJET PCR Purification kit (Fermentas). Semi-quantitative RT-PCR was performed via incorporation of [^{32}P] dCTP [56]. Amplification products were subjected to polyacrylamide sequencing gel electrophoresis. Products were visualized by exposure to X-ray film at -80° C. Quantitative RT-PCR was performed using Light Cycler (Roche Diagnostics) [57]. All transcript values shown are relative to *Actb* expression and are mean values ± standard error measurement (SEM). Primer sequences are provided in Table S1 in File S1.

Immunoblotting (Western blot)

Total whole cell lysates (WCL) were generated from thymus, spleen, bone marrow, and testes via lysis in Radio-Immunoprecipitation Assay (RIPA) buffer following standard methods. Protease inhibitors were added to RIPA before use (Roche, 04693132001). Protein amounts equivalent to 2.5–5 million (M) cells were electrophoresed in 4-20% gradient SDS-PAGE gels (Thermo Scientific, 0025204). After transfer to PVDF membranes, blots were stained with Ponceau Red and cut into strips to allow for simultaneous probing of target antigens. After removing Ponceau staining via TBS-T washing, blots were blocked in 5% NFDM/TBS-T for 1 hour at room temperature. Blots were then probed at 4° C overnight with the following primary antibodies at the indicated dilutions: Snai1 (Santa Cruz, sc-10432, 1:250), Snai2 (Santa Cruz, sc-10436, 1:100), Snai3 (Harlan Bioproducts, P070240, 1:250) [21], and β-actin (Sigma, A2066, 1:10,000). The next day, blots were washed with TBS-T and incubated for 2 hours at room temperature with the following secondary antibodies: peroxidase-conjugated bovine anti-goat (Jackson ImmunoResearch, 805-035-180, 1:10,000) or peroxidase-conjugated goat anti-rabbit (Bio-Rad, 170-6515, 1:10,000). Blots were washed sequentially with TBS-T and then TBS to remove unbound antibody and excess Tween, respectively. Bound antibody was detected by standard ECL detection (Thermo Scientific, 34080) methodology and exposure to X-ray film.

DNA isolation and genotyping

Approximately 5 mm tail sections were boiled in 50 mM NaOH for at least one hour. 1 M Tris was added to neutralize the NaOH. Following centrifugation to remove insoluble material, DNA was precipitated from supernatants following standard ethanol precipitation guidelines. *Snai2* and *Snai3* genotyping was performed with Fermentas *Taq* DNA Polymerase (EP0402) using 2 µl of DNA per reaction. Cycling parameters are available upon request. Primer sequences are provided in Supplemental Table 1. Products were electrophoresed in 2% agarose gels.

FACS analysis and cell sorting

All experiments were performed using mice ≥ 4 weeks of age. Cells were prepared for FACS analysis as previously described [49]. The following antibodies were used with the dilutions indicated: CD16/32 (BioLegend, 101302, 1:1000), CD3-FITC (eBioscience, 11-0031-82, 1:100), CD4-PerCPCy5.5 (BioLegend, 100434, 1:200), CD8-PE (eBioscience, 12-0083-83, 1:200), CD19-FITC (eBioscience, 11-0193-85, 1:500), B220-PE (BioLegend, 103208, 1:500), CD11b-PerCPCy5.5 (BioLegend, 101227, 1:500), and Gr1-PECy7 (BioLegend, 108415, 1:2300). Population analysis was performed on the FACS Canto II (BD Biosciences) and results are presented as percentages of the total live cells analyzed per tissue. Cell sorting of specific populations was performed on the Aria Cell Sorter (BD Biosciences) at the University of Utah Flow Cytometry Core.

Tissue Preparation and Analysis

Spleen and thymus were dissected from mice and briefly rinsed in 1x PBS. Tissues were fixed overnight at 4° C in 4% paraformaldehyde following by sequential dehydration steps in 5% sucrose: 1x PBS, 15% sucrose: 1x PBS, and 30% sucrose: 1x PBS. Following dehydration, tissues were OCT embedded on dry ice. Sections were cut to a thickness of 10 µm using a cryostat.

Hematoxylin and eosin staining were performed following manufacturer protocols. Cytospins were prepared using 30 µl of blood following lysis of erythrocytes. Slide preparations were stained with Wright-Giemsa stain (Ricca, 9380-16) to differentiate cell types. Samples were imaged with an Olympus

BX-51 microscope. Image processing was performed using cellSens Dimension software (Olympus).

Statistical analysis

One-way ANOVA followed by the Bonferroni post hoc test was utilized for all statistical measurements performed. Statistical cutoffs are noted in the figure legends.

Supporting Information

File S1. Figure S1, S2, S3, S4, S5, S6, S7, S8, S9 and Table S1. (PDF)

References

1. Barrallo-Gimeno A, Nieto MA (2009) Evolutionary history of the Snail/Scratch superfamily. Trends Genet 25: 248-252. doi:10.1016/j.tig.2009.04.001. PubMed: 19427053.
2. Manzanares M, Blanco MJ, Nieto MA (2004) Snail3 orthologues in vertebrates: divergent members of the Snail zinc-finger gene family. Dev Genes Evol 214: 47-53. doi:10.1007/s00427-003-0373-1. PubMed: 14655014.
3. Boulay JL, Dennefeld C, Alberga A (1987) The Drosophila developmental gene snail encodes a protein with nucleic acid binding fingers. Nature 330: 395-398. doi:10.1038/330395a0. PubMed: 3683556.
4. Nieto MA (2002) The snail superfamily of zinc-finger transcription factors. Nat Rev Mol Cell Biol 3: 155-166. doi:10.1038/nrm757. PubMed: 11994736.
5. Soleimani VD, Yin H, Jahani-Asl A, Ming H, Kockx CE et al. (2012) Snail Regulates MyoD Binding-Site Occupancy to Direct Enhancer Switching and Differentiation-Specific Transcription in Myogenesis. Mol: Cell Publishing House.
6. Lin Y, Wu Y, Li J, Dong C, Ye X et al. (2010) The SNAG domain of Snail1 functions as a molecular hook for recruiting lysine-specific demethylase 1. EMBO J 29: 1803-1816. doi:10.1038/emboj.2010.63. PubMed: 20389281.
7. Peinado H, Ballestar E, Esteller M, Cano A (2004) Snail mediates E-cadherin repression by the recruitment of the Sin3A/histone deacetylase 1 (HDAC1)/HDAC2 complex. Mol Cell Biol 24: 306-319. doi:10.1128/MCB.24.1.306-319.2004. PubMed: 14673164.
8. Lomelí H, Starling C, Gridley T (2009) Epiblast-specific Snai1 deletion results in embryonic lethality due to multiple vascular defects. BMC Res Notes 2: 22. doi:10.1186/1756-0500-2-22. PubMed: 19284699.
9. Carver EA, Jiang R, Lan Y, Oram KF, Gridley T (2001) The mouse snail gene encodes a key regulator of the epithelial-mesenchymal transition. Mol Cell Biol 21: 8184-8188. doi:10.1128/MCB.21.23.8184-8188.2001. PubMed: 11689706.
10. Kataoka H, Murayama T, Yokode M, Mori S, Sano H et al. (2000) A novel snail-related transcription factor Smuc regulates basic helix-loop-helix transcription factor activities via specific E-box motifs. Nucleic Acids Res 28: 626-633. doi:10.1093/nar/28.2.626. PubMed: 10606664.
11. Hemavathy K, Ashraf SI, Ip YT (2000) Snail/slug family of repressors: slowly going into the fast lane of development and cancer. Gene 257: 1-12. doi:10.1016/S0378-1119(00)00371-1. PubMed: 11054563.
12. Cobaleda C, Pérez-Caro M, Vicente-Dueñas C, Sánchez-García I (2007) Function of the zinc-finger transcription factor SNAI2 in cancer and development. Annu Rev Genet 41: 41-61. doi:10.1146/annurev.genet.41.110306.130146. PubMed: 17550342.
13. Inoue A, Seidel MG, Wu W, Kamizono S, Ferrando AA et al. (2002) Slug, a highly conserved zinc finger transcriptional repressor, protects hematopoietic progenitor cells from radiation-induced apoptosis in vivo. Cancer Cell 2: 279-288. doi:10.1016/S1535-6108(02)00155-1. PubMed: 12398892.
14. Pérez-Losada J, Sánchez-Martín M, Pérez-Caro M, Pérez-Mancera PA, Sánchez-García I (2003) The radioresistance biological function of the SCF/kit signaling pathway is mediated by the zinc-finger transcription factor Slug. Oncogene 22: 4205-4211. doi:10.1038/sj.onc.1206467. PubMed: 12833143.
15. Wu WS, Heinrichs S, Xu D, Garrison SP, Zambetti GP et al. (2005) Slug antagonizes p53-mediated apoptosis of hematopoietic progenitors by repressing puma. Cell 123: 641-653. doi:10.1016/j.cell.2005.09.029. PubMed: 16286009.
16. Shirley SH, Hudson LG, He J, Kusewitt DF (2010) The skinny on Slug. Mol Carcinog 49: 851-861. doi:10.1002/mc.20674. PubMed: 20721976.
17. Parent AE, Newkirk KM, Kusewitt DF (2010) Slug (Snai2) expression during skin and hair follicle development. J Invest Dermatol 130: 1737-1739. doi:10.1038/jid.2010.22. PubMed: 20147965.
18. Inukai T, Inoue A, Kurosawa H, Goi K, Shinjyo T et al. (1999) SLUG, a ces-1-related zinc finger transcription factor gene with antiapoptotic activity, is a downstream target of the E2A-HLF oncoprotein. Mol Cell 4: 343-352. doi:10.1016/S1097-2765(00)80336-6. PubMed: 10518215.
19. Pérez-Losada J, Sánchez-Martín M, Rodríguez-García A, Sánchez ML, Orfao A et al. (2002) Zinc-finger transcription factor Slug contributes to the function of the stem cell factor c-kit signaling pathway. Blood 100: 1274-1286. PubMed: 12149208.
20. Sun Y, Shao L, Bai H, Wang ZZ, Wu WS (2010) Slug deficiency enhances self-renewal of hematopoietic stem cells during hematopoietic regeneration. Blood 115: 1709-1717. doi:10.1182/blood-2009-07-232934. PubMed: 20032500.
21. Dahlem T, Cho S, Spangrude GJ, Weis JJ, Weis JH (2012) Overexpression of Snai3 suppresses lymphoid- and enhances myeloid-cell differentiation. Eur J Immunol 42: 1038-1043. doi:10.1002/eji.201142193. PubMed: 22531927.
22. Zhuge X, Kataoka H, Tanaka M, Murayama T, Kawamoto T et al. (2005) Expression of the novel Snai-related zinc-finger transcription factor gene Smuc during mouse development. Int J Mol Med 15: 945-948. PubMed: 15870897.
23. Nguyen TV, Ke Y, Zhang EE, Feng GS (2006) Conditional deletion of Shp2 tyrosine phosphatase in thymocytes suppresses both pre-TCR and TCR signals. J Immunol 177: 5990-5996. PubMed: 17056523.
24. Hagenbeek TJ, Spits H (2008) T-cell lymphomas in T-cell-specific Pten-deficient mice originate in the thymus. Leukemia 22: 608-619. doi:10.1038/sj.leu.2405056. PubMed: 18046443.
25. Tang SH, Silva FJ, Tsark WM, Mann JR (2002) A Cre/loxP-deleter transgenic line in mouse strain 129S1/SvImJ. Genesis 32: 199-202. doi:10.1002/gene.10030. PubMed: 11892008.
26. Katoh M (2005) Comparative genomics on SNAI1, SNAI2, and SNAI3 orthologs. Oncol Rep 14: 1083-1086. PubMed: 16142376.
27. Akhtar MW, Kim MS, Adachi M, Morris MJ, Qi X et al. (2012) In vivo analysis of MEF2 transcription factors in synapse regulation and neuronal survival. PLOS ONE 7: e34863. doi:10.1371/journal.pone.0034863. PubMed: 22496871.
28. Katoh M (2005) Epithelial-mesenchymal transition in gastric cancer (Review). Int J Oncol 27: 1677-1683 PubMed: 16273224.
29. Larriba MJ, Martín-Villar E, García JM, Pereira F, Peña C et al. (2009) Snail2 cooperates with Snail1 in the repression of vitamin D receptor in colon cancer. Carcinogenesis 30: 1459-1468. doi:10.1093/carcin/bgp140. PubMed: 19502595.
30. Peinado H, Olmeda D, Cano A (2007) Snail, Zeb and bHLH factors in tumour progression: an alliance against the epithelial phenotype? Nat Rev Cancer 7: 415-428. doi:10.1038/nrc2131. PubMed: 17508028.
31. Jiang R, Lan Y, Norton CR, Sundberg JP, Gridley T (1998) The Slug gene is not essential for mesoderm or neural crest development in mice. Dev Biol 198: 277-285. doi:10.1016/S0012-1606(98)80005-5. PubMed: 9659933.

Acknowledgements

The authors would like to thank members of both Weis labs for their insightful and stimulating critiques of this work. The authors would also like to thank the University of Utah Knockout/Transgenic Mouse Core and the University of Utah Flow Cytometry Core for their expertise and support.

Author Contributions

Conceived and designed the experiments: PP TD JHW. Performed the experiments: PP TD. Analyzed the data: PP TD JHW. Contributed reagents/materials/analysis tools: PP TD JHW JJW. Wrote the manuscript: PP TD JHW JJW.

32. Egawa T (2009) Runx and ThPOK: a balancing act to regulate thymocyte lineage commitment. J Cell Biochem 107: 1037-1045. doi: 10.1002/jcb.22212. PubMed: 19479890.
33. Egawa T, Taniuchi I (2009) Antagonistic interplay between ThPOK and Runx in lineage choice of thymocytes. Blood Cells Mol Dis 43: 27-29. doi:10.1016/j.bcmd.2009.03.004. PubMed: 19375362.
34. Lee J, Kim JC, Lee SE, Quinley C, Kim H et al. (2012) Signal transducer and activator of transcription 3 (STAT3) protein suppresses adenoma-to-carcinoma transition in Apcmin/+ mice via regulation of Snail-1 (SNAI) protein stability. J Biol Chem 287: 18182-18189. doi: 10.1074/jbc.M111.328831. PubMed: 22496368.
35. Wang SP, Wang WL, Chang YL, Wu CT, Chao YC et al. (2009) p53 controls cancer cell invasion by inducing the MDM2-mediated degradation of Slug. Nat Cell Biol 11: 694-704. doi:10.1038/ncb1875. PubMed: 19448627.
36. Kumarswamy R, Mudduluru G, Ceppi P, Muppala S, Kozlowski M et al. (2012) MicroRNA-30a inhibits epithelial-to-mesenchymal transition by targeting Snai1 and is downregulated in non-small cell lung cancer. Int J Cancer 130: 2044-2053. doi:10.1002/ijc.26218. PubMed: 21633953.
37. Parent AE, Choi C, Caudy K, Gridley T, Kusewitt DF (2004) The developmental transcription factor slug is widely expressed in tissues of adult mice. J Histochem Cytochem 52: 959-965. doi:10.1369/jhc.4A6277.2004. PubMed: 15208362.
38. Marahrens Y, Panning B, Dausman J, Strauss W, Jaenisch R (1997) Xist-deficient mice are defective in dosage compensation but not spermatogenesis. Genes Dev 11: 156-166. doi:10.1101/gad.11.2.156. PubMed: 9009199.
39. Tian D, Sun S, Lee JT (2010) The long noncoding RNA, Jpx, is a molecular switch for X chromosome inactivation. Cell 143: 390-403. doi:10.1016/j.cell.2010.09.049. PubMed: 21029862.
40. Lee JT (2000) Disruption of imprinted X inactivation by parent-of-origin effects at Tsix. Cell 103: 17-27. doi:10.1016/S0092-8674(00)00101-X. PubMed: 11051544.
41. Bain G, Engel I, Robanus Maandag EC, te Riele HP, Voland JR et al. (1997) E2A deficiency leads to abnormalities in alphabeta T-cell development and to rapid development of T-cell lymphomas. Mol Cell Biol 17: 4782-4791. PubMed: 9234734.
42. Gatzka M, Newton RH, Walsh CM (2009) Altered thymic selection and increased autoimmunity caused by ectopic expression of DRAK2 during T cell development. J Immunol 183: 285-297. doi:10.4049/jimmunol.0803530. PubMed: 19542440.
43. Siggs OM, Makaroff LE, Liston A (2006) The why and how of thymocyte negative selection. Curr Opin Immunol 18: 175-183. doi: 10.1016/j.coi.2006.01.001. PubMed: 16459069.
44. Zhang K, Zhang B, Lu Y, Sun C, Zhao W et al. (2011) Slug inhibition upregulates radiation-induced PUMA activity leading to apoptosis in cholangiocarcinomas. Med Oncol 28 Suppl 1: S301-S309. doi:10.1007/s12032-010-9759-x. PubMed: 21120639.
45. Metzstein MM, Horvitz HR (1999) The C. elegans cell death specification gene ces-1 encodes a snail family zinc finger protein. Mol Cell 4: 309-319. doi:10.1016/S1097-2765(00)80333-0. PubMed: 10518212.
46. Geier JK, Schlissel MS (2006) Pre-BCR signals and the control of Ig gene rearrangements. Semin Immunol 18: 31-39. doi:10.1016/j.smim.2005.11.001. PubMed: 16386923.
47. Lam QL, Lo CK, Zheng BJ, Ko KH, Osmond DG et al. (2007) Impaired V(D)J recombination and increased apoptosis among B cell precursors in the bone marrow of c-Abl-deficient mice. Int Immunol 19: 267-276. doi:10.1093/intimm/dxl143. PubMed: 17229817.
48. Diamond RA, Ward SB, Owada-Makabe K, Wang H, Rothenberg EV (1997) Different developmental arrest points in RAG-2 -/- and SCID thymocytes on two genetic backgrounds: developmental choices and cell death mechanisms before TCR gene rearrangement. J Immunol 158: 4052-4064. PubMed: 9126963.
49. Debnath I, Roundy KM, Weis JJ, Weis JH (2007) Analysis of the regulatory role of BAFF in controlling the expression of CD21 and CD23. Mol Immunol 44: 2388-2399. doi:10.1016/j.molimm.2006.10.019. PubMed: 17140663.
50. Saito Y, Miyagawa Y, Onda K, Nakajima H, Sato B et al. (2008) B-cell-activating factor inhibits CD20-mediated and B-cell receptor-mediated apoptosis in human B cells. Immunology 125: 570-590. doi:10.1111/j.1365-2567.2008.02872.x. PubMed: 18540961.
51. Deed RW, Jasiok M, Norton JD (1998) Lymphoid-specific expression of the Id3 gene in hematopoietic cells. Selective antagonism of E2A basic helix-loop-helix protein associated with Id3-induced differentiation of erythroleukemia cells. J Biol Chem 273: 8278-8286. doi:10.1074/jbc.273.14.8278. PubMed: 9525934.
52. Massari ME, Murre C (2000) Helix-loop-helix proteins: regulators of transcription in eucaryotic organisms. Mol Cell Biol 20: 429-440. doi: 10.1128/MCB.20.2.429-440.2000. PubMed: 10611221.
53. Suh HC, Leeanansaksiri W, Ji M, Klarmann KD, Renn K et al. (2008) Id1 immortalizes hematopoietic progenitors in vitro and promotes a myeloproliferative disease in vivo. Oncogene 27: 5612-5623. doi: 10.1038/onc.2008.175. PubMed: 18542061.
54. Ikawa T, Kawamoto H, Goldrath AW, Murre C (2006) E proteins and Notch signaling cooperate to promote T cell lineage specification and commitment. J Exp Med 203: 1329-1342. doi:10.1084/jem.20060268. PubMed: 16682500.
55. Frasca D, Nguyen D, Van der Put E, Riley RL, Blomberg BB (2003) The age-related decrease in E47 DNA-binding does not depend on increased Id inhibitory proteins in bone marrow-derived B cell precursors. Front Biosci 8: a110-a116. doi:10.2741/945. PubMed: 12700059.
56. Tan SS, Weis JH (1992) Development of a sensitive reverse transcriptase PCR assay, RT-RPCR, utilizing rapid cycle times. PCR Methods Appl 2: 137-143. doi:10.1101/gr.2.2.137. PubMed: 1282437.
57. Morrison TB, Ma Y, Weis JH, Weis JJ (1999) Rapid and sensitive quantification of Borrelia burgdorferi-infected mouse tissues by continuous fluorescent monitoring of PCR. J Clin Microbiol 37: 987-992. PubMed: 10074514.

CHAPTER 3

FATAL AUTOIMMUNITY RESULTS FROM THE CONDITIONAL DELETION OF SNAI2 AND SNAI3

Reprinted from Fatal Autoimmunity Results from the Conditional Deletion of *Snai2* and *Snai3*.
Cellular Immunology 295(1):1-18. Peter D. Pioli, Xinjian Chen, Janis J. Weis, and John H. Weis.

Cellular Immunology 295 (2015) 1–18

Contents lists available at ScienceDirect

Cellular Immunology

journal homepage: www.elsevier.com/locate/ycimm

Fatal autoimmunity results from the conditional deletion of *Snai2* and *Snai3*

Peter D. Pioli *, Xinjian Chen, Janis J. Weis, John H. Weis

Division of Cell Biology and Immunology, Department of Pathology, University of Utah School of Medicine, Salt Lake City, UT 84132, United States

ARTICLE INFO

Article history:
Received 12 October 2014
Revised 15 February 2015
Accepted 17 February 2015
Available online 24 February 2015

Keywords:
Autoimmunity
Genetic deficiency
Snail transcription factors
Lymphocytes
Autoantibody

ABSTRACT

Transcriptional regulation of gene expression is a key component of orchestrating proper immune cell development and function. One strategy for maintaining these transcriptional programs has been the evolution of transcription factor families with members possessing overlapping functions. Using the germ line deletion of *Snai2* combined with the hematopoietic specific deletion of *Snai3*, we report that these factors function redundantly to preserve the development of B and T cells. Such animals display severe lymphopenia, alopecia and dermatitis as well as profound autoimmunity manifested by the production of high levels of autoantibodies as early as 3 weeks of age and die by 30 days after birth. Autoantibodies included both IgM and IgG isotypes and were reactive against cytoplasmic and membranous components. A regulatory T cell defect contributed to the autoimmune response in that adoptive transfer of wild type regulatory T cells alleviated symptoms of autoimmunity. Additionally, transplantation of *Snai2*/*Snai3* double deficient bone marrow into *Snai2* sufficient *Rag2*$^{-/-}$ recipients resulted in autoantibody generation. The results demonstrated that appropriate expression of *Snai2* and *Snai3* in cells of hematopoietic derivation plays an important role in development and maintenance of immune tolerance.

1. Introduction

Proper development and function of various cell lineages is a critical component in the viability of not only the whole organism, but also individual organ systems. These events are precisely controlled by the coordinated efforts of various gene expression networks. Throughout hematopoiesis, cell (or lineage) fate decisions are constantly being regulated by a multitude of transcriptional regulators. Some factors such as PU.1 may augment lineage bifurcation [1]. Alternatively, other factors may act to regulate the specialization of effector cells within a given lineage. For example, Foxp3 propagates a transcriptional program leading to the generation and function of regulatory T cells (T_{Regs}), necessary for the prevention of lethal autoimmune disease [2,3]. In many instances, these decisions are absolutely required for the viability of the organism leading to the evolution of functional redundancy within various transcription factor families. One such example is the ability of GATA-1 and GATA-2 to functionally overlap within the earliest stages of primitive hematopoiesis [4]. These types of redundancies serve as a potential failsafe mechanism to protect against the loss of a cell type (or specific function) as a result of a germ line or somatic mutation.

The Snail family of transcriptional regulators has been conserved throughout metazoan evolution and consists of three members: *Snai1*, *Snai2* and *Snai3* [5–7]. The protein products of each member share two common features. Within the C-terminus are multiple C_2H_2 zinc finger DNA-binding domains (DBDs). While Snai2 and Snai3 possess five DBDs, Snai1 only has four of these domains [8]. Using these zinc fingers, Snail proteins recognize and bind to canonical E-box sequences (CANNTG) preferentially targeting GC-rich central di-nucleotides [9]. At the extreme N-terminus, each protein contains a SNAG (Snail/Gfi-1) domain used to recruit various chromatin modifiers such as HDACs and EZH2 [10–12]. Due to the similarity between all three Snail members, the potential to function in a redundant manner is highly likely [13]. Historically, the Snail family is most well known for roles in embryonic development [14] however, Snail proteins have also been shown to play a prominent role in hematopoiesis [15]. Due to embryonic lethality resulting from germline deletion of *Snai1*, the hematopoietic functions of this family member have not yet been defined [16,17]. The germline deletion of *Snai2* (g2KO) is viable with piebaldism of variable penetrance [18]. Steady state hematopoiesis shows minimal perturbations with only a slight skewing of thymocyte population frequencies (i.e. decreased CD4

* Corresponding author at: 15 N Medical Dr East Rm 2100, Salt Lake City, UT 84112-5650, United States. Tel.: +1 (801) 581 4447.
E-mail address: peter.pioli@path.utah.edu (P.D. Pioli).

http://dx.doi.org/10.1016/j.cellimm.2015.02.009
0008-8749/

and CD8 double positive versus increased CD4 single positive cell ratios) [18]. Deletion of *Snai3* in the germ line has no significant phenotype [19,20].

Given the relative lack of hematopoietic phenotypes at steady-state conditions in both single knockouts of *Snai2* and *Snai3*, we recently generated and analyzed a *Snai2*/*Snai3* germline double knockout (gDKO) animal [20]. These mice demonstrated multiple lymphopoietic defects with reduced bone marrow B cell frequencies and increased CD4 single positive thymocyte percentages. Of significance, these phenotypes were only evident in the gDKO revealing a previously unappreciated functional redundancy between *Snai2* and *Snai3*. To better understand the hematopoietically intrinsic roles of these proteins in a stromal-independent manner, we generated and analyzed a *Snai2*/*Snai3* conditional double knockout (cDKO) animal. Surprisingly the cDKO animals had more dramatic phenotypes that the gDKO animals including severe runting and mortality at about 30 days. Additionally, these cDKO animals demonstrated a florid autoimmunity after birth involving a wide array of tissues. The symptoms of autoimmunity were reversible upon the adoptive transfer of wild type (WT) T_{Regs}. Finally, deletion of *Snai2* and *Snai3* in bone marrow-derived cells contributed to the autoimmune phenotype as transplantation of cDKO bone marrow into *Snai2* sufficient *Rag2*$^{-/-}$ hosts resulted in the production of autoantibodies.

2. Methods and materials

2.1. Animal strains and care

Animals were housed in the Animal Resource Center (University of Utah Health Science Center, Salt Lake City, UT) according to the guidelines of the National Institute of Health for the care and use of laboratory animals. All animal protocols were reviewed and approved by the University of Utah Institutional Animal Use and Care Committee. For transcriptional profiling experiments, C57BL/6 mice were bred and maintained in house. Foxp3–GFP reporter mice were a kind gift from Dr. June Round. *Vav-Cre* (Stock #: 008610) and *Rag2*$^{-/-}$ (Stock #: 008449) mice were purchased from The Jackson Laboratory and bred in house. All iterations of *Snai2* and *Snai3* wildtype, single and double knockouts were derived from *Snai2*$^{+/-}$ *Snai3*$^{Fl/Fl}$ *Vav-Cre*$^{+/-}$ breeding pairs. Unless otherwise noted, all animals used approximated three to 4 weeks of age. Animal numbers used per experiment are noted in the figure legends. Paraffin sectioning and H&E staining was performed at the University of Utah Hospital, Pathology, following their standard protocol. Sections were cut to thickness of 5 microns.

2.2. DNA isolation and genomic DNA PCR

Approximately 5 mm portions of tail were boiled in 50 mM NaOH until fully dissolved. 1 M Tris was added to neutralize the NaOH. Following centrifugation to remove insoluble material, DNA was precipitated from supernatants following standard ethanol precipitation guidelines. In the case of purified cells, DNA was extracted using the Qiagen DNeasy Blood and Tissue Kit. *Snai2*, *Snai3* and *Vav-Cre* genotyping was performed with Thermo Scientific *Taq* DNA Polymerase (Cat. #: FEREP0402) using 2 μL of DNA per reaction. Products were electrophoresed in 2% agarose gels. When quantification was necessary, PCR was performed via incorporation of [^{32}P] deoxycytidine triphosphate. Products were electrophoresed in polyacrylamide sequencing gels. Products were visualized after exposure to X-ray film at −80 °C or PhosphorImager plates at room temperature. Cycling parameters are available upon request. Primer sequences are provided in Supplementary Table 1.

2.3. RNA isolation, cDNA synthesis and RT-PCR

Total RNA was isolated from cells using the Qiagen miRNeasy Mini Kit (Cat. #: 217004) according to the manufacturer's instructions. Random hexamer primers (Invitrogen, Cat. #: 58875) were used in combination with SuperScript III Reverse Transcriptase (Invitrogen, Cat. #: 56575) to synthesize cDNA. Reactions were purified using the Thermo Scientific GeneJET Purification Kit (Cat. #: K0702). Quantitative RT-PCR was performed using Light Cycler (Roche Diagnostics) technology. All transcript values shown are relative to *Actb* expression within the same sample and are mean values ± standard error measurement (SEM). Cycling parameters are available upon request. Primer sequences are provided in Supplementary Table 1.

2.4. FACS analysis and sorting of hematopoietic cell populations

Upon dissection, the plunger of a 5 mL syringe was used to dissociate thymus and spleen tissues. Cells were strained through a 100 μM filter and collected in 10 mL of FACS buffer (1× PBS + 0.1% BSA). Bone marrow was collected from both femurs and tibias. Removing the ends of each bone with a razor blade exposed bone cavities. Marrow was flushed from cavities using a 25$^{5/8}$G syringe and FACS buffer. Contents were collected in 5 mL of FACS buffer. After centrifugation, erythrocytes were lysed on ice for 10 min using ACK buffer. Following lysis, cells were respun, resuspended in FACS buffer and counted using a Hemoctyometer. Cells were stained on ice for 30 min using the appropriate antibody cocktail. Samples were washed with FACS buffer, centrifuged and resuspended in FACS buffer. To discriminate between live and dead cells, 4′,6-diamidino-2-phenylindole (DAPI) was added at a final concentration of 3 μM. For intracellular staining, cells were processed using the BioLegend Nuclear Factor Fixation and Permeabilization Buffer Set (Cat. #: 422601) following the manufacturer's instructions. DAPI was not used for these samples. The antibodies utilized with their indicated dilutions are available in Supplementary Table 2. Population analysis was performed on the FACS Canto II (BD Biosciences) and results for a given cell type are graphically represented as mean values ± standard error measurement (SEM). Cell sorting of select populations was performed on the FacsAria Cell Sorter (BD Biosciences) at the University of Utah Flow Cytometry Core.

2.5. Thymocyte-based assay for autoantibody reactivity

Thymocytes were utilized as a substrate to proxy for systemic antibody-mediated autoreactivity. Organs were harvested from four-weeks-old C57BL/6 mice as described for FACS analysis and sorting of hematopoietic cell populations. Samples were split into two 15-mL conical tubes. One tube was resuspended in 5 mL of 4% PFA and fixed at room temperature for one hour. The other tube was resuspended in 5 mL of methanol (MeOH) at −20 °C for 1 h to fix and permeabilize cells. Following incubation, each tube was taken to 10 mL of volume with FACS buffer. Tubes were centrifuged at 1600 rpm (rpm) for 5 min at room temperature. Supernatants were aspirated and cells were washed once more with 10 mL of FACS buffer. The resultant cell pellets were resuspended in FACS buffer at a concentration of 10^7 cells per mL and stored at 4 °C until used.

Mouse blood was collected retro-orbitally in heparinized capillary tubes. Samples were centrifuged at ⩾13,000 rpm for 5 min at 4 °C. Plasma was transferred to 1.5-mL tubes at stored at −80 °C until further use. For each assay, plasma was pre-diluted 1:50 in FACS buffer. Plasma from *H2-O*$^{-/-}$ deficient animals served as a positive control. 10 μL of diluted plasma was mixed with 10^6 previously fixed thymocytes yielding a final sample dilution of 1:500

and incubated at room temperature for 30 min in 96-well plates. Wells were washed with 100 μL of FACS buffer and centrifuged at 2000 rpm for 5 min at 10 °C. A second wash was performed with 200 μL of FACS buffer. Samples were then resuspended in 100 μL of diluted fluorophore-conjugated secondary antibody and incubated for 30 min at room temperature. Wells were washed as above and samples were resuspended in 300 μL of FACS buffer/1% PFA for analysis on a FACS Canto II. "Intact" cells were gated on and the geometric mean fluorescence intensity (gMFI) was measured for each sample. Graphical representation of the data depicts the Autoreactivity Index (AI) for each sample (calculated as such: AI = sample gMFI/mean WT gMFI). The mean for a given genotype is represented by the middle horizontal bar while the standard error measurement (SEM) is indicated by the upper and lower horizontal bars. Animals were considered autoantibody positive with an AI $\geqslant 2$. The antibodies utilized with their indicated dilutions are available in Supplementary Table 2.

2.6. Immunofluorescence of mouse 3T3 fibroblasts

Mouse 3T3 fibroblasts were seeded at a density of 10^3 cells per well in 96-well plates and cultured in DMEM/10% FCS/1× Pen-Strep. The next day, media was removed and cells were fixed with 4% PFA for 20 min at room temperature. Cells were washed with 200 μL of 1× PBS and subsequently permeabilized with 1× PBS/αCD16 + 32/0.5% BSA/0.25% Triton X-100 for 30 min at room temperature then washed 2 times with 1× PBS. Plasma samples were diluted 1:500 in 1× PBS/αCD16 + 32/0.5% BSA and directly applied to cells for 30 min at room temperature. Plasma from *H2-O*$^{-/-}$ deficient animals served as a positive control. Cells were washed 2 times with 1× PBS and then incubated with fluorophore-conjugated antibody diluted in 1× PBS/0.5% BSA for 30 min at room temperature. Following incubation, cells were washed as above and stained with 1× PBS/DAPI (3 μM) to demarcate nuclei. Cells were washed once more with 1× PBS then visualized and recorded with a camera-mounted Olympus BX 51 microscope. The antibodies utilized with their indicated dilutions are available in Supplementary Table 2.

2.7. Thymocyte-based plasma western blot

Thymocytes from four-weeks-old C57BL/6 mice were harvested as described in FACS analysis and sorting of hematopoietic cell populations. After cell counting, cells were washed twice with 1× PBS to remove any residual BSA from FACS buffer. Pellets were resuspended in RIPA (25 mM Tris ph 7.5, 50 mM NaCl, 1 mM EDTA, 0.1% SDS, 1% DOC, 1% NP-40) at a concentration of 10^6 cells per 10 μL. Protease inhibitors (Roche, Cat. #: 04 693 132 001) were included to prevent degradation of samples. Cells suspensions were incubated on ice for 20–30 min and insoluble material was pelleted via a 15 min, $\geqslant$13,000 rpm centrifugation at 4 °C. Supernatants were collected as whole cell lysates and stored at −80 °C until further use. The protein equivalent of 10^7 total thymocytes was electrophoresed in 1.5 mm, 2D-well, NuPage 4–12% Bis-Tris gels (Invitrogen, Cat. #: NP0337BOX) using 1× MOPS SDS–PAGE running buffer (Invitrogen, Cat. #: NP0001). Following separation, protein was transferred to PVDF membranes. Membranes were stained with 0.1% Ponceau S/1% glacial acetic acid to verify equivalent protein distribution across the entirety of the membrane. Blots were washed at 5-min intervals, 4 times with 1× TBS/0.2% Tween-20 at room temperature. Following complete removal of Ponceau staining, membranes were blocked for one hour at room temperature with 1× TBS/0.2% Tween-20/5% BSA. Membranes were then positioned in the Mini-Protean II Multi Screen chamber from Bio-Rad (Cat. #: 170-4017). This allowed for the simultaneous screening of multiple plasma samples on the same lysate without introducing gel-to-gel variation. Plasma sample from C57BL/6 and *Snai2*/*Snai3* cDKO mice were diluted 1:500 in 1× TBS/0.2% Tween-20/5% BSA and applied to each chamber of the slot blot device. Plasma from *H2-O*$^{-/-}$ deficient animals served as a positive control. Following room temperature incubation for 2 h, blots were washed at 5-min intervals, 5 times with 1× TBS/0.2% Tween-20 at room temperature. Membranes were incubated with the appropriate secondary antibody diluted in 1× TBS/0.2% Tween-20/5% BSA for two hours at room temperature (see Supplementary Table 2 for antibody details). Membranes were washed as above and further rinsed 1 time with 1× TBS for 5 min at room temperature. Blots were incubated with an appropriate amount of chemi-illuminescence reagent (Thermo Scientific, Cat. #: 34080) to ensure full coverage. After 5 min at room temperature, membranes were blotted on a paper towel to remove excess reagent, wrapped in plastic wrap and exposed to film to detect reactive self-antigens.

2.8. Enzyme-linked immunosorbent assay (ELISA)

Immulon 4HBX microtiter plates (Thermo Scientific, Cat. #: 3855) were incubated with αIgG + IgM + IgA capture antibody diluted to 5 μg/mL in 100 mM Carbonate buffer overnight at 4 °C. The next day, plates were washed 3 times with 1× PBS/0.1% Tween-20 and then blocked for 1.5 h at room temperature with 1× PBS/0.1% Tween-20/1% BSA. Plates were washed again and 100 μL of plasma sample or immunoglobulin-specific standard were added to each well (diluted in 1× PBS/0.1% Tween-20/1% BSA). Following a 1.5-h incubation, plates were washed as above. Immunoglobulin-specific secondary antibodies (diluted in 1× PBS/1% BSA) were added to each well and plates were incubated for an additional 1.5 h. Following six consecutive washes with 1× PBS/0.1% Tween-20, wells were incubated as needed with 100 μL Developing Solution (0.33 μL of 30% hydrogen peroxide (H_2O_2) and 8.8 μg of *o*-Phenylenediamine dihydrochloride (OPD) per 20 mL of Citrate buffer). Developing reactions were stopped with the addition of 100 μL of 1 N HCl. Absorbance for each well was recorded at 490 nm by a Synergy H1 microplate reader (Bio Tek). Standard curves were generated in Microsoft Office Excel and fitted with a logarithmic trend line. Plasma sample dilutions that fell within standard curves were used to calculate antibody titers for each isotype assayed. Isotype standards included mouse IgM (eBioscience, Clone 11E10), IgG1 (Invitrogen, Cat. #: 026100), IgG2b (eBioscience, Clone eBMG2b), IgG2c (Southern Biotech, Cat. #: 0122-01) and IgG3 (eBioscience, Cat. #: 14-4742-85). Details about antibody usage are available in Supplementary Table 2.

2.9. Immunofluorescence of frozen skin and thymus sections

Dorsal (back) skin and thymus were harvested and washed briefly in 1× PBS. Tissue was immersed in 4% PFA at 4 °C for a minimum of 72 h. Following fixation, tissue was washed at 5-min intervals for 5 times with 1× PBS at room temperature. Samples were embedded in OCT compound (Tissue-Tek) on dry ice and then sectioned to an approximate thickness of 10 μM using a Microm HM 505N cryostat (Mikron Instruments). To evaluate morphology, sections were stained with hematoxylin and eosin using standard methodology. For immunofluorescence, sections were post-fixed to slides with 4% PFA at room temperature for 10 min. Slides were washed at 5-min intervals for 3 times with 1× PBS at room temperature. Endogenous tissue autofluorescence was quenched via 0.1% Sudan Black B/70% EtOH staining for 20 min at room temperature. If necessary, sections were permeabilized with a 10-min incubation in 1× PBS/0.5% BSA/0.25% Triton X-100. Slides were washed at 5-min intervals for 3 times with 1× PBS/0.2% Tween-20 at room temperature. Sections were blocked for 1 h at room temperature with 1× PBS/0.2% Tween-20/αCD16 + 32/1%

BSA (Blocking Buffer). Tissue sections were stained with the appropriate fluorophore-conjugated antibody (diluted in Blocking Buffer) at room temperature for 1 h in an enclosed humidity chamber. Slides were washed at 5-min intervals for 3 times with 1× PBS/0.2% Tween-20 at room temperature. To visualize nuclei, tissue sections were incubated for 5 min at room temperature with 1× PBS/DAPI (3 μM). Excess DAPI solution was removed by a one-time wash with 1× PBS/0.2% Tween-20. Stained sections were mounted with Image-iT FX signal enhancer (Invitrogen, Cat. #: I36933). Images were visualized and recorded with a camera-mounted Olympus BX 51 microscope. The antibodies utilized with their indicated dilutions are available in Supplementary Table 2.

2.10. Regulatory T cell (T_{Reg}) adoptive transfer

Spleens were excised from Foxp3–GFP reporter mice approximating two months of age. Following erythrocyte lysis, B cells were depleted using CD45R (B220) Microbeads (Miltenyi Biotec, Cat. #: 130-049-501). T_{Regs} were FACS-sorted based on forward scatter (FSC), side scatter (SSC) and GFP positivity. Cells were washed with 1× PBS and resuspended at a final concentration of 7.5×10^4 cells per 100 μL. 7.5×10^4 cells were delivered retro-orbitally (r.o.) to 21-day-old C57BL/6 and *Snai2*/*Snai3* cDKO recipients. As a negative control, a group of cDKO animals were left untransferred. Animals were monitored out to 60 days of total lifespan. Bodyweight was measured over the first 4 weeks post-transfer and plasma samples were collected at four weeks post-transfer. At the completion of the each experiment, WT and cDKO animals were euthanized and analyzed via FACS.

2.11. Bone marrow transplantation

One day prior to transplantation, 8–12 weeks old *Rag2*$^{-/-}$ or WT recipient mice were lethally irradiated with two doses of 500 cGy split 6 h apart. WT and cDKO bone marrow was isolated from pooled tibias and femurs. Samples were lineage depleted using the mouse-specific Lineage Depletion Kit from Miltenyi (Cat. #: 130-090-858). Isolated progenitors were washed and resuspended in 1× PBS at a concentration of 1×10^6 cells/mL. A total of 1×10^5 cells (100 μL) were delivered r.o. to each recipient animal. Three WT and three cDKO donors were used to transplant five and seven *Rag2*$^{-/-}$ mice, respectively. Two WT and two cDKO donors were used to transplant two WT mice apiece. Animals were maintained on Sulfamethoxazole and Trimethoprim antibiotic-treated water for the duration of all experiments. Post-transplant, animals were periodically analyzed for systemic autoantibodies as described in Section 2.5. Animals with multiple autoantibody subtypes or persistent autoantibodies (2 consecutive positive tests for a particular autoantibody subtype) were euthanized and analyzed at time of presentation. Otherwise, all animals were analyzed nine (*Rag2*$^{-/-}$) or twelve (WT) weeks post-transplant.

2.12. Statistical analysis

Using Prism GraphPad software, two-tailed unpaired Student's *t*-tests were applied for all RT-PCR, body/organ mass measurements, FACS-based cell population analysis and ELISA experiments. Thymocyte autoantibody experiments were analyzed using the Mann–Whitney test. Kaplan–Meier survival analysis using the Mantel-Cox log-rank test was applied to the T_{Reg} adoptive transfer experiments. Fisher's exact test was used to compare autoantibody occurrence rates. Statistical cutoffs are described in the figure legends.

3. Results

3.1. Generation of the *Snai2*$^{-/-}$ *Snai3*$^{Fl/Fl}$ *Vav-Cre conditional double knockout (cDKO)*

Our previous study identified a functional redundancy for *Snai2* and *Snai3* in lymphocyte development [20]. That analysis used a germline deletion of both gene products such that loss of both Snail gene products in the stromal cells could potentially influence T and B cell development. Currently, there only exists a germline deletion allele of *Snai2* (g2KO). Therefore, we bred *Snai2*$^{-/-}$ animals to mice possessing a LoxP-targeted allele of *Snai3* (*Snai3*$^{Fl/Fl}$) [20]. The progeny of this cross were further bred to animals expressing the *Vav-Cre* transgene allowing for the conditional deletion of *Snai3* within the hematopoietic lineages. This animal will be referred to as the *Snai2*/*Snai3* conditional DKO (cDKO) throughout the text. Analysis of genomic DNA isolated from the tail, bone marrow and thymus of the cDKO demonstrated appropriate deletion of the *Snai3*$^{Fl/Fl}$ allele in the cells of the bone marrow and thymus (Supplementary Fig. 1). Unexpectedly, the *Snai2*/*Snai3* cDKO animals demonstrated a severe runting compared to WT littermates (Fig. 1A) that was evident post natal. Overall, the cDKO animals were approximately half the body mass of WT littermates (Fig. 1B). Additionally within the pre-weaning period (<21 days of age), cDKO animals consistently developed severe alopecia and dermatitis. This "pathology" was not apparent in the previously studied gDKO model [20]. Macroscopic analysis of hematopoietic tissues such as the bone marrow, spleen and thymus showed no gross abnormalities aside from an overall reduction in mass (DNS). Histological cross sections of thymus samples taken from the cDKO animals (3 weeks of age) displayed a lack of normal cortex to medulla organization when examined by hematoxylin and eosin (H&E) staining (Fig. 1C). However, immunofluorescence staining for MHC II (cortical and medullary epithelium) and AIRE (medullary epithelium) was normal in the cDKO thymus (Supplementary Fig. 2) [21]. This suggested that the abnormal H&E staining pattern in the cDKO thymus was not due to an inability of mature thymic epithelium to develop. Additionally, H&E staining of the spleen revealed severely disorganized lymphoid follicles in cDKO samples (Fig. 1D). Analysis of bone marrow cellularity demonstrated that the cDKO had an approximately 50% reduction in total cells (Supplementary Fig. 3A). Analysis of the thymus showed a reduction in cDKO thymic mass relative to overall body mass (Supplementary Fig. 3B). Furthermore, the cDKO thymus had less cell density compared to all other genotypes. Relative splenic mass was normal in the cDKO animals however the cDKO spleen demonstrated a reduced cell density (Supplementary Fig. 3C).

3.2. Snai1,2,3 gene expression in developing lymphocytes

Previously we transcriptionally profiled the expression patterns of *Snai1*, *Snai2* and *Snai3* in hematopoietic cells delineated by fluorescence-activated cell sorting (FACS) with the CD4, CD8, B220 and CD11b surface markers [20]. This analysis demonstrated that multiple Snail genes were expressed within a given cell type. To further clarify Snail gene expression profiles in lymphocyte precursors, we FACS sorted pre-Pro B cell progenitors ($CD11b^-$ $CD19^-$ $B220^+$) and B cell subsets at various stages of maturation from the bone marrow and spleen [22]. Transcriptional analysis of isolated RNA demonstrated that *Snai1* was expressed by all marrow and splenic B cell subsets with specific points of enrichment at the pre-Pro, newly formed (NF), marginal zone (MZ) and follicular (FO) B cell stages (Supplementary Fig. 4A). In contrast, *Snai2* was restricted in expression pattern being detectable only in pre-Pro, Pre and NF B cells (Supplementary Fig. 4B). *Snai3* demonstrated a

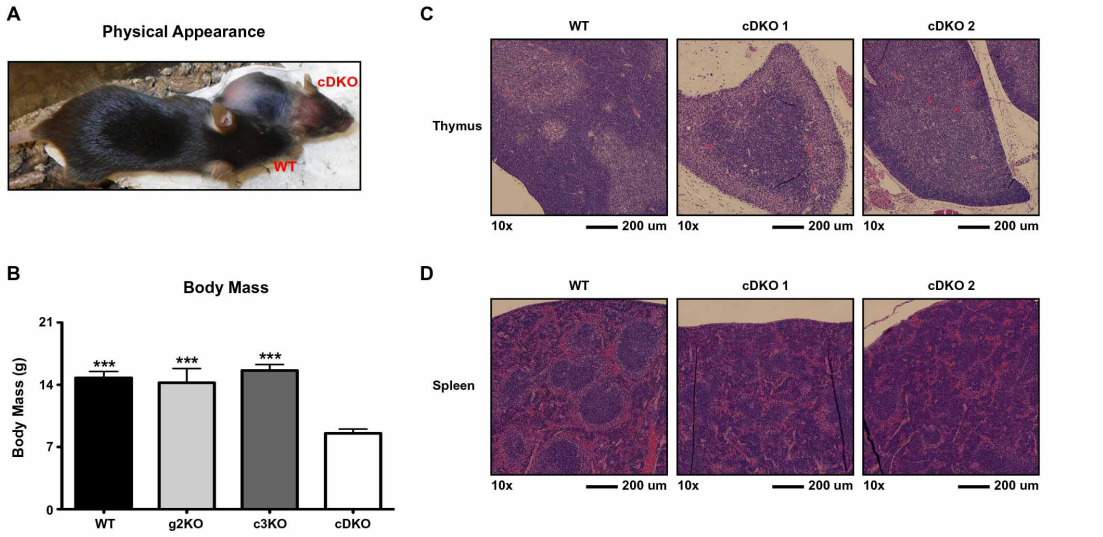

Fig. 1. Germline deletion of *Snai2* in conjunction with the hematopoietic specific deletion of *Snai3* results in a failure to thrive combined with reduced hematopoietic output. (A) Representative image depicting three-week-old sex-matched wildtype (WT) and *Snai2*/*Snai3* conditional double knockout (cDKO) littermates. The cDKO animals are consistently runted and present with alopecia and dermatitis. (B) Body mass comparisons of wildtype WT, *Snai2* germline knockout (g2KO), *Snai3* conditional knockout (c3KO) and cDKO mice. Number of animals per group: WT = 13, g2KO = 4, c3KO = 6, cDKO = 10. Histological H&E staining of paraffin embedded cross sections of thymus (C) and spleen (D) from WT and two different cDKO animals. Images were captured at 10× magnification and scale bars represent 200 microns.

highly overlapping pattern of expression as compared to *Snai1* (Supplementary Fig. 4A versus 4C).

All three Snail members have been shown to be expressed during various stages of T cell development [20]. The thymic double negative (DN) population contains a heterogeneous collection of cells: T cell progenitors (early thymic progenitors, ETP), uncommitted (DN1-2) and committed (DN3-4) maturing T cells. We FACS sorted the DN compartment into stages one through four and transcriptionally profiled each population for Snail gene expression. *Snai1* was expressed at low levels at the stages proceeding T cell commitment (DN1-2) with significantly increased expression at the DN3-4 stages marking T cell commitment (Supplementary Fig. 4D). *Snai2* was expressed in all double negative stages at relatively equivalent levels (Supplementary Fig. 4E). The *Snai3* expression pattern of double negative thymocytes highly overlapped with *Snai1* (Supplementary Fig. 4D versus 4F).

3.3. Impaired generation of B and T lymphocytes in the Snai2/Snai3 cDKO

Given the reduced cellular output from primary lymphoid organs, we examined at what stage(s) of hematopoietic development these deficiencies were occurring. To do this, we initially evaluated lineage negative (Lin^-) hematopoietic progenitors in the marrow that were further subdivided into Sca-$1^{+/-}$ populations and further analyzed using c-Kit and L-selectin (CD62L) (Supplementary Fig. 5A) [23,24]. All genotypes demonstrated equivalent numbers of Lin^- cells (Supplementary Fig. 5B, left). Subdivision of Sca-1^+ cells into the most primitive progenitor (c-Kit^+ $CD62L^-$) and lymphoid-primed multipotent progenitor (LMPP) (c-Kit^+ $CD62L^+$) containing fractions also displayed no apparent differences (Supplementary Fig. 5B, middle). Cell numbers of the less well-defined Sca-1^- c-Kit^+ $CD62L^{+/-}$ populations were equivalent between all four genotypes as well (Supplementary Fig. 5B, right). This data suggested that reduced hematopoietic output of cDKO mice was not due to a hematopoietic progenitor defect.

Next we examined the bone marrow for generation of myeloid and B cell lineages (Supplementary Fig. 5C). The number of myeloid-derived cells such as monocytes ($CD11b^+$ Gr-$1^{INT/-}$) and neutrophils (PMN, $CD11b^+$ Cr-1^{HI}) were reduced 30% in the cDKO animals compared to WT and single knockouts (Supplementary Fig. 5D). However, the B cell lineage showed a greater degree of impairment with pre-Pro B ($B220^+$ $CD19^-$) and committed B cells ($B220^+$ $CD19^+$) reduced by 43% and 67%, respectively (Supplementary Fig. 5D). Although, pre-Pro B cells were reduced, the greatest loss of B cells came within the committed B cell lineage ($CD19^+$).

The loss in B cells was further quantified by an assessment of the various stages of bone marrow B cell development in the cDKO mouse. Marrow B cells were divided into immature ($CD19^+$ $AA4.1^+$) and mature recirculating ($CD19^+$ $AA4.1^-$) subpopulations (Supplementary Fig. 6A). As shown in Supplementary Fig. 6B, AA4.1 and CD22 demarcated separate populations of B cells in both WT and cDKO animals. $CD19^+$ $AA4.1^+$ immature B cells were further subdivided into Pro ($CD43^+$ surface IgM^-), Pre ($CD43^-$ surface IgM^-) and NF ($CD43^-$ surface IgM^+) stages of maturation (Supplementary Fig. 6A). Quantification of these subsets demonstrated equivalent production between WT, g2KO and c3KO genotypes, which was in stark contrast to the cDKO (Fig. 2A). Similar to the pre-Pro stage, cDKO Pro B cell numbers were reduced by 40% compared to WT while the production of Pre B cells was impaired by 76% in the cDKO. This decrease was similar in magnitude at the NF stage of B cell development (81% reduction). These data identified the Pre B cell stage as the major point of constriction within the B cell lineage.

We then determined if the loss of Snai2 and Snai3 could alter the production of mature splenic B cell populations with mature follicular and marginal zone phenotypes (Fig. 2B). B cells were gated for CD19 expression and further subdivided into immature ($AA4.1^+$) and mature ($AA4.1^-$) subsets. Immature B cells were divided into Transitional 1 (T1, $CD23^-$ IgM^+) and Transitional 2 (T2, $CD23^+$ IgM^+) subsets. Mature B cells were subdivided into follicular (FO, IgD^{HI} IgM^{INT}) and marginal zone (MZ, IgD^{INT} IgM^{HI})

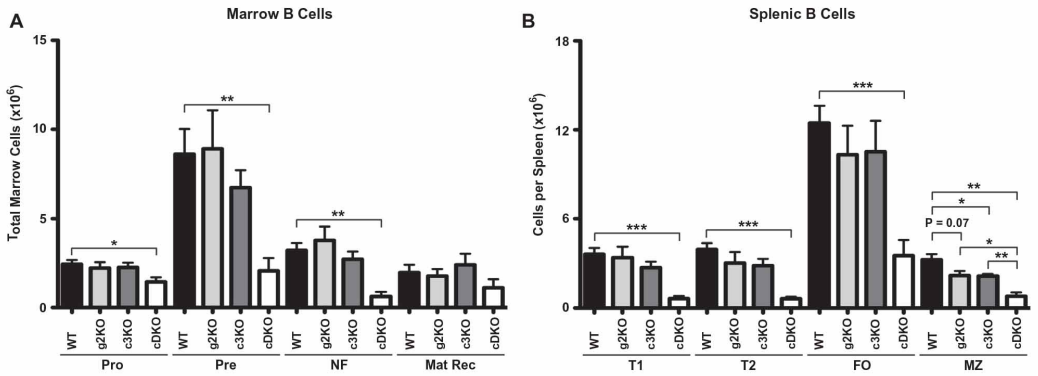

Fig. 2. Deletion of *Snai2* and *Snai3* significantly impairs B cell generation. (A) Quantification of marrow B cell subsets as described in Supplemental Fig. 4. (B) Quantification of splenic B cell subsets as described in Supplemental Fig. 4. Total cell numbers of a given population are displayed for all four genotypes. Bars represent mean ± SEM. Number of animals per group: WT = 5, g2KO = 4, c3KO = 4, cDKO = 4; Statistical comparisons: $^{*}P \leqslant 0.05$, $^{**}P \leqslant 0.01$, $^{***}P \leqslant 0.001$.

subsets (Supplementary Fig. 6C). Comparison of the various genotypes demonstrated a continued B cell pipeline defect in the cDKO as all subsets analyzed were significantly reduced. Of note, g2KO and c3KO single knockout animals both demonstrated similar reductions within the marginal zone compartment (33% decrease).

As shown in Supplementary Fig. 3B, the cDKO animals demonstrated impaired generation of the T cell lineage. Examination of early thymic progenitors ($CD44^{+}$ $CD25^{-}$ c-Kit^{HI}) demonstrated a 95% reduction of these cells in the cDKO thymus (Fig. 3A–C) as compared to WT animals. The cDKO animals also demonstrated severe reductions in all of the thymic DN1-4 compartments (Fig. 3D). The greatest deficiencies were seen earliest in T lineage maturation with DN1 reduced by 88%, DN2 by 78%, DN3 by 66% and DN4 by 56%. CD4 and CD8 surface markers were used to differentiate between CD4 and CD8 double positive (DP), CD4 single positive (CD4SP) and CD8 single positive (CD8SP) thymocytes (Fig. 3E). The cDKO had significant reductions in DP (86%), CD4SP (91%) and CD8SP (86%) populations as compared to WT (Fig. 3F). Similar to B cells, we examined peripheral T cells in the spleen to determine any obvious differences in the persistence of CD4SP and CD8SP T cells upon emigration from the thymus (Fig. 3G). Both CD4SP and CD8SP splenic populations were significantly reduced in the cDKO (Fig. 3H, 72% and 58%).

3.4. Snai2 and Snai3 cDKO animals generate systemic autoimmunity

The above data demonstrated obvious lymphopoietic defects in the *Snai2*/*Snai3* cDKO that were evident in the first days of life. The lack of lymphocytes alone, however, would not account for the evident "failure to thrive" phenotype of the cDKO. Instead the cDKO animals closely paralleled the phenotype of acute autoimmunity similar to that seen for the *Scurfy* mice, which are deficient for T_{Reg} generation [25].

To test determine if the cDKO animals had evidence of autoimmunity, we utilized a FACS-based assay using WT thymocytes as the source of self-antigen. Thymocytes were incubated with plasma from various animals and bound autoreactive antibodies are detected with fluorophore-conjugated anti-IgM and anti-IgG. Representative histograms demonstrating positive results for cDKO autoreactivity to permeabilized thymocyte antigens are shown for IgM (Fig. 4A, left) and IgG (Fig. 4B, left). In both instances, clear increases in fluorescence intensity (autoantibody binding) are observable in the cDKO samples as compared to all other genotypes. To quantify these results, the geometric mean fluorescence intensity (gMFI) for each individual sample was normalized to the mean WT gMFI to derive the Autoreactivity Index (AI) per each sample. An AI $\geqslant 2$ was required for an animal to be considered as having a particular subtype of autoantibody (AA). Quantification of IgM reactivity to total cellular antigens (permeabilized cells) is presented in the middle panel of Fig. 4A. Six of eleven cDKO animals possessed IgM autoantibodies (AA) by three weeks of age. When we skewed the analysis to examine IgM autoantibodies to surface antigens, eight of eleven cDKOs tested positive (Fig. 4A, right). Importantly, both single knockouts were normal. IgM AA are indicative of a loss of B cell tolerance as previously shown in various autoimmune models [25,26].

Next, we analyzed the generation of IgG AA, an indicator of a break in T cell tolerance [27]. Our initial analysis of permeabilized cell reactivity showed that seven of eleven cDKO mice had circulating IgG AA (Fig. 4B, middle). Similar to IgM, the majority (seven of eleven) cDKO animals also had IgG AA reactive to surface antigens (Fig. 4B, right). Again, these results were specific to the deletion of both *Snai2* and *Snai3*. Overall, >80% of cDKO animals (nine of eleven) possessed detectable levels of circulating autoantibodies.

To evaluate B cell activity in the cDKO, we quantified Ig from the plasma of approximately three-week-old animals via enzyme-linked immunosorbent assay (ELISA). Analysis of thymus independent (TI) isotypes demonstrated increased production of both IgM and IgG3 by the cDKO (Fig. 4C, IgM mean titer: WT = 9.7 μg/mL, cDKO = 52.3 μg/mL; IgG3 mean titer: WT = 10.5 μg/mL, cDKO = 22.9 μg/mL). The c3KO also demonstrated a significant increase in IgM titers albeit not to the degree of the cDKO (IgM mean titer: c3KO = 26.6 μg/mL). Next we examined titers of thymus dependent (TD) Ig such as IgG1, IgG2b and IgG2c. For both IgG1 and IgG2c (Fig. 4D, left and right), the cDKO had equivalent titers to WT animals. However, IgG2b was significantly increased in the cDKO (Fig. 4D, middle, IgG2b mean titer: WT = 76.1 μg/mL, cDKO = 175.0 μg/mL). Interestingly, the c3KO showed a clear impairment in the generation of class-switched TD antibodies.

We then sought to characterize the autoantibodies generated by the cDKO to determine if they displayed nuclear and/or cytoplasmic reactivity. Fixed and permeabilized 3T3 fibroblasts were treated with cDKO and control plasma samples and analyzed by immunofluorescence microscopy (Fig. 5A). WT plasma served as a negative control. Plasma from *H2-O*$^{-/-}$ deficient animals served as a positive control: these animals have been shown to develop IgG2a autoantibodies specific for nuclear antigens due to defects in MHC II presentation [27]. cDKO plasma samples demonstrated

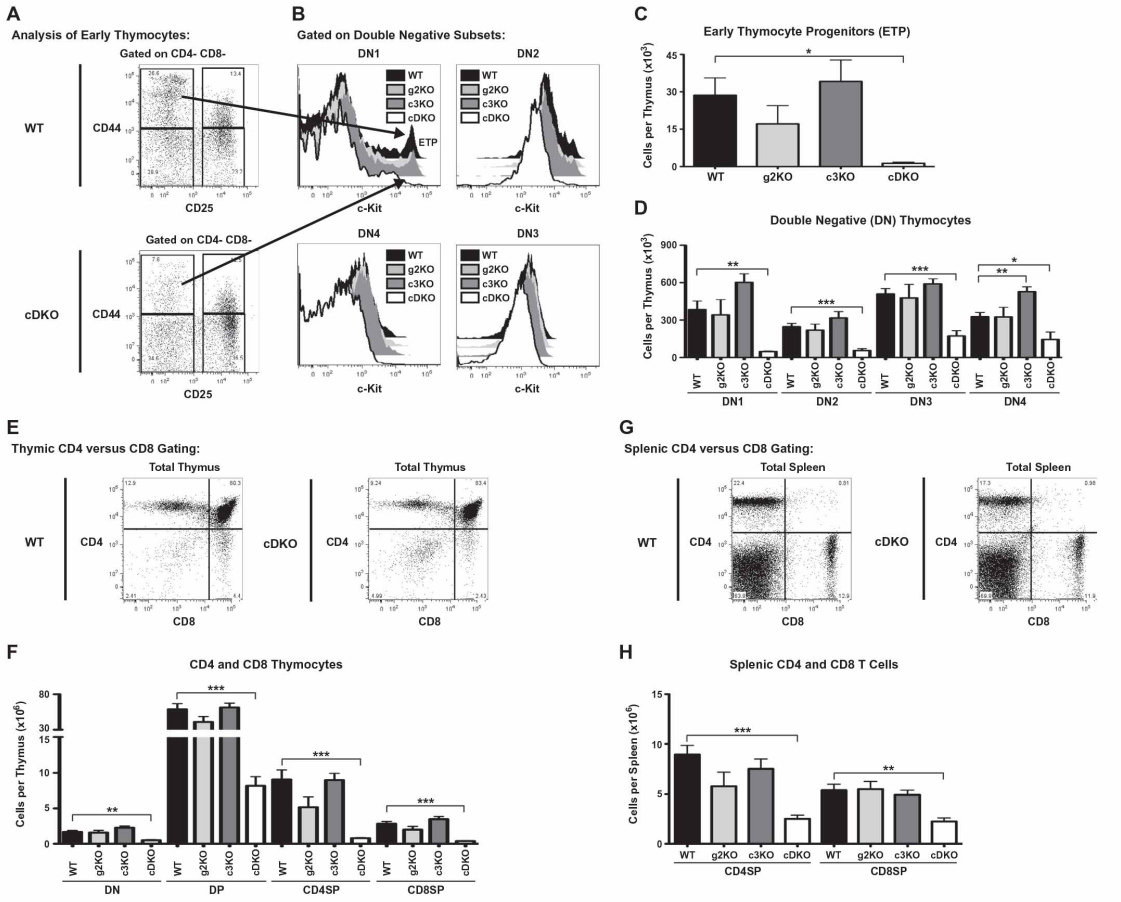

Fig. 3. Deletion of both *Snai2* and *Snai3* severely reduces early thymic progenitors (ETP) and subsequent generation of T cells. (A) Representative WT and cDKO FACS gating for the analysis of double negative thymocytes. Double Negative 1 (DN1): $CD44^{+}$ $CD25^{-}$; Double Negative 2 (DN2): $CD44^{+}$ $CD25^{+}$; Double Negative 3 (DN3): $CD44^{-}$ $CD25^{+}$; Double Negative 4 (DN4): $CD44^{-}$ $CD25^{-}$. (B) Representative histograms for all four genotypes demonstrating c-Kit fluorescence intensity within DN1-4 compartments. ETP can be identified within the DN1 compartment as the $c\text{-}Kit^{HI}$ peak (see arrow). Quantification of ETP (C) and DN1-4 (D) compartments within the thymus of three-week-old animals as outlined in A, B. Results are represented as total cells per thymus. (E) Representative WT and cDKO thymic analysis using CD4 and CD8 surface markers. (F) Quantification of the number CD4 and CD8 double negative (DN), CD4 and CD8 double positive (DP), CD4 single positive (CD4SP) and CD8 single positive (CD8SP) cells per thymus. (G) Representative gating of WT and cDKO animals depicted the analysis of CD4 and CD8 T cells. (H) Quantification of splenic CD4 and CD8 T cell numbers using the strategy depicted in G. (C, D, F and H) Bars represent mean ± SEM. Number of animals per group: WT = 5, g2KO = 4, c3KO = 4, cDKO = 4; Statistical comparisons: $^{*}P \leqslant 0.05$, $^{**}P \leqslant 0.01$, $^{***}P \leqslant 0.001$.

a diffuse pattern of IgM reactivity present in the cytoplasm with an apparent absence of nuclear staining (Fig. 5A). As expected, WT samples were devoid of reactivity. *H2-O*$^{-/-}$ animals displayed a similar pattern of IgM staining as the cDKO. Similar to IgM, cDKO IgG reactivity was clearly dominated by a commonly shared diffuse cytoplasmic staining (Fig. 5A). Again, WT samples displayed an absence of staining. In contrast, plasma from *H2-O*$^{-/-}$ animals demonstrated a high level of IgG nuclear reactivity (Fig. 5A).

Western blot analysis was used to simultaneously analyze the immunoreactive patterns of multiple cDKO samples against thymocyte whole cell extracts (Fig. 5B). The left panel of Fig. 5B displays results for IgM autoreactivity comparing six cDKO samples versus WT and *H2-O*$^{-/-}$ samples. As expected, the WT sample had very minor levels of reactivity while the *H2-O*$^{-/-}$ sample served as a definitive positive control (Fig. 5B, left, lanes W and H). All six cDKO samples displayed a varying degree of IgM autoreactivity representative of an oligoclonal response. Some cDKO samples displayed reactive bands unique to a particular sample; however, the majority of samples displayed an amount of shared antigenic reactivity based on molecular weight.

Next we analyzed IgG reactivity among the six cDKO samples. The WT plasma displayed very little IgG autoreactivity with the *H2-O*$^{-/-}$ sample, again, validating the assay (Fig. 5B, right, lanes W and H). Interestingly, cDKO samples displayed a much more limited repertoire of IgG reactive antigens as compared to IgM (Fig. 5B, left versus right, cDKO 1-6). The cDKO samples demonstrated some acquisition of IgG reactive antigens not present in the IgM analysis (Fig. 5B, left versus right, cDKO 3, ~68 kD). Additionally, there was the apparent expansion of dominant IgG secreting B cell clones in some animals (Fig. 5B, left versus right, cDKO 4, 38–40 kD). However, these types of events would not completely account for the dramatic reduction of diverse IgG autoreactivity when compared

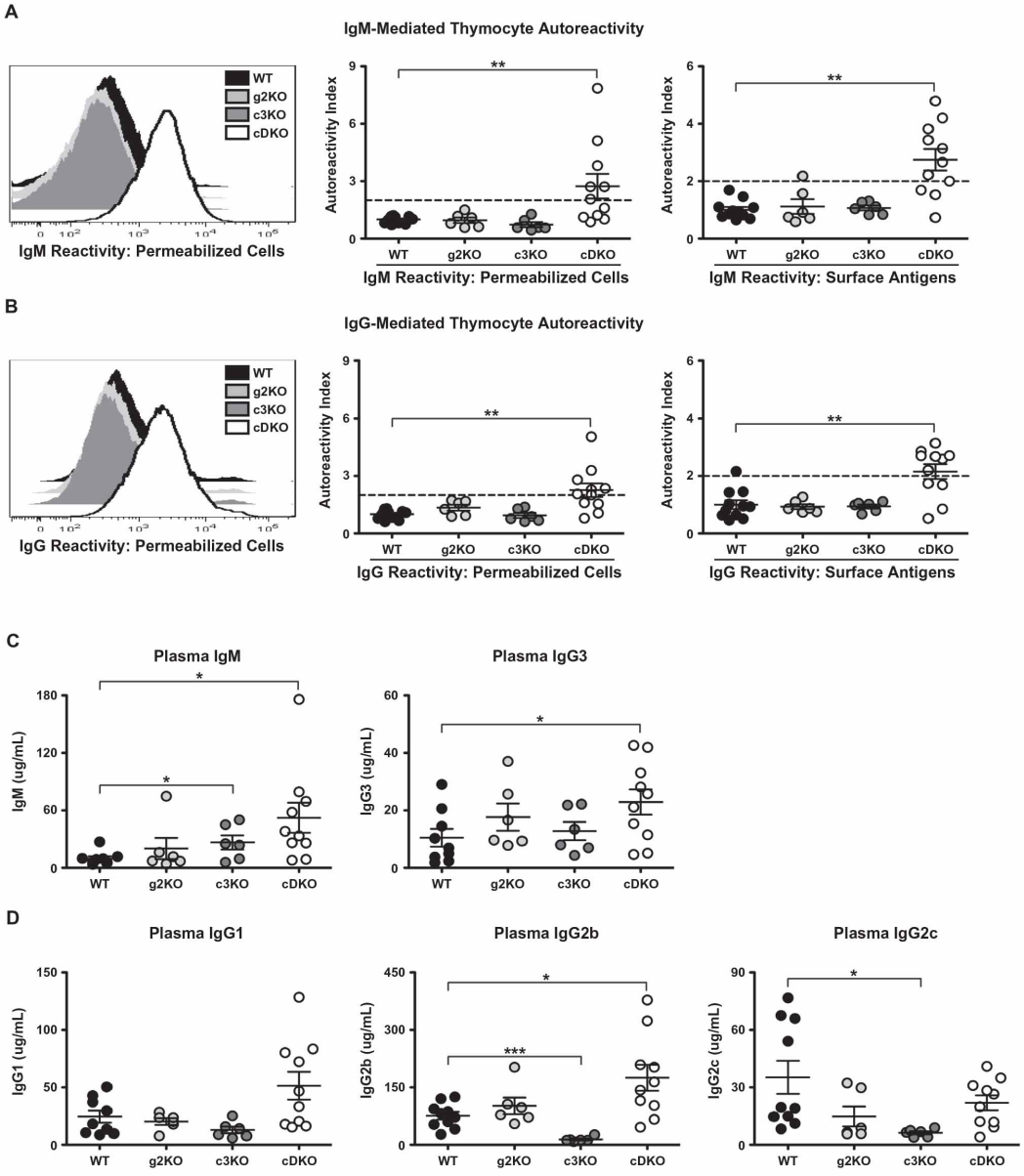

Fig. 4. cDKO animals have increased circulating immunoglobulins due to the presence of IgM and IgG autoantibodies. (A) Analysis of IgM autoantibodies generated by the cDKO. Representative histograms of IgM autoreactivity to permeabilized cell antigens (left). Quantified IgM reactivity towards permeabilized cell (middle) and surface antigens (right). (B) Analysis of IgG autoantibodies generated by the cDKO. Representative histograms of IgG autoreactivity to permeabilized cell antigens (left). Quantified IgG reactivity towards permeabilized cell (middle) and surface antigens, right. (A and B) Autoreactivity Index (AI) = gMFI per sample/mean WT gMFI, AI $\geqslant$ 2 (indicated by dotted line) is considered autoreactive; (C) Plasma titers of thymus independent isotypes. Total IgM (left) and total IgG3 (right) are depicted for WT, g2KO, c3KO and cDKO animals. (D) Plasma titers of thymus dependent isotypes. Data from all four genotypes is shown for IgG1 (left), IgG2b (middle) and IgG2c (right). (C and D) Number of animals per group: WT = 9–10, g2KO = 6, c3KO = 6, cDKO = 10. Number of animals per group: WT = 11–12, g2KO = 6, c3KO = 6, cDKO = 11 (A–D). The mean value per genotype is represented by the middle horizontal bar with SEM measured by upper and lower horizontal bars. Statistical comparisons: $^{*}P \leqslant 0.05$, $^{**}P \leqslant 0.01$, $^{***}P \leqslant 0.001$.

to IgM. The most likely factor contributing to the relative loss of diversified IgG reactivity would be a deficiency in T cell help.

The above *in vitro*-based assays clearly demonstrated that *Snai2*/*Snai3* cDKO mice generate autoantibodies. However, we were curious as to whether the generation of these autoantibodies could be correlated with any *in vivo* consequences. Presented in Fig. 1 was a representative three-week-old cDKO animal with severe alopecia and dermatitis. Histological examination of dorsal

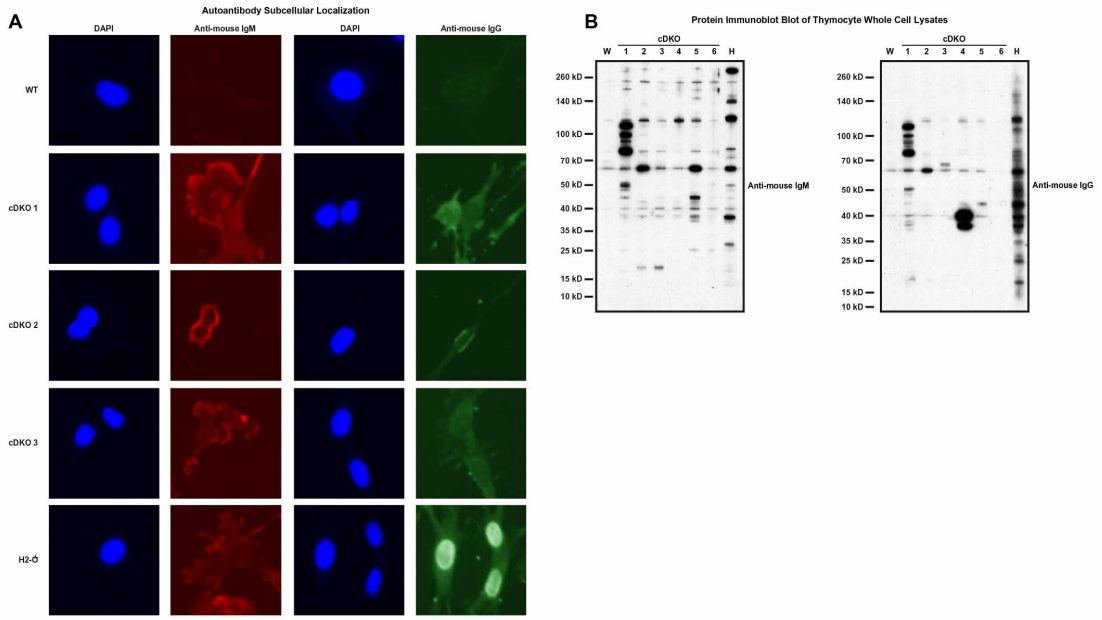

Fig. 5. cDKO autoantibodies are dominated by reactivity to cytoplasmic antigens. (A) Immunofluorescence microscopy demonstrating the subcellular localization of reactive autoantibodies in cDKO plasma. Columns 1 and 3 demarcate nuclei with 4′,6-diamidino-2-phenylindole (DAPI). Columns 2 and 4 show the detection of autoreactive IgM and IgG, respectively. Row 1 corresponds to a representative WT sample. Rows 2–4 present 3 individual cDKO replicates (cDKO 1–3). Row 5 shows staining with *H2-O*$^{-/-}$ plasma, a positive control for anti-nuclear IgG. (B) Western immunoblot analysis of thymocyte extracts examining IgM (left) and IgG (right) autoantibodies from six cDKO mice (cDKO 1–6). Molecular weights are indicated on the left side of each blot. W = WT; H = *H2-O*$^{-/-}$.

(back) skin from multiple cDKO mice demonstrated a varying range of abnormalities compared to WT animals (Fig. 6A). cDKOs 1 and 2 displayed an enhanced cellularity in the dermis. In conjunction with this, cDKO 1 also demonstrated an obvious thickening of the dermis, a phenomenon common to skin disorders such as dermatitis [28]. Overall, the dermal layer of cDKO 3 was normal. Examination of the epidermal layer of all three cDKOs showed what appeared to be a rough and ruffled outermost layer of skin with obvious thickening of the layer. In contrast, the skin of WT animals possessed a smooth appearance along the epidermal layer. As with the histological examination, deposition of IgM in the skin of cDKO animals demonstrated a graded level of staining (Fig. 6B). cDKO 1 displayed the highest level of bound IgM with a non-discriminating pattern of staining in both epidermal and dermal layers which may be due to reactivity to highly prevalent self-antigens similar to what has been observed in *Scurfy* mice[29,30]. cDKO 2 had moderate amounts of IgM reactivity in the dermis. The pattern of IgM reactivity for cDKO 2 was more focused with the most intense staining surrounding the sebaceous glands. Unlike both cDKO 1 and 2, cDKO 3 tested negative for IgM deposition.

Next we evaluated skin tissue for the deposition of IgG (Fig. 6C). Again, cDKO 1 demonstrated widespread staining of endogenous IgG to both epidermal and dermal layers. IgG staining for cDKO 2 was minimal and relatively similar to background levels seen with the WT sample. Interestingly, cDKO 3 skin samples had a high level of IgG deposition in both epidermal and dermal regions of the tissue, which was in direct contrast to the IgM staining. Finally, we analyzed the deposition of complement C3 that can be locally recruited through both IgM and IgG. As shown in Fig. 6D, C3 was most heavily deposited in cDKO 1. cDKO 2 showed a marginal amount of C3 and cDKO 3 was completely negative for complement activation when compared to WT. Overall, the level of C3 deposition correlated with the level of IgM deposition (cDKO 1 > cDKO 2 > cDKO3). The data clearly demonstrated that autoantibodies are functionally present in cDKO animals.

3.5. Snai2/Snai3 cDKO mice have reduced T_{Reg} generation and function

The sum of the phenotypes of the cDKO animals suggests they possess an autoimmune disease similar to that of immunodysregulation polyendocrinopathy enteropathy X-linked syndrome (IPEX) [31] which is caused by Foxp3 mutations that impair the generation and/or function of T_{Regs} [32]. Considering this, we analyzed WT, g2KO, c3KO and cDKO mice for the generation of natural, thymic derived (nT_{Reg}, Foxp3$^+$ Helios$^+$) and peripherally induced (iT_{Reg}, Foxp3$^+$ Helios$^-$) T_{Regs}. Representative WT and cDKO FACS plots from analysis of both thymus and spleen are shown in Fig. 7A. Percentage of T_{Regs} within the CD4$^+$ compartment of the thymus and spleen is shown in top panel of Fig. 7B and the quantification of absolute cell numbers is shown in the middle panel of Fig. 7B, and demonstrated a 94% reduction of thymic T_{Regs} compared to WT animals. Importantly, this numerical loss of T_{Regs} was not due solely to the global reduction in thymocyte generation as the percentage of cDKO T_{Regs} within the CD4$^+$ compartment was reduced by 35% when compared to WT. This result is suggestive of impaired differentiation into the cDKO T_{Reg} lineage or alternatively, impaired survival of those cells. In contrast, the g2KO had a non-significant trend towards reduced output while the c3KO completely phenocopied WT. The cDKO showed depressed numbers of peripheral T_{Regs} with nT_{Regs} reduced 63% and iT_{Regs} reduced 61% compared to WT.

It has previously been reported that reductions in Foxp3 protein levels can impair proper T_{Reg} function [33,34]. Analysis of the gMFI

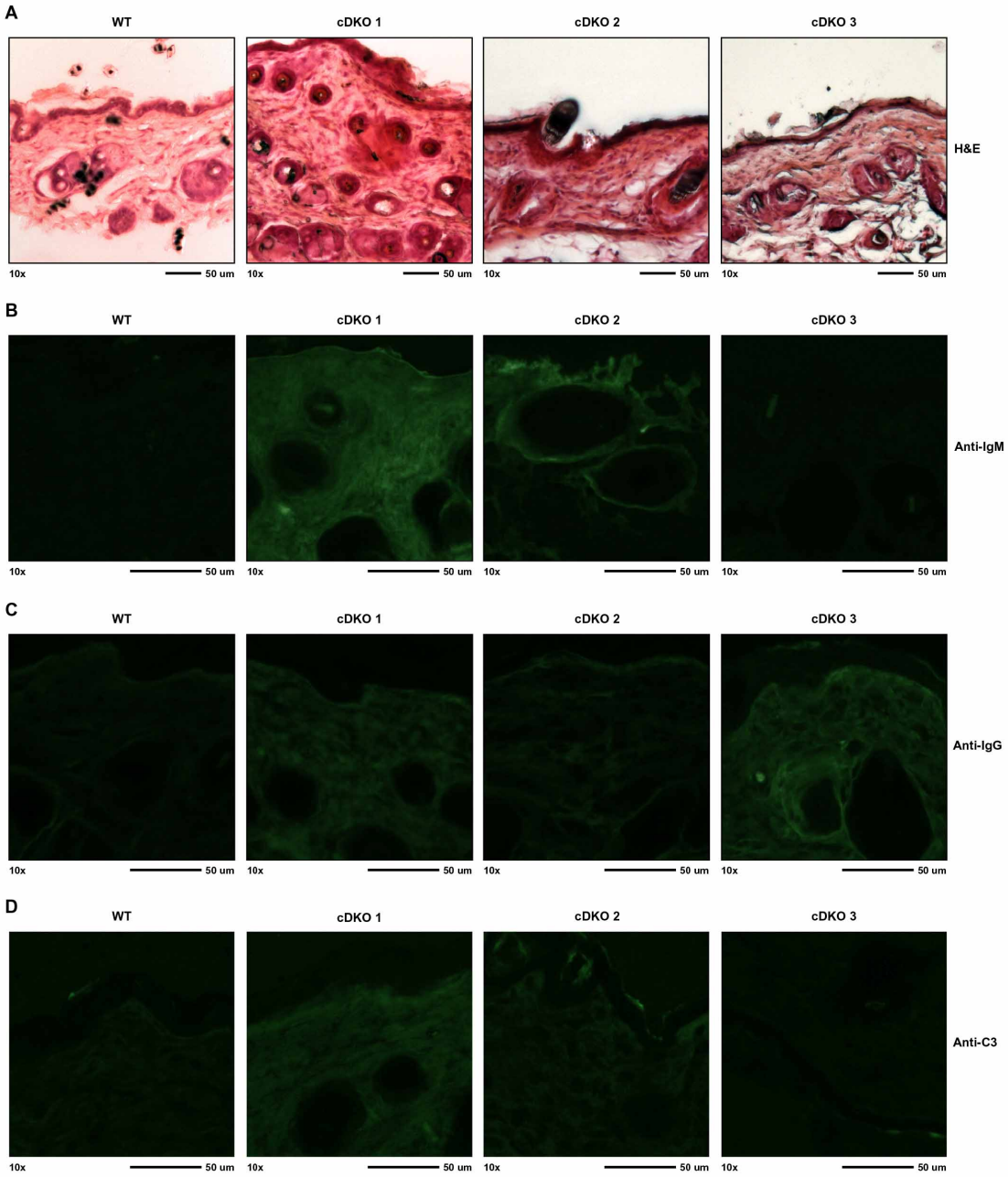

Fig. 6. Immune reactivity and pathology in the skin of the cDKO animals. (A) Hematoxylin and eosin (H&E) staining of frozen dorsal skin sections from one representative WT and three cDKO mice. (B–D) Immunofluorescence images demonstrating endogenous IgM (B), IgG (C) and complement C3 (D) deposition in skin samples from (A). Images were taken with a 10× objective and scale bars represent 50 μM.

from FACS data verified that Foxp3 protein was expressed at equivalent levels between all four genotypes (Fig. 7B, bottom panel). While the data do not answer the question of whether Foxp3 is properly regulating its gene targets, it does suggest that any T_{Reg} functional defect is independent of a dysregulated *Foxp3* gene locus. To further support a role for Snail family members as regulators of T_{Reg} function, we transcriptionally profiled T_{Regs} FACS-sorted from the thymus and spleen of Foxp3–GFP reporter mice

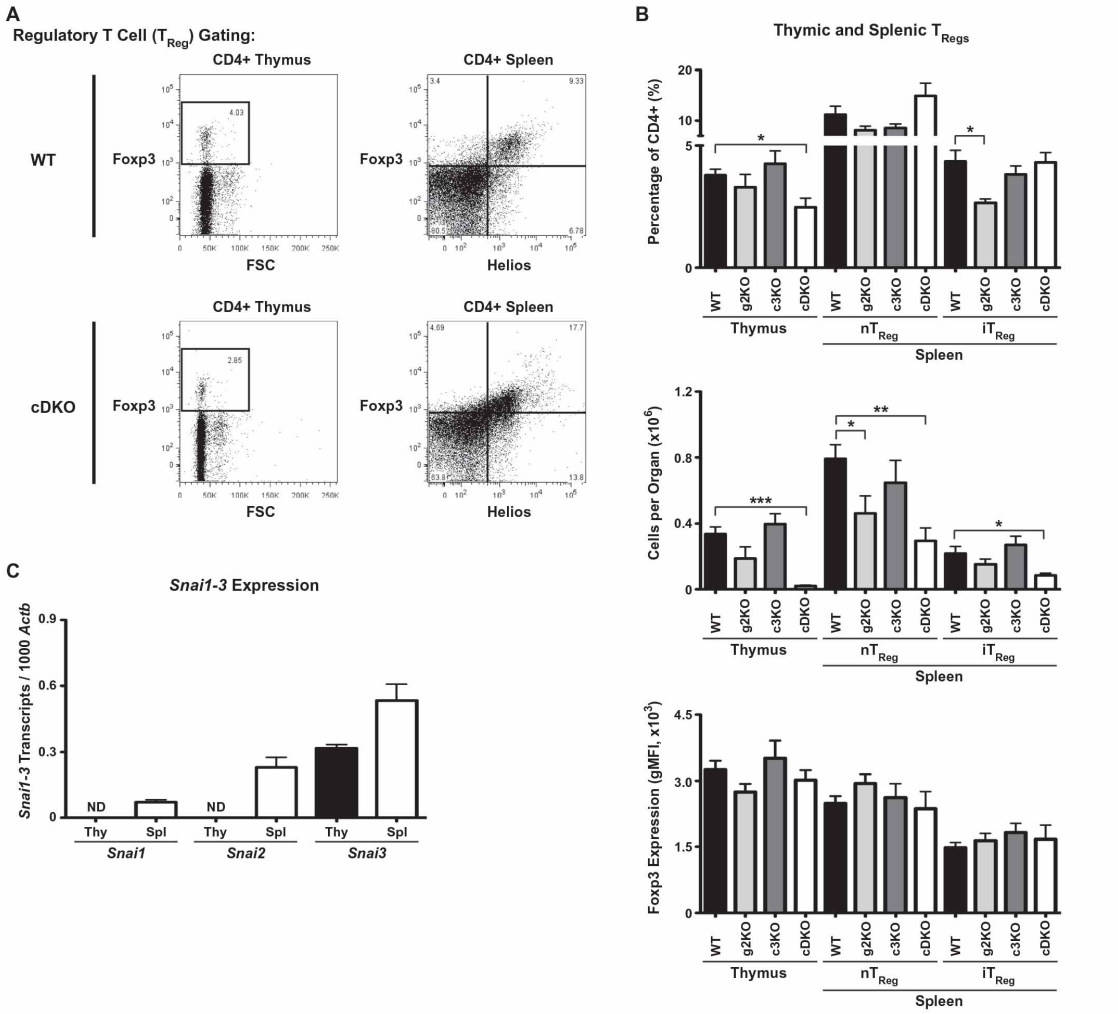

Fig. 7. T_{Regs} express Snail family members and are severely decreased in cDKO animals. (A) Representative WT and cDKO FACS gating of thymic (left) and splenic (right) T_{Regs}. $CD4^+$ T cells were gated as $Foxp3^+$ T_{Regs} in the thymus. In the spleen, $CD4^+$ T cells were divided into $Foxp3^+$ $Helios^+$ natural T_{Regs} (nT_{Reg}) and $Foxp3^+$ $Helios^-$ induced T_{Regs} (iT_{Reg}). (B) Quantification of T_{Regs} per category analyzed for all genotypes (top two panels). FACS-based quantification of Foxp3 gMFI for each T_{Reg} subset (bottom panel). Bars represent mean ± SEM. Number of animals per group: WT = 5, g2KO = 4, c3KO = 4, cDKO = 4; Statistical comparisons: $^*P \leqslant 0.05$, $^{**}P \leqslant 0.01$, $^{***}P \leqslant 0.001$ (C) Transcriptional analysis of Snail gene expression in thymic and splenic T_{Regs} isolated from Foxp3-GFP reporter mice. *Snai1*, *Snai2* and *Snai3* expression levels are depicted as transcripts per 1000 *Actb*. ND = not detected; Bars represent mean ± SEM. Three animals were analyzed per group.

(Fig. 7C). While *Snai3* was the only member expressed in thymic T_{Regs}, all three family members were present in splenic T_{Regs}.

To determine if the autoimmunity seen in the cDKO animals was due to defective T_{Regs}, we adoptively transferred 7.5×10^4 GFP^+ T_{Regs} isolated from the spleens of Foxp3–GFP reporter mice into 21 days old cDKO mice and monitored the recipients. For these experiments, a cohort of WT mice also received GFP^+ T_{Regs} to control for any procedural effects and a cohort of cDKO mice did not receive T_{Regs} to assess the lifespan of unmanipulated animals. Fig. 8A shows the outward appearance of a representative cDKO on the day of T_{Reg} transfer and the same animal 28 days after receiving WT T_{Regs}. It was clear that after receiving WT T_{Regs}, cDKO animals had reduced dermatitis and were able to regrow their hair. All unmanipulated cDKO animals succumbed to disease and died before reaching 30 days of age (Fig. 8B, red line). However, if given WT T_{Regs} at 21 days of age (Fig. 8B, downward arrow), cDKO animals achieved a significant extension of lifespan equivalent to that of WT animals (Fig. 8B, blue and black lines). During these experiments, two cDKOs that received WT T_{Regs} died at days twenty-three and twenty-four of age. Analysis of growth rates over a 4-week period following WT T_{Reg} transfer demonstrated that cDKOs receiving WT T_{Regs} were able to gain weight at kinetics equivalent to WT animals (Fig. 8C). Importantly, analysis of IgM and IgG autoantibodies (Fig. 8D and E) revealed that within 4 weeks of receiving WT T_{Regs}, cDKO animals were essentially devoid of detectable circulating autoantibodies and possessed normal levels of total serum immunoglobulin. To support that these phenotypic reversals were due to transferred GFP^+ WT T_{Regs}, we

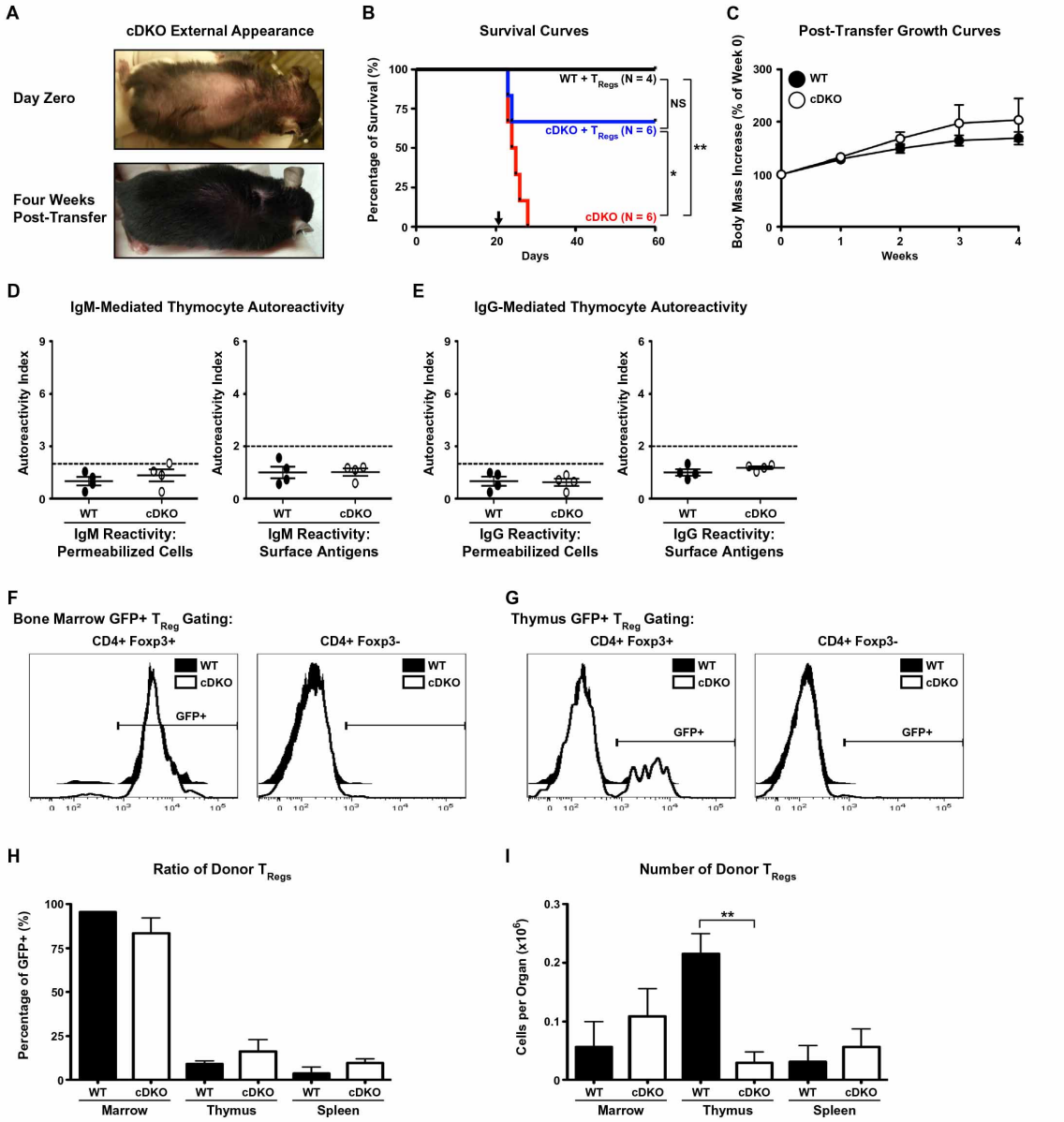

Fig. 8. Adoptive transfer of WT T_{Regs} rescues fatal autoimmune disease of cDKO animals. (A) Representative image of the same cDKO animal before (top) and 4 weeks after receiving WT T_{Regs} (bottom). (B) Kaplan–Meier survival plot illustrating the extension of lifespan afforded cDKO animals upon transfer of WT T_{Regs}. The black arrow marks the animal age when T_{Regs} were transferred. Black line: WT animals + WT T_{Regs} ($N = 4$); Blue line: cDKO animals + WT T_{Regs} ($N = 6$); Red line: cDKO animals, no transfer ($N = 6$); Statistical comparisons: $^{*}P \leqslant 0.05$, $^{**}P \leqslant 0.01$. (C) Four week analysis of body mass increase following the transfer of WT T_{Regs}. (D and E) Quantification of IgM (D) and IgG (E) autoreactivity to permeabilized cell (left) and surface antigens (right). Autoreactivity Index (AI) = gMFI per sample/mean WT gMFI, AI $\geqslant 2$ (indicated by dotted line) is considered autoreactive; Number of animals per group: WT = 4, cDKO = 4. (F and G) Representative FACS histograms demonstrating the prevalence of GFP^+ cells in the bone marrow (F) and thymus (G) of WT and cDKO recipients following WT T_{Reg} transfer. Representative histograms depicting analysis of $CD4^+$ $Foxp3^+$ (left) and $CD4^+$ $Foxp3^-$ (right) cells are shown. (H and I) Quantification of GFP^+ donor T_{Regs} from multiple organs. Shown are percentages (H) and absolute numbers (I) of GFP^+ donor T_{Regs} in bone marrow, thymus and spleen. Bars represent mean ± SEM. Numbers of animals per group: 2–3 for marrow, 3–4 for thymus and spleen; Statistical comparisons: $^{**}P \leqslant 0.01$.

analyzed the $CD4^+$ populations of various organs by FACS (Fig. 8F and G). In the bone marrow, the vast majority of $CD4^+$ $Foxp3^+$ cells were also GFP^+ (Fig. 8F, left). This was specific to the T_{Reg} compartment as $CD4^+$ $Foxp3^-$ cells were GFP^- by comparison (Fig. 8F, right). In the thymus, both WT and cDKO animals had detectable $CD4^+$ $Foxp3^+$ GFP^+ cells indicating that mature T_{Regs} are capable of recirculating to the thymus (Fig. 8G). Quantification showed that donor GFP^+ WT T_{Regs} contributed to the total T_{Reg} pool of various WT and

cDKO organs in an equivalent fashion (Fig. 8H). Unlike in the bone marrow and spleen, WT recipients had a significantly greater number of donor GFP$^+$ WT T_{Regs} than the cDKO (Fig. 8I). This may reflect limitations of the cDKO thymus to support high levels of T_{Reg} residence perhaps due to prior autoimmune damage or the lack of *Snai2* in the stromal environment. In total, these data suggest that GFP$^+$ WT T_{Regs} were able to suppress autoimmunity in cDKO mice. Additionally, this may be illustrative of a functional gap between WT and cDKO T_{Regs} as donor WT T_{Regs} were still the minority population in the cDKO thymus and spleen.

3.6. Deletion of Snai2 and Snai3 in bone marrow-derived cells is sufficient to induce autoantibody generation

The above data has demonstrated that autoimmunity resulted from the combined deletion of both *Snai2* and *Snai3*. However, the question remained as to whether autoimmunity was due to a cell intrinsic defect or also required the stromal (i.e. non-hematopoietic) deletion of *Snai2*. To address this, we transplanted WT or cDKO lineage-depleted bone marrow into *Rag2*$^{-/-}$ recipients. We chose this experimental system for two reasons: (1) the use of lineage-depleted marrow would evaluate *de novo* generation of autoimmunity rather than the carryover of autoreactive donor B and/or T cells and (2) *Rag2*$^{-/-}$ mice never develop T_{Regs} which have been previously shown to be radio-resistant in bone marrow transplant models and thus would suppress the development of autoimmunity in recipients of cDKO bone marrow [35]. Starting at three weeks post-transplant, we bled mice retro-orbitally once every two weeks and analyzed plasma for IgM and IgG autoantibodies. Animals were euthanized upon presentation of persistent autoantibodies (i.e. consecutive positive tests for the same autoantibody subtype) or positivity for multiple autoantibody subtypes at a given time point. Otherwise, all animals were euthanized at a pre-determined nine weeks post-transplant endpoint. As shown in Table 1, five out of seven recipients of cDKO bone marrow developed at least one subtype of autoantibody with the earliest detected onset being at 5 weeks post-transplant. Overall, transplantation of cDKO bone marrow into *Rag2*$^{-/-}$ mice resulted in an approximately 71% occurrence of autoantibody generation, similar albeit slightly reduced when compared to "whole" cDKO mice (see above). As such, the deletion of *Snai2* in the stromal compartment is not required for the loss of tolerance and subsequent generation of autoantibodies.

Of note, there was a reduction in autoantibody subtypes concomitantly generated by autoreactive cDKO bone marrow transplants when compared to autoreactive "whole" cDKOs (Fig. 9A). While five of nine "whole" cDKOs possessed all four subtypes of autoantibodies, none of the cDKO bone marrow recipients had more than two subtypes. Previous analysis of "whole" cDKOs showed a propensity to generate IgM and IgG autoantibodies reactive to surface antigens (see Fig. 4). Re-evaluation of "whole" cDKO animals positive for autoantibodies revealed that 89% (eight of nine) and 78% (seven of nine) possessed surface reactive IgM and IgG, respectively (Fig. 9B). This was in contrast to *Rag2*$^{-/-}$ animals receiving cDKO bone marrow, which developed very limited surface reactivity with a 20% (one of five) incidence rate of surface reactive IgM and no instances of surface reactive IgG (zero of five). In contrast, all five recipients of cDKO bone marrow generated IgM cross-reactive to total cellular antigens (permeabilized cells) and two of these animals progressed to the generation of IgG cross-reactive to total cellular antigens.

Gross physical examination of cDKO bone marrow recipients showed no signs of alopecia or skin inflammation (Fig. 10A). Nor did these animals display any indicators of illness such as weight loss when compared to WT bone marrow recipients (Fig. 10B). This suggested that the autoimmune disease of these animals was either limited in scope (i.e. limited target tissues) or in its relative infancy. Next we characterized cDKO bone marrow recipient hematopoiesis in a manner similar to that used for the "whole" cDKOs (see above). Recipients of WT and cDKO bone marrow showed no disparities in lymphoid organ mass (Fig. 10C) and the thymus and spleen had equivalent cellularity (Fig. 10D). Interestingly, the bone marrow had a non-significant ($p = 0.11$) trend that represented a 25% reduction in total cell numbers (Fig. 10D). Analysis of bone marrow constituents demonstrated that while B cell development was unperturbed in the cDKO recipients, both monocytes ($P = 0.06$) and neutrophils (PMN) ($P = 0.10$) were reduced by 27% and 29%, respectively (Fig. 11A). Similar to B cell development in the bone marrow, thymic T cell development in cDKO recipients displayed no abnormalities (Fig. 11B). The lack of lymphocyte defects was not an artifact of potentially examining animals at a point of homeostasis. Analysis of lineages in the blood starting at three weeks post-transplant further demonstrated equivalent generation of B and T lymphocytes between the two genotypes (Supplementary Fig. 7). Finally, we examined the T_{Reg} compartment; which was previously shown to be developmentally deficient in the "whole" cDKO (see Fig. 7). As a percentage of CD4$^+$ T cells and as total cell numbers, cDKO bone marrow was equivalent to WT in the ability to generate T_{Regs} when transplanted into the *Rag2*$^{-/-}$ background (Fig. 12). This meant that even in a scenario where normal numbers of cDKO T_{Regs} were present, self-tolerance still was not maintained. Overall, these results support the conclusion that the loss of immune tolerance is, at the very least, partially attributable to the combined deletion of *Snai2* and *Snai3* in hematopoietic lineages. However, the deletion of *Snai2* in the stroma appears to significantly contribute to disease progression and severity. Further bone marrow transplantation experiments comparing disease parameters using *Rag2*$^{-/-}$ and *Snai2*$^{-/-}$ *Rag2*$^{-/-}$ double knockout recipients will be essential in determining the role of *Snai2* expressing stromal compartments in immune tolerance.

Table 1
Summary of autoimmune occurrence in *Rag2*$^{-/-}$ mice transplanted with *Snai2*/*Snai3* cDKO lineage-depleted bone marrow. Three individual cDKO mice were used as donors for a total of seven *Rag2*$^{-/-}$ recipients. Time of termination, reason for termination and autoreactive indices (AI) are shown for each individual recipient. All cDKO AI are relative to the WT values for a given time point. AI indices greater than 2.0 are in bold to signify autoantibody generation.

Recipient #	cDKO donor #	Week of termination	Reason	Surface IgM AI	Total IgM AI	Surface IgG AI	Total IgG AI
1	1	9	Predetermined endpoint	0.68	0.44	0.42	0.09
2	1	9	Persistent autoantibodies, Multiple autoantibody subtypes	1.78	**2.10**	1.39	**2.10**
3	1	9	Predetermined endpoint	1.88	**8.74**	1.00	0.49
4	2	7	Persistent autoantibodies	1.78	**2.37**	0.90	0.71
5	2	9	Predetermined endpoint	0.83	1.20	0.79	0.24
6	3	7	Multiple autoantibody subtypes	**2.20**	**4.52**	1.13	1.55
7	3	5	Multiple autoantibody subtypes	1.60	**2.40**	1.23	**2.17**

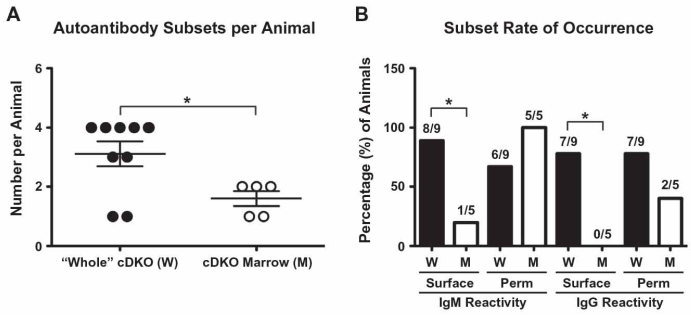

Fig. 9. *Rag2*$^{-/-}$ recipients of cDKO bone marrow predominantly generate autoantibodies to total cellular antigens. (A) The number of autoantibody subtypes per autoimmune "whole" cDKO (W) and *Rag2*$^{-/-}$ recipient of cDKO bone marrow (M). Number of animals per group: $W = 9$, $M = 5$. The mean value per genotype is represented by the middle horizontal bar with SEM measured by upper and lower horizontal bars. (B) Analysis of surface versus total cellular (permeabilized cells, Perm) antigen reactivity in "whole" cDKOs (W) and *Rag2*$^{-/-}$ animals receiving cDKO bone marrow (M). Bars represent percentage of animals positive for a subtype within the total population. Actual numbers of animals are shown above each bar. Statistical comparisons: $^{*}P \leqslant 0.05$.

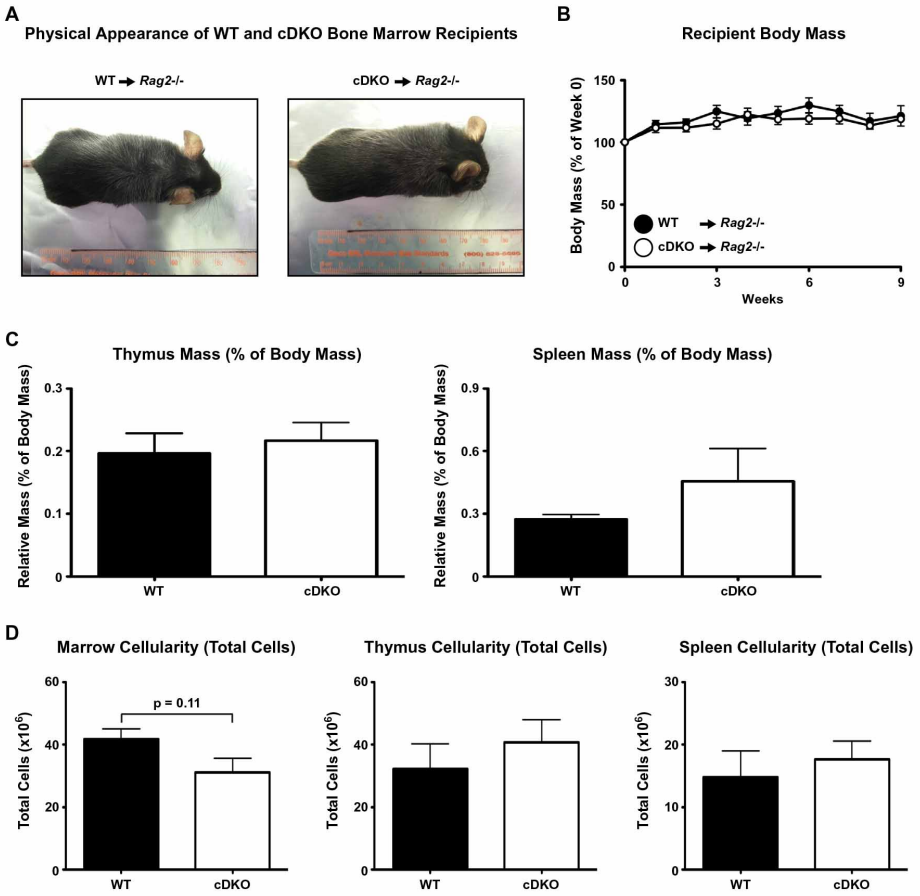

Fig. 10. *Rag2*$^{-/-}$ recipients of cDKO bone marrow are physically indistinguishable from animals receiving WT bone marrow. (A) Representative images of *Rag2*$^{-/-}$ receiving WT (left) and cDKO (right) bone marrow. (B) Longitudinal analysis of body mass change over the course of nine weeks post-transplant. Thymus and spleen relative masses (C) and bone marrow, thymus and spleen total cell counts (D) from *Rag2*$^{-/-}$ recipients of WT and cDKO bone marrow. Five *Rag2*$^{-/-}$ mice received WT bone marrow from three individual donors. Seven *Rag2*$^{-/-}$ mice received cDKO bone marrow from three individual donors.

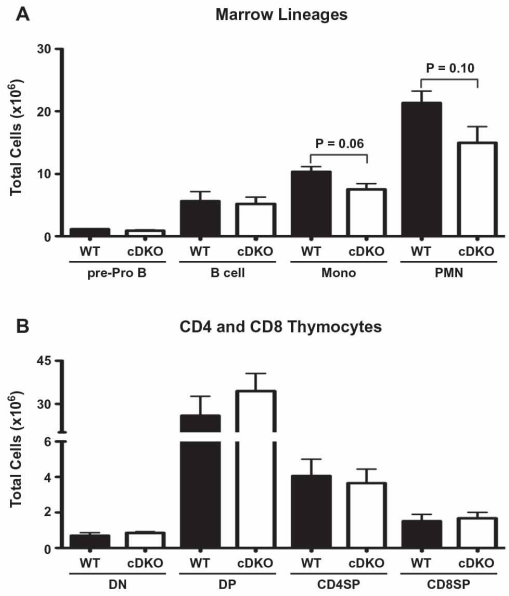

Fig. 11. *Rag2*$^{-/-}$ recipients of cDKO bone marrow develop normal numbers of B and T cells but still retain a deficiency in myeloid lineage development. (A) Quantification of total cell numbers of pre-Pro B cells, committed B cells, monocytes and neutrophils. pre-Pro B cells: B220^{+} CD19^{-}; committed B cells: B220^{+} CD19^{+}; Monocytes: CD11b^{+} Gr-1$^{LO/INT}$; Neutrophils (PMN): CD11b^{+} Gr-1^{HI} (B) Quantification of the number CD4 and CD8 double negative (DN), CD4 and CD8 double positive (DP), CD4 single positive (CD4SP) and CD8 single positive (CD8SP) cells per thymus. (A and B) Bars represent mean ± SEM. Number of animals per group: WT = 5, cDKO = 6–7.

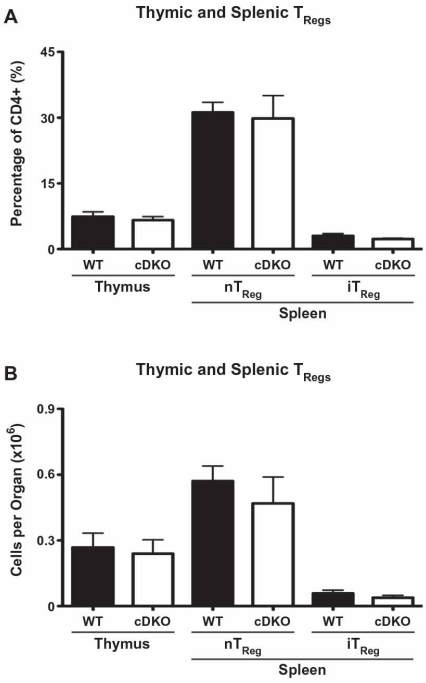

Fig. 12. *Rag2*$^{-/-}$ recipients of cDKO bone marrow develop normal numbers of T_{Regs}. (A) Quantification of T_{Regs} as a percentage of CD4 single positive T cells in both the thymus and spleen. (B) Quantification of total numbers of T_{Regs} in both the thymus and spleen. (A and B) CD4^{+} T cells were gated as Foxp3^{+} T_{Regs} in the thymus. In the spleen, CD4^{+} T cells were divided into Foxp3^{+} Helios^{+} natural T_{Regs} (nT_{Reg}) and Foxp3^{+} Helios^{-} induced T_{Regs} (iT_{Reg}). Bars represent mean ± SEM. Number of animals per group: WT = 5, cDKO = 6–7.

3.7. Wildtype T_{Regs} block autoantibody generation in recipients of cDKO bone marrow

Data from Fig. 8 clearly demonstrated that the adoptive transfer of WT T_{Regs} was capable of suppressing autoimmune disease in the "whole" cDKO. However, *Rag2*$^{-/-}$ recipients that received cDKO bone marrow generated IgM and IgG autoantibodies even with normal numbers of T_{Regs} present (Table 1 and Fig. 12). In an effort to further support the hypothesis of dysfunctional cDKO T_{Regs}, we repeated the bone marrow transplantation using WT recipients. As stated above, these animals would possess a pool of radioresistant WT T_{Regs} native to the recipient animals and thus should not develop autoimmunity. Indeed, that was the case. By twelve weeks post-transplant, none of the cDKO recipients developed autoantibodies (Table 2).

As with *Rag2*$^{-/-}$ recipients, WT recipients of cDKO bone marrow demonstrated normal B and T cell development (Fig. 13 and DNS). However, WT recipients also demonstrated normal myeloid development (Fig. 13). This suggested that the loss of myeloid cells in *Rag2*$^{-/-}$ recipients was due to the autoimmune environment rather than a cell intrinsic defect of *Snai2/3* cDKO bone marrow.

To validate that the observed differences were due to the persistence of radioresistant WT T_{Regs}, we FACS-sorted various splenic cell populations and quantified the presence of *Snai2* WT and KO alleles via PCR of genomic DNA (gDNA). Fig. 14A shows representative genotyping of T_{Conv} (C, CD4^{+} CD25^{-}), T_{Reg} (R, CD4^{+} CD25^{+}) and B (CD19^{+}) cells sorted from one WT and two cDKO reconstituted animals. In total, four animals from each "genotype" were analyzed. Tail gDNA from *Snai2*$^{+/-}$ animals was used to normalize amplicon signal intensity relative to genetic contribution. PhosphorImager-based quantification of ^{32}P radioactivity demonstrated that approximately 59% of T_{Conv} were derived from cDKO donor marrow at twelve weeks post-transplant (Fig. 14B). In contrast, only approximately 39% of T_{Regs} were generated from cDKO marrow. Not surprisingly, almost all B cells were derived from cDKO donor marrow. In summary, we used two bone marrow

Table 2
Summary of autoimmune occurrence in WT mice transplanted with *Snai2/Snai3* cDKO lineage-depleted bone marrow. Two individual cDKO mice were used as donors for a total of four WT recipients. Time of termination, reason for termination and autoreactive indices (AI) are shown for each individual recipient. All cDKO AI are relative to the WT values for a given time point.

Recipient #	cDKO donor #	Week of termination	Reason	Surface IgM AI	Total IgM AI	Surface IgG AI	Total IgG AI
1	1	12	Predetermined endpoint	0.65	0.19	0.40	0.17
2	1	12	Predetermined endpoint	0.95	0.41	0.53	0.25
3	2	12	Predetermined endpoint	1.43	0.99	0.76	0.52
4	2	12	Predetermined endpoint	1.03	0.68	0.74	1.33

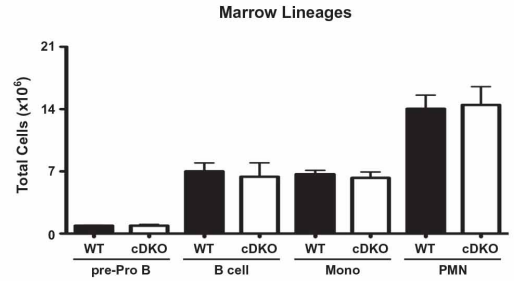

Fig. 13. WT recipients of cDKO bone marrow develop normal levels of bone marrow lineages. Quantification of total cell numbers of pre-Pro B cells, committed B cells, monocytes and neutrophils. pre-Pro B cells: $B220^{+}$ $CD19^{-}$; committed B cells: $B220^{+}$ $CD19^{+}$; Monocytes: $CD11b^{+}$ $Gr\text{-}1^{LO/INT}$; Neutrophils (PMN): $CD11b^{+}$ $Gr\text{-}1^{HI}$; Bars represent mean ± SEM. Number of animals per group: WT = 4, cDKO = 4.

transplantation systems where essentially the only variable was the presence or absence of a radioresistant T_{Reg} pool. Only animals lacking a WT T_{Reg} pool demonstrated the capacity to develop autoimmunity (i.e. autoantibodies) further suggesting a functional gap between WT and cDKO T_{Regs}. However, further studies will be needed to formally address this issue.

4. Discussion

In this report, we describe the generation and characterization of the *Snai2*/*Snai3* conditional double knockout. These animals developed a florid autoimmunity in conjunction with severe impairment in both B and T cell generation. The cDKO animals demonstrated an autoimmune phenotype inclusive of alopecia and the generation of both IgM and IgG autoantibodies, which culminated in the demise of mice by 30 days post birth. Adoptive transfer of WT T_{Regs} into cDKO animals alleviated autoimmune symptoms and significantly extended the lifespan of cDKO animals. This suggested that cDKO B and T cells were ultimately responsive to peripheral regulatory mechanisms and that a cDKO T_{Reg} defect may contribute to autoimmune disease.

Since cDKO mice possessed a germline deletion of *Snai2*, it was important to determine whether or not the stromal loss of *Snai2* contributed to the phenotypes observed in the "whole" cDKO. To test this, we transplanted cDKO marrow into *Rag2*$^{-/-}$ recipients and analyzed these animals for hematopoietic defects and various autoimmune symptoms. Rather interestingly, the reconstitution of *Snai2* into the stromal environment blunted many of the phenotypes observed in the "whole" cDKO. Unlike "whole" cDKO animals, *Rag2*$^{-/-}$ recipients of cDKO marrow displayed unperturbed B and T cell development. However, myeloid development was still impaired in these animals. The simplest interpretation is that gene products regulated by *Snai2* in the stroma may interact with gene products regulated by *Snai3* (and possibly also *Snai2*). This would likely involve receptor-ligand pairs important for lymphocyte development such as IL-7/IL-7Rα, CXCL12/CXCR4 and others [36,37]. Previous analysis of protein expression demonstrated detectable Snai2 in bone marrow whole cell lysates. In contrast, Snai2 protein was only faintly detectable in the thymus suggesting that the ETP defect originated in the bone marrow [20,37]. This was not directly assayed here. An alternative hypothesis is that the observed B and T cell defects were directly affected by autoimmunity in the "whole" cDKO. In regards to B cells, this has been previously observed in *Scurfy* mice in which pro-inflammatory cytokines were presumed to be the driving force [25,38].

In total, five of the seven *Rag2*$^{-/-}$ recipients of cDKO bone marrow developed autoantibodies by nine weeks post-transplant demonstrating a hematopoietic cell intrinsic redundancy for *Snai2*/*Snai3* in regulating some level of immune tolerance. Curiously, unlike the "whole" cDKOs, there was very little reactivity to surface antigens. Since we used WT thymocytes to detect autoreac-

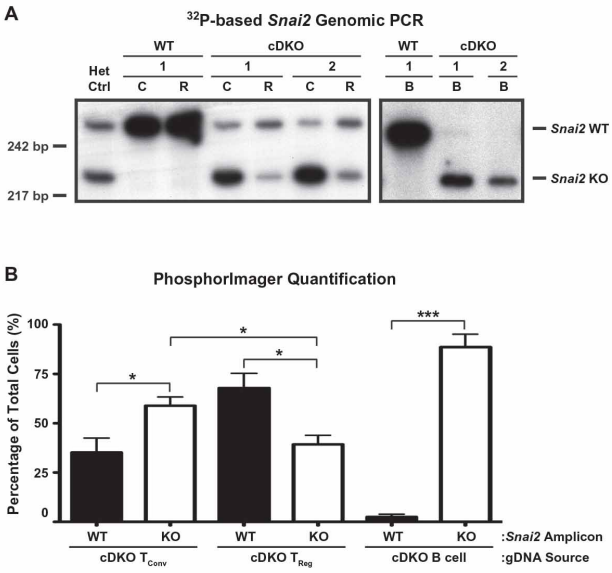

Fig. 14. Autoimmune-resistant WT recipients of cDKO bone marrow possess a persistent pool of WT T_{Regs}. (A) Representative genotyping PCR performed via incorporation of [^{32}P] deoxycytidine triphosphate. Samples from one WT and two cDKO animals are shown. Het Ctrl = *Snai2*$^{+/-}$ tail gDNA, C = T_{Conv}, R = T_{Reg}. (B) Quantification of *Snai2* WT and KO genetic contribution per cell population analyzed. Bars represent mean ± SEM. Number of animals per group: WT = 4, cDKO = 4; Statistical comparisons: $^{*}P \leqslant 0.05$, $^{***}P \leqslant 0.001$.

tivity, it is possible that the lack of surface reactivity may explain the non-existent T cell developmental defects in *Rag2*$^{-/-}$ recipients. Along these lines, surface reactive autoantibodies would contribute to direct killing of T cells through antibody-dependent cell-mediated cytotoxicity (ADCC) and complement activation. The resultant inflammation may further poison the thymic microenvironment. This might also account for the impaired B cell pipeline in the "whole" cDKO [38].

Surface autoreactivity would be expected to drive autoimmunity more potently than reactivity to intracellular components. The reasoning behind this is that surface antigens are continuously exposed to the extracellular environment and thus, potential autoantibodies. In contrast, intracellular antigens are "hidden" the majority of the time. An obvious question then becomes, how does stromal expression of Snai2 regulate autoantibody repertoire? A potential explanation for this is that *Snai2* may augment the expression of a particular set of surface proteins in a tissue specific manner. In this model, *Snai2* would repress the expression of certain "autoreactive" surface proteins so that low-to-moderate affinity autoreactive B cells would not encounter these proteins at levels required for activation. However, if *Snai2* is deleted, then these "autoreactive" proteins would be overexpressed leading to a more robust activation of autoreactive B cells. It is also possible that germline deletion of *Snai2* contributes to disease though the sensitization of animals to apoptosis. Multiple systems have shown that Snai2 repression of *Puma* is crucial in preserving cell survival when challenged with various "stressors" [39–41]. These non-mutually exclusive models would position the stromal deletion of *Snai2* as a disease accelerator rather than a gatekeeper. This hypothesis would be in line with our data showing that although cDKO bone marrow in itself leads to a loss of tolerance, the overall severity of disease (i.e. alopecia, lethality), but not occurrence (i.e. autoantibody generation), were seemingly diminished in a *Snai2* sufficient background. To fully evaluate these possibilities, we will need to compare the transplantation of cDKO bone marrow into *Snai2*$^{-/-}$, *Rag2*$^{-/-}$and *Rag2*$^{-/-}$ *Snai2*$^{-/-}$ double knockout recipients not only examining hematopoiesis but also autoimmune disease parameters.

Adoptive transfer of WT T_{Regs} was able to dampen autoimmunity in cDKO mice. This meant that cDKO B and T_{Conv} cells still retained sensitivity to peripheral regulatory mechanisms. WT T_{Reg} expansion was evident in cDKO recipients as the combined output from the thymus and spleen was more than that initially transferred (8.6×10^4 versus 7.5×10^5 GFP$^+$ T_{Regs}). However, at least in the thymus and spleen, donor T_{Regs} were still a minority contributor to the total T_{Reg} pool. Interestingly, both WT and cDKO recipients demonstrated an equivalent accumulation of GFP$^+$ T_{Regs} in the bone marrow. The significance of this is not currently understood. However, the data in total suggested that perhaps enhanced function of WT T_{Regs} rather than inflated cellular number may have been the main contributor to disease alleviation. In support of this, *Rag2*$^{-/-}$ recipients of cDKO bone marrow developed autoantibodies in spite of normal numbers of cDKO T_{Regs}. In contrast, WT recipients of cDKO bone marrow maintained a pool of radioresistant WT T_{Regs} (approximately 61% of total T_{Regs}) and did not generate autoantibodies. Essentially, the only difference between these two bone marrow transplantation studies was the presence of radioresistant WT T_{Regs} further supporting that a cDKO regulatory T cell defect contributes to cDKO autoimmune disease. However, future experiments will be needed to define the potential defect(s) of cDKO T_{Regs}.

The final question to address is why the phenotype of the cDKO animal is so much more profound than that found in the genomic *Snai2*/*Snai3* deletion model. While both models demonstrated an approximately 50% reduction in animal masses, only the cDKO presented with alopecia, dermatitis and the generation of autoantibodies. Within the first days of life, cDKO animals developed autoimmune disease while we were able to age gDKO animals to six months of age with no indication of autoimmunity [20]. To the extent of our knowledge, the conditional deletion of a gene(s) has always resulted in phenotypes less severe than a whole-organism germline deletion. That is not the case in this instance. One possible explanation may be the global epigenetic upregulation of *Snai1* in the gDKO to compensate for the whole-organism loss of the *Snai2* and *Snai3* genes. It has been previously shown that *Snai1* and *Snai2* can reciprocally antagonize the gene expression of the other family member [42]. Indeed, germline deletion of *Snai2* has led to the upregulation of *Snai1* in tissues previously devoid of *Snai1* gene expression [13]. Introduction of a conditional *Snai1* allele into the gDKO background (along with *Vav-Cre*) would provide a model to test this hypothesis.

In summary, we have identified the Snail family as novel transcriptional regulators necessary for the maintenance of immune tolerance. The autoimmunity generated in the cDKO mice is identifiable proximal to birth and quickly leads to the death of the animal unless they are rescued by the introduction of exogenous WT T_{Regs}. Importantly, hematopoietically intrinsic defects contribute to cDKO autoimmunity as *Rag2*$^{-/-}$ recipients of cDKO bone marrow generated autoantibodies.

Acknowledgments

The authors would like to thank the University of Utah Flow Cytometry Core Facility. We would like to thank the Weis labs for their critique of this work and many intellectual contributions. Thank you to Hannah Pioli and KimAnh Pioli for assistance with genotyping.

The Department of Pathology and the Weber Presidential Endowed Chair in Immunology provided research funding. Usage of the FacsAria flow cytometer was supported by NIH #1S10RR026802-01. J.J.W. was supported by NIH AR43521 and AI32223. P.D.P. was supported as a pre-doctoral trainee on the NIH Hematology T32 training Grant, #T-32DK007115-38.

The authors have no competing financial interests.

Appendix A. Supplementary data

Supplementary data associated with this article can be found, in the online version, at http://dx.doi.org/10.1016/j.cellimm.2015.02.009.

References

[1] E.W. Scott, R.C. Fisher, M.C. Olson, E.W. Kehrli, M.C. Simon, H. Singh, PU.1 functions in a cell-autonomous manner to control the differentiation of multipotential lymphoid-myeloid progenitors, Immunity 6 (1997) 437–447.
[2] J.D. Fontenot, J.P. Rasmussen, L.M. Williams, J.L. Dooley, A.G. Farr, A.Y. Rudensky, Regulatory T cell lineage specification by the forkhead transcription factor foxp3, Immunity 22 (2005) 329–341.
[3] S. Sakaguchi, Regulatory T Cells: key controllers of immunologic self-tolerance, Cell 101 (2000) 455–458.
[4] Y. Fujiwara, A.N. Chang, A.M. Williams, S.H. Orkin, Functional overlap of GATA-1 and GATA-2 in primitive hematopoietic development, Blood 103 (2004) 583–585.
[5] M. Manzanares, A. Locascio, M.A. Nieto, The increasing complexity of the Snail gene superfamily in metazoan evolution, Trends Genet. 17 (2001) 178–181.
[6] M. Manzanares, M.J. Blanco, M.A. Nieto, Snail3 orthologues in vertebrates: divergent members of the Snail zinc-finger gene family, Dev. Genes. Evol. 214 (2004) 47–53.
[7] A. Barrallo-Gimeno, M.A. Nieto, Evolutionary history of the Snail/Scratch superfamily, Trends Genet. 25 (2009) 248–252.
[8] H. Kataoka, T. Murayama, M. Yokode, S. Mori, H. Sano, H. Ozaki, et al., A novel snail-related transcription factor Smuc regulates basic helix-loop-helix transcription factor activities via specific E-box motifs, Nucleic Acids Res. 28 (2000) 626–633.
[9] V.D. Soleimani, H. Yin, A. Jahani-Asl, H. Ming, C.E. Kockx, W.F. van Ijcken, et al., Snail regulates MyoD binding-site occupancy to direct enhancer switching and

differentiation-specific transcription in myogenesis, Mol. Cell 47 (2012) 457–468.
[10] G. Ferrari-Amorotti, V. Fragliasso, R. Esteki, Z. Prudente, A.R. Soliera, S. Cattelani, et al., Inhibiting interactions of lysine demethylase LSD1 with snail/slug blocks cancer cell invasion, Cancer Res. 73 (2013) 235–245.
[11] N. Herranz, D. Pasini, V.M. Diaz, C. Franci, A. Gutierrez, N. Dave, et al., Polycomb complex 2 is required for E-cadherin repression by the Snail1 transcription factor, Mol. Cell. Biol. 28 (2008) 4772–4781.
[12] H. Peinado, E. Ballestar, M. Esteller, A. Cano, Snail mediates E-cadherin repression by the recruitment of the Sin3A/histone deacetylase 1 (HDAC1)/HDAC2 complex, Mol. Cell. Biol. 24 (2004) 306–319.
[13] Y. Chen, T. Gridley, Compensatory regulation of the Snai1 and Snai2 genes during chondrogenesis, J. Bone Miner. Res. 28 (2013) 1412–1421.
[14] A. Barrallo-Gimeno, M.A. Nieto, The Snail genes as inducers of cell movement and survival: implications in development and cancer, Development 132 (2005) 3151–3161.
[15] P.D. Pioli, J.H. Weis, Snail transcription factors in hematopoietic cell development: a model of functional redundancy, Exp. Hematol. 42 (2014) 425–430.
[16] H. Lomeli, C. Starling, T. Gridley, Epiblast-specific Snai1 deletion results in embryonic lethality due to multiple vascular defects, BMC Res. Notes 2 (2009) 22.
[17] E.A. Carver, R. Jiang, Y. Lan, K.F. Oram, T. Gridley, The mouse snail gene encodes a key regulator of the epithelial-mesenchymal transition, Mol. Cell. Biol. 21 (2001) 8184–8188.
[18] J. Perez-Losada, M. Sanchez-Martin, A. Rodriguez-Garcia, M.L. Sanchez, A. Orfao, T. Flores, et al., Zinc-finger transcription factor Slug contributes to the function of the stem cell factor c-kit signaling pathway, Blood 100 (2002) 1274–1286.
[19] C.K. Bradley, C.R. Norton, Y. Chen, X. Han, C.J. Booth, J.K. Yoon, et al., The snail family gene snai3 is not essential for embryogenesis in mice, PLoS ONE 8 (2013) e65344.
[20] P.D. Pioli, T.J. Dahlem, J.J. Weis, J.H. Weis, Deletion of Snai2 and Snai3 results in impaired physical development compounded by lymphocyte deficiency, PLoS ONE 8 (2013) e69216.
[21] G. Anderson, Y. Takahama, Thymic epithelial cells: working class heroes for T cell development and repertoire selection, Trends Immunol. 33 (2012) 256–263.
[22] P.D. Pioli, I. Debnath, J.J. Weis, J.H. Weis, Zfp318 regulates IgD expression by abrogating transcription termination within the Ighm/Ighd locus, J. Immunol. (2014).
[23] S. Cho, G.J. Spangrude, Enrichment of functionally distinct mouse hematopoietic progenitor cell populations using CD62L, J. Immunol. 187 (2011) 5203–5210.
[24] S.S. Perry, H. Wang, L.J. Pierce, A.M. Yang, S. Tsai, G.J. Spangrude, L-selectin defines a bone marrow analog to the thymic early T-lineage progenitor, Blood 103 (2004) 2990–2996.
[25] S.M. Leonardo, J.A. Josephson, N.L. Hartog, S.B. Gauld, Altered B cell development and anergy in the absence of Foxp3, J. Immunol. 185 (2010) 2147–2156.
[26] M.L. Hibbs, D.M. Tarlinton, J. Armes, D. Grail, G. Hodgson, R. Maglitto, et al., Multiple defects in the immune system of Lyn-deficient mice, culminating in autoimmune disease, Cell 83 (1995) 301–311.
[27] Y. Gu, P.E. Jensen, X. Chen, Immunodeficiency and autoimmunity in H2-O-deficient mice, J. Immunol. 190 (2013) 126–137.
[28] T. Ando, W. Xiao, P. Gao, S. Namiranian, K. Matsumoto, Y. Tomimori, et al., Critical role for mast cell Stat5 activity in skin inflammation, Cell Rep. 6 (2014) 366–376.
[29] E.N. Huter, K. Natarajan, T.R. Torgerson, D.D. Glass, E.M. Shevach, Autoantibodies in scurfy mice and IPEX patients recognize keratin 14, J. Invest. Dermatol. 130 (2010) 1391–1399.
[30] S. Aschermann, C.H. Lehmann, S. Mihai, G. Schett, D. Dudziak, F. Nimmerjahn, B cells are critical for autoimmune pathology in Scurfy mice, Proc. Natl. Acad. Sci. U.S.A. 110 (2013) 19042–19047.
[31] C.L. Bennett, H.D. Ochs, IPEX is a unique X-linked syndrome characterized by immune dysfunction, polyendocrinopathy, enteropathy, and a variety of autoimmune phenomena, Curr. Opin. Pediatr. 13 (2001) 533–538.
[32] C.L. Bennett, J. Christie, F. Ramsdell, M.E. Brunkow, P.J. Ferguson, L. Whitesell, et al., The immune dysregulation, polyendocrinopathy, enteropathy, X-linked syndrome (IPEX) is caused by mutations of FOXP3, Nat. Genet. 27 (2001) 20–21.
[33] W. Ouyang, O. Beckett, Q. Ma, J.H. Paik, R.A. DePinho, M.O. Li, Foxo proteins cooperatively control the differentiation of Foxp3+ regulatory T cells, Nat. Immunol. 11 (2010) 618–627.
[34] M. Miyazaki, K. Miyazaki, S. Chen, M. Itoi, M. Miller, L.F. Lu, et al., Id2 and Id3 maintain the regulatory T cell pool to suppress inflammatory disease, Nat. Immunol. 15 (2014) 767–776.
[35] N. Komatsu, S. Hori, Full restoration of peripheral Foxp3+ regulatory T cell pool by radioresistant host cells in scurfy bone marrow chimeras, Proc. Natl. Acad. Sci. U.S.A. 104 (2007) 8959–8964.
[36] T. Nagasawa, Microenvironmental niches in the bone marrow required for B-cell development, Nat. Rev. Immunol. 6 (2006) 107–116.
[37] A.Y. Lai, M. Kondo, Identification of a bone marrow precursor of the earliest thymocytes in adult mouse, Proc. Natl. Acad. Sci. U.S.A. 104 (2007) 6311–6316.
[38] K. Nakamura, T. Kouro, P.W. Kincade, A. Malykhin, K. Maeda, K.M. Coggeshall, Src homology 2-containing 5-inositol phosphatase (SHIP) suppresses an early stage of lymphoid cell development through elevated interleukin-6 production by myeloid cells in bone marrow, J. Exp. Med. 199 (2004) 243–254.
[39] W.S. Wu, S. Heinrichs, D. Xu, S.P. Garrison, G.P. Zambetti, J.M. Adams, et al., Slug antagonizes p53-mediated apoptosis of hematopoietic progenitors by repressing puma, Cell 123 (2005) 641–653.
[40] S. Kim, J. Yao, K. Suyama, X. Qian, B.Z. Qian, S. Bandyopadhyay, et al., Slug promotes survival during metastasis through suppression of puma-mediated apoptosis, Cancer Res. 74 (2014) 3695–3706.
[41] C. Arienti, A. Tesei, S. Carloni, P. Ulivi, A. Romeo, G. Ghigi, et al., SLUG silencing increases radiosensitivity of melanoma cells in vitro, Cell. Oncol. 36 (2013) 131–139.
[42] Y. Chen, T. Gridley, The SNAI1 and SNAI2 proteins occupy their own and each other's promoter during chondrogenesis, Biochem. Biophys. Res. Commun. 435 (2013) 356–360.

CHAPTER 4

DISCUSSION

Summary

This dissertation details novel contributions of *Snai2* and *Snai3* in hematopoietic biology. Overall, *Snai2* and *Snai3* functioned redundantly to preserve the development and function of lymphocytes as the conditional deletion of both genes led to lymphopenia and autoimmunity. Importantly, autoimmunity was still generated when *Snai2/Snai3* double knockout bone marrow was transplanted into *Rag2*$^{-/-}$ *Snai2*$^{+/+}$ animals. This supported a cell intrinsic role for these regulators in immune tolerance. However, some interesting questions remain. Why does the *Snai2/Snai3* conditional double knockout (cDKO) develop autoimmunity but the germline double knockout (gDKO) does not? What are the individual contributions of various cell types to autoimmunity? What are the transcriptional targets of *Snai2* and *Snai3* in these cell types? Finally, does *Snai1* play a role in the immune system?

No Autoimmunity in the Germline Double Knockout

From an immunological standpoint, the most interesting contrast between the *Snai2/Snai3* double knockout models was the apparent lack of autoimmunity in the gDKO. This result was supported by a lack of alopecia and inflammation, a lifespan of up to six months of age, and the lack of autoantibody generation in the germline deleted mice. Perhaps overly simplistic, one explanation may be the general epigenetic upregulation of *Snai1* due to the global loss of four Snail alleles (i.e., *Snai2* and *Snai3* in the gDKO). While no data currently support this notion, the hypothesis would be testable via the introduction of a *Snai1* conditional allele which could be specifically deleted via a *Vav-Cre* transgene. If

this really is a question of gene dosage, then deletion of one *Snai1* allele would be predicted to result in the induction of autoimmunity.

An alternative hypothesis is that *Snai3* has functional roles in the stromal compartment in regard to promoting an immune response. As above, this is another very testable hypothesis. One could simply introduce an inducible Cre such as *Mx1-Cre* into the already existing conditional double knockout that normally deletes *Snai3* only in the hematopoietic system (1). If stromal expression of *Snai3* is crucial for autoimmunity, the administration of poly(I:C) and subsequent stromal deletion of *Snai3* would be "curative" for cDKO mice. Given that this is an interferon-inducible system, "leaky" expression may occur as disease progresses in the cDKO. As such, an alternative inducible system would be required (e.g., Doxycycline-inducible). However, if this scenario is true then how does Snai3 function in the stroma to regulate an immune response?

Given the history of Snail proteins, the most likely contribution may be in immune cell migration and localization. The Immunological Genome Project (ImmGen) has collected data from multiple cell types including stromal cells from secondary lymphoid organs. Analysis of fibroblastic reticular cells has demonstrated a significant level of *Snai3* expression. These cells are key determinants of secondary lymphoid structure and immune function through the expression of various chemokines such as CXCL12, CCL19, and CCL21 (2-4). Interestingly enough, these cytokines can induce Snail expression through CXCR4 and CCR7 signaling setting the stage for a stromal/hematopoietic interdependence on Snail factors (5, 6). Previous data have demonstrated that

Snai3 is also a repressor of E-cadherin (7). Keratinocytes in the mouse dermis express E-cadherin. The inappropriate expression of E-cadherin would thus result in the sequestration and tolerization of Langerhans cells (LC), a specialized dendritic cell subset (8). Mechanistically, this occurs through homotypic interactions with LC-expressed E-cadherin (9). Additional work has since shown that crosslinking of β-catenin by E-cadherin induces a toleragenic state in dendritic cells through the blockade of costimulatory molecules such as B7 (10). Considering these data, it becomes easy to see how the stromal deletion of *Snai3* on top of the loss of *Snai2* would potentiate an immunosuppressive environment.

Contributing Cell Types and Gene Targets

Snai2/Snai3 conditional double knockout mice develop a fatal autoimmunity that includes both IgM and IgG isotypes. This suggests a loss of both B and T cell tolerance. Additionally, these phenotypes were reversible upon the adoptive transfer of wildtype regulatory T cells (T_{Regs}) indicative of a cDKO T_{Reg} defect. Unlike *Rag2*$^{-/-}$ recipients, wildtype animals that received cDKO bone marrow did not develop autoimmunity due to residual radioresistant T_{Regs}. PCR-based genotyping of cell populations demonstrated that approximately seventy-five percent of conventional T cells (T_{Conv}) were derived from cDKO bone marrow (Pioli et al. unpublished data). In stark contrast, only roughly twenty-five percent of T_{Regs} were derived from cDKO donor cells. These data further support the idea that cDKO T_{Regs} are defective compared to their wildtype counterparts. Currently, these experiments are being repeated with *Ubc-GFP* mice. This will

allow for a more accurate quantification of donor cell contribution as the source of T_{Regs} ($CD4^+$ $CD25^+$) can be identified by GFP expression. More importantly, cDKO T_{Regs} can be isolated for the purpose of transcriptional profiling using RNA sequencing (RNA-Seq). These experiments will be fundamental in understanding how the loss of *Snai2* and *Snai3* affects the T_{Reg} transcriptional program and thus, cellular function.

Our initial evaluation of cDKO mice demonstrated a propensity to generate autoantibodies that targeted cell surface antigens. This suggested impaired B cell central tolerance as B cells would normally be expected to undergo negative selection. This would prevent peripheral recognition of surface exposed self-antigens and the induction of autoimmunity. Rather interestingly, transplant of cDKO marrow into *Rag2*$^{-/-}$ animals that had intact *Snai2* alleles demonstrated a shift in autoantibody reactivity. These animals generated a high level of autoantibodies that recognized intracellular self-antigens but with almost a complete absence of reactivity to surface antigens. Since these animals still possessed *Snai2*, the results suggested that deletion of *Snai2* might have led to inappropriate expression of self-antigens in the periphery thus shifting the autoantibody repertoire. Additionally, recipients of cDKO marrow did not die due to disease by nine weeks posttransplant. This result is indicative of a limited scope (or progression) of disease; an interpretation supported by the autoantibody data. Additionally, the germline deletion of *Snai2* (an anti-apoptotic gene) may sensitize mice to cell death as a result of autoimmune-induced inflammation. Overall, the data hint to a role for the stromal deletion of *Snai2* as

a disease accelerator rather than an initiator. It is important to note that we were not able to compare the transplantation of cDKO bone marrow into both *Rag2*$^{-/-}$ and *Rag2*$^{-/-}$ *Snai2*$^{-/-}$ mice so it impossible to draw too firm of conclusions in regards to the differences between the intact, or "whole" cDKO and *Rag2*$^{-/-}$ recipients receiving cDKO bone marrow. Further studies will be needed to fully assess these questions.

Given all this, it becomes tempting to speculate that T_{Regs} are the only hematopoietic cells intrinsically responsible for cDKO autoimmunity. Although not readily appreciated, T_{Regs} are important mediators of peripheral B cell tolerance as well as that of T cells (11, 12). Importantly, cDKO B cells were ultimately susceptible to regulation by wildtype regulatory T cells. One way to assess this question will be to generate strains that delete *Snai3* just in T_{Regs} (i.e., *Foxp3-Cre*) and delete *Snai3* in both T_{Regs} and B cells (i.e., *Foxp3-Cre* and *Mb-1-Cre* combined). If both strains demonstrate similar disease severity, then it can be concluded that T_{Reg} dysfunction is the essential, and main, component of the *Snai2/Snai3* cDKO autoimmune model. Similar types of comparisons can be made using alternatives such as *Cd4-Cre* to specifically delete *Snai3* in T cells while leaving the B cell compartment intact.

Snai1 **in Hematopoiesis**

The body of work presented here has focused on *Snai2* and *Snai3*. However, the role of *Snai1* in hematopoiesis is unknown. Current work in our lab has demonstrated that the conditional deletion of *Snai1* via *Vav-Cre* (1cKO) has very few consequences at steady state. Perhaps this is not surprising given the

overlapping expression pattern of *Snai1* and *Snai3* in both B and T cells (Chapter 3) (13). As such, the effort to generate and characterize *Snai1/Snai3* conditional double knockout mice is underway.

Still, maybe a lack of *Snai1* cKO phenotypes is not due to redundancy. Rather, *Snai1* may play a subtler role that requires the system under study to be stressed before a phenotype is evident. *Snai1* is a critical mediator of differentiation during early embryonic stem cell differentiation (14). Previous work in the immune system has shown a crucial role for *Snai2* as a progenitor stress "response" gene (15, 16). So does *Snai1* play a similar role in hematopoietic stem cells (HSCs)? HSCs require strict control of programs driving self-renewal and differentiation in order to properly respond to cellular demands such as infection while also maintaining a long-term progenitor pool (17, 18). As such, it is appropriate to analyze this potential function for *Snai1* under conditions of stress. This can be done by the administration of sublethal doses of irradiation or the provision of 5-fluorouracil (5-FU), both of which would induce the need to replenish blood cells. From there, one can assay the ability of *Snai1* cKO mice to reconstitute various lineages while also maintaining a long-term HSC pool. These assays mainly focus on progenitor biology. However, it is important to consider how *Snai1* might function in mature lineages.

Transcriptional profiling suggests that *Snai1* may play a role in mature lymphocyte populations. Recently, it has been shown that NR2F6 is a key repressor of T helper 17 (T_H17) cell differentiation (19, 20). Biochemical analysis demonstrated a direct repression of NR2F6 function as a result of PKC-mediated

phosphorylation. Of interest, pathways induced by T cell receptor signaling such as AKT and ERK signaling have been shown to induce Snai1 in other model systems (5, 21). Additionally, it has been shown that Snai1 negatively regulates adipocyte differentiation through the direct repression of *Nr2f6* (22). This leads one to speculate that Snai1 may be upregulated in T_H17 cells in order to suppress Nr2f6 at the gene level, essentially creating a T_H17 feed forward loop. This becomes more reasonable when one considers the fact that IL-17 induces *Snai1* expression in multiple myeloma (23). Whatever the roles of Snai1 turn out to be, surely they will add to the ever-growing contributions of the Snail family to hematopoiesis.

References

1. Gudmundsson, K. O., K. Oakley, Y. Han, and Y. Du. 2014. Analyzing gene function in adult long-term hematopoietic stem cells using the interferon inducible Mx1-Cre mouse system. *Methods in Molecular Biology* 1194: 313-325.

2. Alvarenga, H. G., and L. Marti. 2014. Multifunctional roles of reticular fibroblastic cells: more than meets the eye? *Journal of Immunology Research* 2014: 402038.

3. Cremasco, V., M. C. Woodruff, L. Onder, J. Cupovic, J. M. Nieves-Bonilla, F. A. Schildberg, J. Chang, F. Cremasco, C. J. Harvey, K. Wucherpfennig, B. Ludewig, M. C. Carroll, and S. J. Turley. 2014. B cell homeostasis and follicle confines are governed by fibroblastic reticular cells. *Nature Immunology* 15: 973-981.

4. Suenaga, F., S. Ueha, J. Abe, M. Kosugi-Kanaya, Y. Wang, A. Yokoyama, Y. Shono, F. H. Shand, Y. Morishita, J. Kunisawa, S. Sato, H. Kiyono, and K. Matsushima. 2015. Loss of lymph node fibroblastic reticular cells and high endothelial cells is associated with humoral immunodeficiency in mouse graft-versus-host disease. *Journal of Immunology* 194: 398-406.

5. Lv, B., X. Yang, S. Lv, L. Wang, K. Fan, R. Shi, F. Wang, H. Song, X. Ma, X. Tan, K. Xu, J. Xie, G. Wang, M. Feng, and L. Zhang. 2014. CXCR4 signaling induced epithelial-mesenchymal transition by PI3K/AKT and ERK pathways in glioblastoma. *Molecular Neurobiology*.

6. Zhang, J., Y. Zhou, and Y. Yang. 2015. CCR7 pathway induces epithelial-mesenchymal transition through up-regulation of Snail signaling in gastric cancer. *Medical Oncology* 32: 467.

7. Gras, B., L. Jacqueroud, A. Wierinckx, C. Lamblot, F. Fauvet, J. Lachuer, A. Puisieux, and S. Ansieau. 2014. Snail family members unequally trigger EMT and thereby differ in their ability to promote the neoplastic transformation of mammary epithelial cells. *PloS One* 9: e92254.

8. Van den Bossche, J., B. Malissen, A. Mantovani, P. De Baetselier, and J. A. Van Ginderachter. 2012. Regulation and function of the E-cadherin/catenin complex in cells of the monocyte-macrophage lineage and DCs. *Blood* 119: 1623-1633.

9. Riedl, E., J. Stockl, O. Majdic, C. Scheinecker, W. Knapp, and H. Strobl. 2000. Ligation of E-cadherin on in vitro-generated immature Langerhans-type dendritic cells inhibits their maturation. *Blood* 96: 4276-4284.

10. Jiang, A., O. Bloom, S. Ono, W. Cui, J. Unternaehrer, S. Jiang, J. A. Whitney, J. Connolly, J. Banchereau, and I. Mellman. 2007. Disruption of E-cadherin-mediated adhesion induces a functionally distinct pathway of dendritic cell maturation. *Immunity* 27: 610-624.

11. Gotot, J., C. Gottschalk, S. Leopold, P. A. Knolle, H. Yagita, C. Kurts, and I. Ludwig-Portugall. 2012. Regulatory T cells use programmed death 1 ligands to directly suppress autoreactive B cells in vivo. *Proceedings of the National Academy of Sciences of the United States of America* 109: 10468-10473.

12. Leonardo, S. M., J. A. Josephson, N. L. Hartog, and S. B. Gauld. 2010. Altered B cell development and anergy in the absence of Foxp3. *Journal of Immunology* 185: 2147-2156.

13. Pioli, P. D., T. J. Dahlem, J. J. Weis, and J. H. Weis. 2013. Deletion of Snai2 and Snai3 results in impaired physical development compounded by lymphocyte deficiency. *PloS One* 8: e69216.

14. Galvagni, F., C. Lentucci, F. Neri, D. Dettori, C. DeClemente, M. Orlandini, F. Anselmi, S. Rapelli, M. Grillo, S. Borghi, and S. Oliviero. 2014. Snai1 promotes ESC exit from the pluripotency by direct repression of self-renewal genes. *Stem Cells*.

15. Inoue, A., M. G. Seidel, W. Wu, S. Kamizono, A. A. Ferrando, R. T. Bronson, H. Iwasaki, K. Akashi, A. Morimoto, J. K. Hitzler, T. I. Pestina, C. W. Jackson, R. Tanaka, M. J. Chong, P. J. McKinnon, T. Inukai, G. C. Grosveld, and A. T. Look. 2002. Slug, a highly conserved zinc finger transcriptional repressor, protects hematopoietic progenitor cells from radiation-induced apoptosis in vivo. *Cancer Cell* 2: 279-288.

16. Wu, W. S., S. Heinrichs, D. Xu, S. P. Garrison, G. P. Zambetti, J. M. Adams, and A. T. Look. 2005. Slug antagonizes p53-mediated apoptosis of hematopoietic progenitors by repressing puma. *Cell* 123: 641-653.

17. Passegue, E., A. J. Wagers, S. Giuriato, W. C. Anderson, and I. L. Weissman. 2005. Global analysis of proliferation and cell cycle gene expression in the regulation of hematopoietic stem and progenitor cell fates. *The Journal of Experimental Medicine* 202: 1599-1611.

18. Wilson, A., E. Laurenti, G. Oser, R. C. van der Wath, W. Blanco-Bose, M. Jaworski, S. Offner, C. F. Dunant, L. Eshkind, E. Bockamp, P. Lio, H. R. Macdonald, and A. Trumpp. 2008. Hematopoietic stem cells reversibly switch from dormancy to self-renewal during homeostasis and repair. *Cell* 135: 1118-1129.

19. Hermann-Kleiter, N., and G. Baier. 2014. Orphan nuclear receptor NR2F6 acts as an essential gatekeeper of Th17 CD4+ T cell effector functions. *Cell Communication and Signaling : CCS* 12: 38.

20. Hermann-Kleiter, N., T. Gruber, C. Lutz-Nicoladoni, N. Thuille, F. Fresser, V. Labi, N. Schiefermeier, M. Warnecke, L. Huber, A. Villunger, G. Eichele, S. Kaminski, and G. Baier. 2008. The nuclear orphan receptor NR2F6 suppresses lymphocyte activation and T helper 17-dependent autoimmunity. *Immunity* 29: 205-216.

21. Yu, H., L. Zhang, and P. Liu. 2014. CXCR7 signaling induced epithelial-mesenchymal transition by AKT and ERK pathways in epithelial ovarian carcinomas. *Tumour Biology: The Journal of the International Society for Oncodevelopmental Biology and Medicine*.

22. Pelaez-Garcia, A., R. Barderas, R. Batlle, R. Vinas-Castells, R. A. Bartolome, S. Torres, M. Mendes, M. Lopez-Lucendo, R. Mazzolini, F. Bonilla, A. G. de Herreros, and J. I. Casal. 2015. A proteomic analysis reveals that Snail regulates the expression of the nuclear orphan receptor nuclear receptor subfamily 2 group F member 6 (Nr2f6) and interleukin 17 (IL-17) to inhibit adipocyte differentiation. *Molecular & Cellular Proteomics: MCP* 14: 303-315.

23. Sun, Y., J. Pan, S. Mao, and J. Jin. 2014. IL-17/miR-192/IL-17Rs regulatory feedback loop facilitates multiple myeloma progression. *PloS One* 9: e114647.

APPENDIX A

SNAIL TRANSCRIPTION FACTORS IN HEMATOPOIETIC CELL DEVELOPMENT: A MODEL OF FUNCTIONAL REDUNDANCY

ELSEVIER

CrossMark

Experimental Hematology

Experimental Hematology 2014;42:425–430

REVIEW

Snail transcription factors in hematopoietic cell development: A model of functional redundancy

Peter D. Pioli and John H. Weis

Division of Cell Biology and Immunology, Department of Pathology, University of Utah, Salt Lake City, UT, USA

(Received 9 January 2014; revised 5 March 2014; accepted 7 March 2014)

Coordinated gene expression is crucial in facilitating proper lymphoid cell development and function. The precise patterns of gene expression during B- and T-cell development are regulated through a complex interplay between a multitude of transcriptional regulators, both activators and repressors. We have recently identified the Snail family of transcription factors as playing significant and overlapping roles in lymphoid cell development, in that deletion of both *SNAI2* and *SNAI3* was required to fully impact the generation of mature T and B cells. Analyses using compound heterozygote animals further demonstrated that *SNAI2* and *SNAI3* were partially haplosufficient and relatively equivalent in their ability to preserve B-cell generation in the bone marrow. In this review, we summarize studies elucidating the role of the Snail family in hematopoiesis, with a focus on lymphoid cell development. Using the Snail family as an example, we discuss the concepts of functional redundancy and strategies employed to assay transcription factor families for intramember compensation.

Embryonic development along with the development of cell lineages with specialized functions requires a properly orchestrated network of gene expression. The Snail family is a primordial metazoan collection of transcriptional regulators consisting of three members: SNAI1 (Snail), SNAI2 (Slug) and SNAI3 (Smuc) [1,2]. Snail family members function as transcriptional repressors. To carry out this function, all three members share two cardinal features. Within the C-terminal portions of each protein reside multiple C_2H_2-type zinc finger DNA-binding domains (DBDs). SNAI1 possesses four DBDs; both SNAI2 and SNAI3 possess five [3]. These DBDs recognize the consensus E-box sequence, CANNTG. In particular, Snail proteins show a strong preference for GC-rich central dinucleotides [4]. At the extreme N-terminus, each protein contains a Snail/Gfi1 (SNAG) domain [5]. Using this domain, the recruitment of various chromatin corepressor modifiers leads to the generation of a transcriptionally silent state. Examples of such modifiers include histone deacetylases (HDACs), such as HDACs 1 and 2, lysine-specific demethylases (e.g., LSD1), and methyltransferases (e.g., EZH2) [6,7].

The Snail family has been demonstrated to participate in a wide variety of physiologic and pathologic processes [8,9]. The founding member, *SNAI1*, was first described in *Drosophila melanogaster* and was shown to be essential in the developing embryo for proper ventral-dorsal patterning, leading to eventual mesoderm formation [10,11]. Analogous to *Drosophila*, deletion of murine *SNAI1* results in embryonic lethality due to gastrulation defects [12]. This points to an evolutionarily conserved role for *SNAI1* in the developing embryo. Deletion of *SNAI1* at the epiblast stage also resulted in embryonic lethality, in this instance due to global defects in vascularization [13]. Continuing to focus on the murine system, deletion of *SNAI2* did not result in organismal catastrophe. *SNAI2* germline knockout mice possess impaired physical and hair follicle developmental kinetics most readily observed in the preweaning period [14,15]. On select genetic backgrounds, these mice develop piebaldism (suggestive of defective melanocyte function) and symptoms analogous to Type II Waardenburg syndrome (characterized by hearing loss and skin or hair pigment

Offprint requests to: Dr. John H. Weis, Division of Cell Biology and Immunology, Department of Pathology, University of Utah School of Medicine, 15 North Medical Drive East, Salt Lake City, UT 84112; E-mail: john.weis@path.utah.edu

0301-472X/$ - see front matter.
http://dx.doi.org/10.1016/j.exphem.2014.03.002

anomalies) [16]. Importantly, a functional redundancy between SNAI1 and SNAI2 in both chondrogenesis and cranial-facial development has been previously shown [17,18]. Recently, two laboratories, including our own, have described the generation of *SNAI3*-deficient animals. Unlike both *SNAI1* and *SNAI2*, no phenotypes were apparent upon the deletion of only *SNAI3* [19,20]. Our studies, however, additionally analyzed the loss of SNAI3 in the context of a SNAI2-deficient animal, a germline double knockout (DKO), which resulted in clear developmental abnormalities [20]. Some of these included severe runting with an overall failure to thrive and a definitive skewing toward generation of the male sex. Additionally, multiple lymphopoietic abnormalities were apparent only upon deletion of both genes (discussed below). This data supported a physiologic role for *SNAI3*, along with a continued theme of functional redundancy among various Snail members.

The Snail family and hematopoiesis

At this time, there is no data elucidating the role of *SNAI1* within the hematopoietic system. Recently, we have generated a hematopoietic-specific deletion of *SNAI1* via the *Vav-Cre* deleter strain and a strain possessing a conditionally targeted *SNAI1* gene. Unlike embryogenesis, *SNAI1* is not required for hematopoiesis, since these conditional *SNAI1*-deleted mice are viable, outwardly healthy, and with no obvious hematopoietic deficiencies (Pioli., unpublished). A more detailed analysis of these mice is underway.

For the rest of this article, we shift our focus to the hematopoietic functions of both SNAI2 and SNAI3. In an initial report, Inukai et al. demonstrated overexpression of SNAI2 in several human B-cell leukemia cell lines. Upregulation of *SNAI2* was dependent upon the E2A-HLF oncoprotein generated from a t(17;19) chromosomal translocation. Usage of the murine interleukin (IL)-3–dependent BaF3 pro-B-cell line demonstrated that overexpression of SNAI2 was sufficient to confer resistance to apoptosis induced by growth factor withdrawal, which was accompanied by exit from the cell cycle [21]. Regarding cancer progression, SNAI2 and SNAI1 are most commonly identified for their ability to induce epithelial-to-mesenchymal transition, resulting in a more migratory and invasive cancer phenotype. This result suggested an alternative mechanism for the survival of transformed cells. Equally significantly, these data may point to a role for SNAI2 in chemotherapeutic resistance. This is most relevant for DNA-damaging agents, such as Doxorubicin, which are most effective in actively cycling cells. Interestingly, Perez-Losada et al. demonstrated the ability of c-Kit signaling to induce *SNAI2* expression. In vitro studies utilized both BaF3 and LAMA-84 cells overexpressing c-Kit. Of note, LAMA-84 cells were originally derived from a chronic myeloid leukemia (CML) patient undergoing blast crisis [22]. The mechanism of *SNAI2* upregulation becomes relevant when one considers that c-Kit is highly expressed on the surface of acute myeloid leukemia (AML) cells [23,24]. For this study, we did not conduct any experiments to assess the downstream consequences of *SNAI2* induction in LAMA-84 cells. Overall, these data provided some interesting insights into the potential role of the Snail family in promoting hematologic malignancies.

Moving forward, the point of emphasis shifted toward the role of SNAI2 in more physiologic hematopoietic settings. The Perez-Losada report included an initial description of hematopoiesis in the *SNAI2* knockout mouse. They observed multiple defects, which mainly related to erythropoiesis [14]. Complete blood counts showed a trend toward lower erythroid output. Using in vivo models of phenylhydrazine (PHZ)- and pregnancy-induced anemia, a lower percentage of $Ter119^{+}$ cells was observed in the spleen. This pointed to a role for *SNAI2* in hematopoietic stress responses as well as to its requirement in reconstituting the erythroid lineage. Intriguingly, $SNAI2^{+/-}$ animals showed similar defects to the $SNAI2^{-/-}$, suggesting a gene dosage component. Examination of steady state hematopoiesis did not show any derivation from normal myeloid and B-cell generation. However, a decreased ratio of developing CD4 and CD8 double positive thymocytes was observed in *SNAI2* knockout animals. This was apparently a result of increased apoptosis, as assayed by terminal deoxynucleotidyl transferase dUTP nick end labeling (TUNEL) staining of thymic cross sections. Almost immediately following this publication, a separate study from the Look lab [14] showed the expression of *SNAI2* in multiple bone marrow progenitor lineages, including the hematopoietic stem cell (HSC), both long term and short term, common lymphoid progenitors, and common myeloid progenitors, among others. Colony forming assays were performed to evaluate the differentiation potential of progenitors in the bone marrow and spleen. Although the $SNAI2^{-/-}$ progenitors trended toward an increase in colony forming units for various lineages, no clear enhancement over wildtype (WT) was observed. Expanding on this, the researchers assayed the ability of $SNAI2^{-/-}$ animals to reconstitute the hematopoietic compartment as a stress response following a median lethal dose of total body irradiation [25]. By 13 days after irradiation, all $SNAI2^{-/-}$ animals had died due to pancytopenia. This contrasted starkly with the outcome for both WT and $SNAI2^{+/-}$ animals, among whom approximately 50% survival was observed after 29 days. Closer examination of these animals demonstrated increased apoptosis within the $SNAI2^{-/-}$ lineage negative bone marrow, leading to the pancytopenia. As such, administration of a thrombopoietin analog rescued irradiation-induced lethality among $SNAI2^{-/-}$ animals. Using bone marrow chimeras, a follow-up study demonstrated that loss of *SNAI2* in the hematopoietic compartment was sufficient to propagate the irradiation phenotype described above [26]. Importantly, WT bone marrow administered to a $SNAI2^{-/-}$ host completely

prevented any lethality, providing further evidence for a hematopoietically cell-intrinsic role for *SNAI2* that was independent of the surrounding bone marrow stroma. Using a well-designed combination of knockout and transgenic animals, it was shown that SNAI2 functioned downstream of p53 to block the activation of the p53 upregulated modulator of apoptosis (PUMA), a pro-apoptotic Bcl-2 homology 3 (BH3)-only family member. This was accomplished via a direct E-box interaction within intron 1 of the *Puma* gene. Somewhat surprisingly, this effect was specific to PUMA, as *SNAI2*$^{-/-}$ *Puma*$^{-/-}$ compound knockout animals were completely radio-resistant. If other apoptotic mediators were playing a role, an intermediate phenotype would have been expected. Finally, a group led by Wen-Shu Wu examined the self-renewal capacity of hematopoietic stem cells with and without *SNAI2* [27]. Using limiting dilution bone marrow chimera transplants, it was determined that *SNAI2*$^{-/-}$ marrow possessed an approximately eightfold higher repopulation efficiency as compared with *SNAI2*$^{+/-}$. Competitive serial transplantation, a gold standard for assessing HSC fidelity, further demonstrated the enhanced ability of the *SNAI2*$^{-/-}$ HSC to reconstitute the entire hematopoietic system. Incorporation of 5-ethynyl-2′-deoxyuridine (Edu), combined with Annexin V cell surface staining, demonstrated that this result was a consequence of higher proliferative capacity rather than augmented apoptosis within the *SNAI2*$^{-/-}$ lineage negative stem cell antigen-1 (Sca1)$^{+}$ compartment. This result is consistent with the previously identified ability of SNAI2 overexpression to induce cell cycle exit by BaF3 cells [21]. Although the molecular targets of SNAI2 were not identified, they may be similar to what has been previously observed for SNAI1. In a nontumorigenic context, SNAI1 is able to inhibit the cell cycle of Madin-Darby canine kidney (MDCK) cells by repressing cyclin D2 at the transcriptional level [28]. A noncanonical role for the Snail family has also been reported, namely, that SNAI1 coassociated with early growth response protein 1 (EGR-1) and SP-1 to upregulate p15INK4b, leading to the arrest of HepG2 cells [29].

The function of the SNAI3 transcriptional regulator in the hemaotopoietic system was first analyzed in an indirect investigation: the analysis of binding proteins to negative regulator elements of the murine *Itgb2l* (Pactolus) gene [30]. Using a combination of electrophoretic mobility shift assay (EMSA) and supershift assays, it was shown that SNAI3 was capable of binding to these transcriptional regulatory sites. The most intriguing aspect of this work was the hypothesis that, in scenarios where diverse cell types, such as B cells and neutrophils, express a common transcriptional activator (e.g., PU.1), differential expression of a negative regulator may augment lineage-specific expression of downstream genes. Thinking more broadly, Dahlem et al. asked whether retroviral-induced overexpression of *SNAI3* in a bone marrow chimera model was capable of impairing hematopoiesis. Using c-Kit– and Sca-1–based analysis of lineage-depleted marrow, it was determined that overexpression of *SNAI3* did not alter ratios of various subsets of hematopoietic progenitors [31]. However, inspection of peripheral blood demonstrated a clear loss of B- and T-cell lineages in cells that were infected with the *SNAI3*-expressing retrovirus (as assayed by green fluorescent protein [GFA] expression). This effect was dose-dependent, as B- and T-cell populations were present when SNAI3 overexpression was at a modest amount (GFP low). Importantly, B and T cells were present when the empty vector was expressed at both low and high levels, providing evidence against any retroviral-induced artifacts. These data suggested that SNAI3 was either capable of saturating endogenous E-boxes necessary for the proper bifurcation of lymphoid and myeloid lineages or capable of directly repressing gene expression by the recruitment of transcriptional control complexes. This data also alluded to a requirement for precise regulation of *SNAI3* within the hematopoietic system.

Phenotypic analysis of animals lacking both SNAI2 and SNAI3 transcription factors

Two groups recently described the deletion of the *SNAI3* gene using both conditional and germline deletion models. Upon deletion of *SNAI3*, no effects were observed in any hematopoietic lineage assayed [19,20]. Indeed, the *SNAI3*$^{-/-}$ strains created by both groups displayed few to no phenotypic changes compared with WT. Gene expression analysis of *SNAI1*, *SNAI2*, and *SNAI3* in bone marrow–derived lineages demonstrated widespread *SNAI1* expression in T and B precursor and mature cells, as well as cells of the myeloid lineage [20]. *SNAI2* expression was more limited, with the highest levels of transcripts found in immature bone marrow cells (B220^{-} and CDllb^{-} cells) and double negative (DN) (CD4^{-}CD8^{-}) T cells of the thymus. *SNAI3* expression was highest in the DN, the double positive (CD4^{+}CD8^{+}), and the CD8^{+} cells of the thymus and spleen. The potential of the Snail family of proteins to functionally complement one another led us to create and analyze a germline DKO animal lacking both the *SNAI2* and *SNAI3* genes [20] (the absence of *SNAI1* in the germline creates an embryonic lethality [13]). In this animal, we observed multiple hematopoietic and nonhematopoietic phenotypes, all of them greater than that found in the single *SNAI2*$^{-/-}$ or *SNAI3*$^{-/-}$ animals. The DKO animals were distinctly smaller than the single deficient animals and had significantly smaller spleens and thymuses, which possessed morphologic distortions. The most striking hematologic phenotype of the DKO animals was a loss of B cells in the bone marrow.

This was correlated with an expanded myeloid compartment. In the DKO thymus, double positive thymocytes were reduced in favor of enhanced percentages of CD4 single positive T cells. Unlike in the marrow, skewing of thymocyte populations displayed variable penetrance. Analysis of compound heterozygotes suggested that, on a per allele basis, one

allele of either *SNAI2* or *SNAI3* equivalently compensated for the loss of the other three alleles. The DKO animals possessed a normal *SNAI1* gene, which is transcriptionally active in immature B- and T-cell subsets. As such, incomplete complementation of the DKO animal via SNAI1 may have continued to mask the full dependence of hematopoietic cell development on members of the Snail family.

One of the unanswered questions from our recent study was the level of stromal contribution to the phenotypes observed. Development of both B and T cells is dependent upon proper organization within their respective sites of generation. For example, pre-pro-B and pro-B cells congregate in bone marrow niches high in C-X-C motif ligand 12 (CXCL12) and IL-7, respectively [32]. In contrast, pre-B cells were not found to associate with either zone, suggesting that precise localization is required for the proper progression along each stage of B-cell maturation. Histologic examination of the germline *SNAI2* and *SNAI3* DKO bone marrow to assess B-cell localization has not been performed. However, as mentioned above, the analysis of thymic cross sections from DKO mice showed gross alterations in overall architecture [20]. In DKO mice, intense hematoxylin staining was observed in the region corresponding to the thymic medulla, the site of single positive thymocyte negative selection. Normally, the thymic cortex demonstrates the highest intensity of hematoxylin staining due to high numbers of CD4 and CD8 double positive thymocytes. Since double positive thymocytes were still the majority population in the DKO thymus, this suggests against preferential staining of an overexpanded single positive compartment. Rather, this may suggest a dysfunctional organization of the thymus due to altered chemokine signaling. Multiple studies have demonstrated the importance of stromal-derived CCL25 and P-selectin in thymic homing and organization [33,34]. Interestingly, competitive bone marrow chimeras using WT and *CCR9*$^{-/-}$ donor marrow revealed deficiencies in *CCR9*$^{-/-}$ thymocyte development that mirrored many of the phenotypes observed upon thymic stromal-specific deletion of *Il7* [35]. This points to a role for CCL25, not only in thymic homing, but perhaps also in positioning developing thymocytes in the proximity of survival/proliferative signals such as IL-7. Given the known role of the Snail family in cellular migration (i.e., gastrulation and epithelial-to-mesenchymal transition), it is possible that the contributions of this family to lymphocyte development include a role in lymphocyte migration. This function would assist in orchestrating lymphocyte maturation by allowing a cell at any given developmental stage to receive signals required for its survival and continued differentiation. Due to the lack of an animal model possessing a *SNAI2* conditional allele, the examination of stromal contributions in providing organizational and/or survival signals will require the use of bone marrow chimera models. Although inconvenient due to such factors as length of time for functional reconstitution, these studies may provide the most flexibility in assaying the stromal versus hematopoietic function of each Snail gene. In this sense, one has the option of selectively deleting *SNAI2* in the stroma while also deleting *SNAI3* in just the hematopoietic compartment and vice versa. Experiments such as these would be virtually impossible using current recombinase deleter strains.

Functional redundancy in the snail gene family

The requirement of *SNAI2* deletion to unveil a role for *SNAI3* in hematopoiesis was somewhat surprising. Traditional thinking has held that, by deleting a particular gene, researchers could, based on the resulting phenotypes, deduce the function of the deleted genes, rather than the function of other genes. However, gene function may not be as simple and linear as traditional thinking assumes, especially regarding multigene families of transcription factors. The question, then, is: can the need for compound knockouts be predicted? The answer is most likely not a simple 'yes' or 'no.' When dealing with a multigene family like Snail, one might transcriptionally profile the cell or tissue type of interest for overlapping expression. Although coexpression of multiple Snail members may suggest a potential for redundancy, it does not exclude the possibility that each factor has a completely independent function for within a given cell. Conversely, nothing can be concluded on the basis of a lack of coexpression. This was demonstrated for *SNAI1* and *SNAI2* during chondrogenesis [18]. In the steady state, *SNAI1* and *SNAI2* were expressed mutually exclusively within hypertrophic and proliferating chondrocytes, respectively. However, deletion of *SNAI1* resulted in expression of *SNAI2* in hypertrophic chondrocytes, and vice versa. It was later shown that SNAI1 and SNAI2 could repress one another at the level of transcription [36]. In that circumstance, analysis of single knockouts provided the evidence for a compound knockout approach.

Within hematopoiesis, functional redundancy among transcription factors is not a new concept. For example, the GATA family of transcriptional regulators possesses six members, three of which (*GATA1*, *GATA2*, and *GATA3*) are highly expressed in hematopoietic lineages. Using mouse deficiency models, the lack of both *GATA1* and *GATA2* has a more profound impact upon primitive hematopoiesis during development than seen with animals lacking only one of those factors [37]. Additionally, all three Runx family members (*Runx1*, *Runx2*, and *Runx3*) are expressed in HSCs and may play redundant roles in influencing stem cell quiescence and cycling [38]. Functional redundancy for transcription factors implies common gene target recognition. However, unique protein sequences present in highly conserved family members can alter target site specificity by recruiting additional targeting factors, as demonstrated by the highly conserved members of the E26 transformation-specific (ETS) family [39].

Once a mechanism of redundancy is validated using compound knockouts, the next question is related to the mechanism. The optimal way to assess this phenomenon would be to determine the transcriptional footprint of each factor involved through the combined use of chromatin

immunoprecipitation sequencing and RNA sequencing. Chromatin immunoprecipitation sequencing will identify direct transcriptional targets, while RNA sequencing of knockout animals will identify additional indirect genetic interactions. In the case of transcriptional repressors, genes downregulated in a knockout would most likely represent an indirect regulation (i.e., derepression of another repressor). Although arduous, this approach is much more globally informative and unbiased compared with the examination of predetermined gene targets. For both forms of analyses, WT and knockout animals are required. WT animals become extremely valuable in their ability to tell us what happens normally (e.g., SNAI2- versus SNAI3-bound genes). Analysis of single and compound knockouts will determine the genetic extent of redundancy and may even narrow the candidate list of essential targets. Consider the following hypothetical (and oversimplified) example SNAI3 binds the *Gene X* and *Gene Y* promoters in WT pre-B cells (Fig. 1A). Upon loss of SNAI3, SNAI2 now binds only the *Gene X* promoter. As such, *Gene X* is still repressed, but now expression of *Gene Y* is enhanced with no resultant phenotype (Fig. 1B). Upon deletion of both *SNAI2* and *SNAI3*, *Gene X* is also transcriptionally enhanced, and a B-cell phenotype is now observable (Fig. 1C). This result would identify two things: (1) common and specific targets for each Snail member and (2) genes potentially responsible for phenotypes observed in the compound knockout. Of course, these scenarios become more complex as the size of the family being studied and its list of in vivo targets grow. One factor not discussed here is how dysregulated expression of known posttranslational modifiers might augment the system being studied. This may be most relevant for factors under the influence of a multitude of posttranslational modifier modalities.

Conclusions

To summarize, the Snail family consists of three evolutionarily conserved members. These factors have been most extensively studied in the fields of developmental and cancer biology. To our knowledge, the examination of how this family regulates various aspects of immunology has been minimal. It is the opinion of the authors that the role of the Snail family in hematopoiesis will prove to be much more expansive than initially realized. This conclusion is based, in part, on the recent discovery of a functional redundancy between *SNAI2* and *SNAI3* during lymphocyte development. These data also point to the evolutionary conservation of all three Snail members as a potential failsafe mechanism, allowing the fidelity of hematopoiesis in the face of single gene loss (i.e., germline or somatic mutation). This suggestion raises a provocative question: how many functions of a particular gene have not been discovered due to redundancy with another family member? To completely unveil the functions of a specific gene product may ultimately require the generation and analysis of various single and compound knockout combinations.

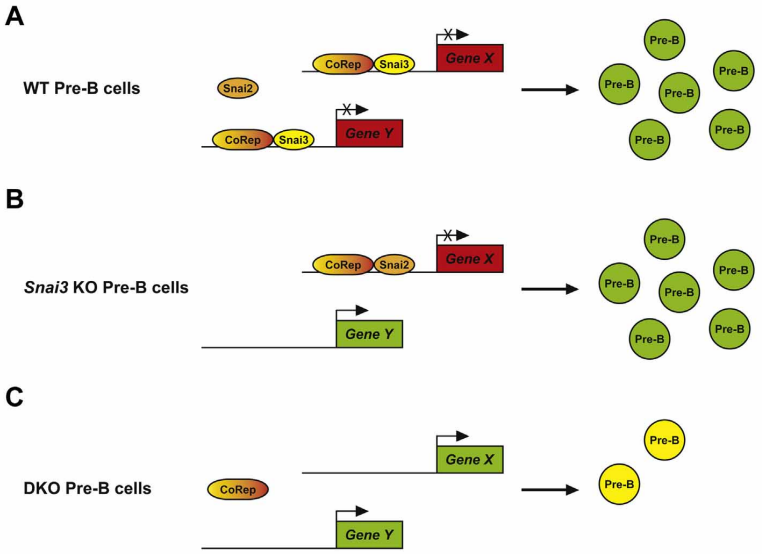

Figure 1. Redundancy model illustrating potential Snail compensation in lymphocyte development. **(A)** In a WT developing pre-B cell, SNAI3 inhibits transcription of its specific hypothetical target genes *X* and *Y* (red boxes), along with CoRep, allowing for normal development of pre-B cells. **(B)** In the absence of SNAI3, the SNAI2 protein can facilitate the transcriptional repression of *Gene X*; however, it lacks the specificity to similarly repress *Gene Y* transcription (green box). The presence of the *Gene Y* protein product does not appreciably influence the development of the pre-B cells. **(C)** The absence of both SNAI2 and SNAI3 allows for the transcription of both *Gene X* and *Gene Y*, resulting in the inhibition of the development of functional pre-B cells (yellow cells). CoRep = Corepressor protein; KO = knockout.

Acknowledgments

John H. Weis was supported by the Weber Presidential Endowed Chair and by the Department of Pathology, University of Utah (Salt Lake City, UT). Peter D. Pioli received a grant from the NIH Hematology Research Training (Grant No. T-32DK007115-38).

Conflict of interest disclosure

No financial interest/relationships with financial interest relating to the topic of this article have been declared.

References

1. Nieto MA. The snail superfamily of zinc-finger transcription factors. Nat Rev Mol Cell Biol. 2002;3:155–166.
2. Manzanares M, Blanco MJ, Nieto MA. Snail3 orthologues in vertebrates: divergent members of the Snail zinc-finger gene family. Dev Genes Evol. 2004;214:47–53.
3. Mingot JM, Vega S, Maestro B, Sanz JM, Nieto MA. Characterization of Snail nuclear import pathways as representatives of C2H2 zinc finger transcription factors. J Cell Sci. 2009;122:1452–1460.
4. Kataoka H, Murayama T, Yokode M, et al. A novel snail-related transcription factor Smuc regulates basic helix-loop-helix transcription factor activities via specific E-box motifs. Nucleic Acids Res. 2000;28:626–633.
5. Lin Y, Wu Y, Li J, et al. The SNAG domain of Snail1 functions as a molecular hook for recruiting lysine-specific demethylase 1. EMBO J. 2010;29:1803–1816.
6. Peinado H, Ballestar E, Esteller M, Cano A. Snail mediates E-cadherin repression by the recruitment of the Sin3A/histone deacetylase 1 (HDAC1)/HDAC2 complex. Mol Cell Biol. 2004;24:306–319.
7. Tong ZT, Cai MY, Wang XG, et al. EZH2 supports nasopharyngeal carcinoma cell aggressiveness by forming a co-repressor complex with HDAC1/HDAC2 and Snail to inhibit E-cadherin. Oncogene. 2012;31:583–594.
8. Bolos V, Peinado H, Perez-Moreno MA, Fraga MF, Esteller M, Cano A. The transcription factor Slug represses E-cadherin expression and induces epithelial to mesenchymal transitions: a comparison with Snail and E47 repressors. J Cell Sci. 2003;116:499–511.
9. Oram KF, Gridley T. Mutations in snail family genes enhance craniosynostosis of Twist1 haplo-insufficient mice: implications for Saethre-Chotzen Syndrome. Genetics. 2005;170:971–974.
10. Boulay JL, Dennefeld C, Alberga A. The Drosophila developmental gene snail encodes a protein with nucleic acid binding fingers. Nature. 1987;330:395–398.
11. Alberga A, Boulay JL, Kempe E, Dennefeld C, Haenlin M. The snail gene required for mesoderm formation in Drosophila is expressed dynamically in derivatives of all three germ layers. Development. 1991;111:983–992.
12. Carver EA, Jiang R, Lan Y, Oram KF, Gridley T. The mouse snail gene encodes a key regulator of the epithelial-mesenchymal transition. Mol Cell Biol. 2001;21:8184–8188.
13. Lomeli H, Starling C, Gridley T. Epiblast-specific SNAI1 deletion results in embryonic lethality due to multiple vascular defects. BMC Res Notes. 2009;2:22.
14. Perez-Losada J, Sanchez-Martin M, Rodriguez-Garcia A, et al. Zinc-finger transcription factor Slug contributes to the function of the stem cell factor c-kit signaling pathway. Blood. 2002;100:1274–1286.
15. Parent AE, Newkirk KM, Kusewitt DF. Slug (SNAI2) expression during skin and hair follicle development. J Invest Dermatol. 2010;130:1737–1739.
16. Sanchez-Martin M, Rodriguez-Garcia A, Perez-Losada J, Sagrera A, Read AP, Sanchez-Garcia I. SLUG (SNAI2) deletions in patients with Waardenburg disease. Hum Mol Genet. 2002;11:3231–3236.
17. Murray SA, Oram KF, Gridley T. Multiple functions of Snail family genes during palate development in mice. Development. 2007;134:1789–1797.
18. Chen Y, Gridley T. Compensatory regulation of the SNAI1 and SNAI2 genes during chondrogenesis. Journal of bone and mineral research: the official journal of the J Bone Miner Res. 2013;28:1412–1421.
19. Bradley CK, Norton CR, Chen Y, et al. The snail family gene snai3 is not essential for embryogenesis in mice. PLoS Curr. 2013;8:e65344.
20. Pioli PD, Dahlem TJ, Weis JJ, Weis JH. Deletion of SNAI2 and SNAI3 results in impaired physical development compounded by lymphocyte deficiency. PLoS One. 2013;8:e69216.
21. Inukai T, Inoue A, Kurosawa H, et al. SLUG, a ces-1-related zinc finger transcription factor gene with antiapoptotic activity, is a downstream target of the E2A-HLF oncoprotein. Mol Cell. 1999;4:343–352.
22. Seigneurin D, Champelovier P, Mouchiroud G, et al. Human chronic myeloid leukemic cell line with positive Philadelphia chromosome exhibits megakaryocytic and erythroid characteristics. Exp Hematol. 1987;15:822–832.
23. Cascavilla N, Musto P, D'Arena G, et al. CD117 (c-kit) is a restricted antigen of acute myeloid leukemia and characterizes early differentiative levels of M5 FAB subtype. Haematologica. 1998;83:392–397.
24. Wakita S, Yamaguchi H, Miyake K, et al. Importance of c-kit mutation detection method sensitivity in prognostic analyses of t(8;21)(q22;q22) acute myeloid leukemia. Leukemia. 2011;25:1423–1432.
25. Inoue A, Seidel MG, Wu W, et al. Slug, a highly conserved zinc finger transcriptional repressor, protects hematopoietic progenitor cells from radiation-induced apoptosis in vivo. Cancer Cell. 2002;2:279–288.
26. Wu WS, Heinrichs S, Xu D, et al. Slug antagonizes p53-mediated apoptosis of hematopoietic progenitors by repressing puma. Cell. 2005;123:641–653.
27. Sun Y, Shao L, Bai H, Wang ZZ, Wu WS. Slug deficiency enhances self-renewal of hematopoietic stem cells during hematopoietic regeneration. Blood. 2010;115:1709–1717.
28. Vega S, Morales AV, Ocana OH, Valdes F, Fabregat I, Nieto MA. Snail blocks the cell cycle and confers resistance to cell death. Genes Dev. 2004;18:1131–1143.
29. Hu CT, Chang TY, Cheng CC, et al. Snail associates with EGR-1 and SP-1 to upregulate transcriptional activation of p15INK4b. FEBJS J. 2010;277:1202–1218.
30. Hale JS, Dahlem TJ, Margraf RL, Debnath I, Weis JJ, Weis JH. Transcriptional control of Pactolus: evidence of a negative control region and comparison with its evolutionary paralogue, CD18 (beta2 integrin). J Leukoc Biol. 2006;80:383–398.
31. Dahlem T, Cho S, Spangrude GJ, Weis JJ, Weis JH. Overexpression of SNAI3 suppresses lymphoid- and enhances myeloid-cell differentiation. Eur J Immunol. 2012;42:1038–1043.
32. Nagasawa T. Microenvironmental niches in the bone marrow required for B-cell development. Nat Rev Immunol. 2006;6:107–116.
33. Gossens K, Naus S, Corbel SY, et al. Thymic progenitor homing and lymphocyte homeostasis are linked via S1P-controlled expression of thymic P-selectin/CCL25. J Exp Med. 2009;206:761–778.
34. Svensson M, Marsal J, Uronen-Hansson H, et al. Involvement of CCR9 at multiple stages of adult T lymphopoiesis. J Leukoc Biol. 2008;83:156–164.
35. Shitara S, Hara T, Liang B, et al. IL-7 produced by thymic epithelial cells plays a major role in the development of thymocytes and TCRgammadelta+ intraepithelial lymphocytes. J Immunol. 2013;190:6173–6179.
36. Chen Y, Gridley T. The SNAI1 and SNAI2 proteins occupy their own and each other's promoter during chondrogenesis. Biochem Biophys Res Commun. 2013;435:356–360.
37. Fujiwara Y, Chang AN, Williams AM, Orkin SH. Functional overlap of GATA-1 and GATA-2 in primitive hematopoietic development. Blood. 2004;103:583–585.
38. Wang CQ, Jacob B, Nah GS, Osato M. Runx family genes, niche, and stem cell quiescence. Blood Cells Mol Dis. 2010;44:275–286.
39. Hollenhorst PC, Shah AA, Hopkins C, Graves BJ. Genome-wide analyses reveal properties of redundant and specific promoter occupancy within the ETS gene family. Genes Dev. 2007;21:1882–1894.

APPENDIX B

ZFP318 REGULATES IGD EXPRESSION BY ABROGATING TRANSCRIPTION TERMINATION WITHIN THE *IGHM/IGHD* LOCUS

Reprinted from Zfp318 regulates IgD expression by abrogating transcription termination within the *Ighm/Ighd* locus. Journal of Immunology 193: 2546-2553.

Peter D. Pioli, Irina Debnath, Janis J. Weis, and John H. Weis.

The Journal of Immunology

Zfp318 Regulates IgD Expression by Abrogating Transcription Termination within the *Ighm/Ighd* Locus

Peter D. Pioli, Irina Debnath, Janis J. Weis, and John H. Weis

The protein Zfp318 is expressed during the transition of naive B cells from an immature to mature state. To evaluate its role in mature B cell functions, a conditional gene deficiency in *Zfp318* was created and deleted in bone marrow lineages via *Vav-Cre*. B cell development was minimally altered in the absence of the protein, although transitional 2 (T2) B cell populations were depressed in the absence of Zfp318. Intriguingly, the analysis of IgM and IgD expression by maturing and mature naive B cells demonstrated an elevated level of IgM gene products and a virtual loss of IgD products. Transcriptome analysis of Zfp318-deficient B cells revealed that only two gene products showed altered expression in the absence of Zfp318 (*Ighd* and *Sva*), demonstrating a remarkable specificity of Zfp318 action. In the absence of Zfp318, *Ighm/Ighd* transcripts, which would normally encode IgM and IgD from heterogeneous nuclear RNA transcripts via alternative splicing, lack intron and exon sequences from the IgD (*Ighd*)–encoding region. This finding indicates that Zfp318, in a novel manner, functions by repressing recognition of the transcriptional termination site at the 3′ end of the terminal IgM-encoding exon, allowing for synthesis of the complete *Ighm/Ighd* heterogeneous nuclear RNA. *The Journal of Immunology*, 2014, 193: 2546–2553.

The differentiation and maturation of immature transitional B cells of the marrow into mature but naive B cells requires the coordinated expression of a number of gene products (1). Pax5 and the E2 transcriptional regulators are widely regarded as central for inducing the expression of many of the early B cell–specific products (such as CD19 and IgM) in maturing marrow B cells (2, 3). Later, as B cells enter the periphery, additional transcription factors, such as Mef2c, NF-κB family members, NFAT proteins, Ciita, and Notch signaling family members, continue the differentiation of immature B cells into mature follicular (FO) or marginal zone (MZ) cells (4, 5). A number of studies have sought to define the key transcriptional regulators and kinetics that control this pathway. In one such analysis, we examined the expression of transcriptional regulators during B cell differentiation, comparing $B220^+$ B cells obtained from the marrow of 2-wk-old animals (thus lacking mature recirculating B cells), from spleens of 2-wk-old animals [enriched for transitional 1 (T1) and transitional 2 (T2) B cells], and from mature but naive spleens (enriched for FO and MZ B cells) (6). That gene expression screen identified a number of candidate transcriptional regulatory proteins whose expression increased with B cell maturation. Zfp318 was one such factor.

Division of Microbiology and Immunology, Department of Pathology, University of Utah School of Medicine, Salt Lake City, UT 84112

Received for publication May 27, 2014. Accepted for publication June 17, 2014.

This work was supported by the Department of Pathology and the Weber Presidential Endowed Chair in Immunology, by National Institutes of Health Grants AI32773 and AR45521 (to J.J.W.), and by Hematology T32 Training Grant T-32DK007115-38 M (to P.D.P. as a predoctoral trainee).

Address correspondence and reprint requests to Dr. John H. Weis, University of Utah School of Medicine, 15 North Medical Drive East, Salt Lake City, UT 84112-5650. E-mail address: john.weis@path.utah.edu

The online version of this article contains supplemental material.

Abbreviations used in this article: AR, androgen receptor; cKO, conditional knockout; FO, follicular; hnRNA, heterogeneous nuclear RNA; MFI, mean fluorescence intensity; MZ, marginal zone; NF, newly formed (B cell); RNA-Seq, RNA-sequencing; T1, transitional 1; T2, transitional 2; WT, wild type.

www.jimmunol.org/cgi/doi/10.4049/jimmunol.1401275

The *Zfp318* gene encodes a primary protein of 2237 aa that includes domains encoding two C_2H_2 zinc fingers and a myosin II-homology sequence as well as regions rich in serine and basic amino acids (7, 8). A smaller truncated form of Zfp318 has also been described in the mouse, but only the full-length form has been found as a homolog in human tissues. Zfp318 has been most extensively studied in the testes (an alternative name for the protein is testicular zinc-finger, or TZF) where it is expressed during spermatogenesis. In transfection analyses, Zfp318 was shown to augment ligand-dependent androgen receptor (AR) control in a dose-dependent fashion (9). The possibility that Zfp318 could also play a role in B cell development via the AR was suggested by a number of studies showing B cell functions dependent upon AR (10, 11). In one such study, using a B cell–specific deletion of AR, B cell development from the marrow was inhibited, accompanied by enhanced autoimmune responses, using a collagen-induced arthritis model (12).

To determine if Zfp318 does have a role in the development and function of B cells, we created a mouse with a conditional (Flox'd) deletion of the gene. Using *Vav-Cre*–dependent deletion of the gene, we have found that B cells deficient in Zfp318 developed from marrow precursors virtually identical to that of wild type (WT). Zfp318-deficient, naive splenic B cells did, however, demonstrate a dramatic loss of both IgD-specific transcripts and protein. IgM and IgD are synthesized from alternatively spliced transcripts positioning the same VDJ domains on either the IgM or the IgD constant domains (13, 14). The gene sequences encoding the IgM transcripts have been denoted *Ighm*, whereas those encoding IgD are identified as *Ighd*. The loss of IgD in the Zfp318-deficient B cell was due to the nearly exclusive use of *Ighm* transcripts to produce the IgM product owing to RNA transcript termination prior to the IgD-encoding exons. The role of Zfp318 in regulating gene products is highly specific for IgD, in that genome-wide transcriptome analysis of B cells obtained from the Zfp318-deficient animal identified only a single additional gene with significantly altered gene expression.

As our data were being prepared for submission, a report by Enders et al. (15) detailed the results of an ethylnitrosourea mutagenesis screen followed by whole-exome sequencing that identified

a single point mutation (a nonsynonymous T > C transition altering the protein sequence I1347T) within *Zfp318* that inhibited the production of IgD. This mutation mapped to the long form of the protein, confirming its necessity versus that of the alternatively spliced, truncated form of the protein. The group also created a germline *Zfp318* null animal by gene targeting that reproduced their point mutation analyses. Those data, along with the findings presented in this article, confirm the necessity of Zfp318 for the production of IgD.

Materials and Methods

Animal strains and care

Animals were housed in the Animal Resource Center (University of Utah Health Science Center, Salt Lake City, UT) according to the National Institutes of Health *Guide for the Care and Use of Laboratory Animals*. All animal protocols were reviewed and approved by the University of Utah Institutional Animal Use and Care Committee. For transcriptional profiling experiments, C57BL/6 mice were bred and maintained in house. B6.Cg-Tg (Vav1-cre)A2Kio/J mice (Stock #008449) were obtained from The Jackson Laboratory and maintained as heterozygotes. *Zfp318*$^{Fl/Fl}$ mice were bred to the *Vav-Cre* deleter strain to obtain progeny with a hematopoietic-specific deletion of *Zfp318* [conditional knockout (cKO)]. Littermates approximating 4 wk of age were used for all experiments. Numbers of animals used per experiment are noted in the figure legends.

Generation of the Zfp318$^{Fl/Fl}$ *animal*

A targeting construct for *Zfp318* was created using a 14-kb homologous fragment containing the first two exons of the gene obtained from a 129/Sv phage library. A neo targeting cassette (flanked by FRT sites) and a single LoxP site was inserted at the Hpa1 site located in the intron between exons 2 and 3. A single LoxP site was inserted at the BspE1 site 5′ of the transcription start site. 129/Sv ES clones possessing the targeted Zfp3818 gene were confirmed by Southern blot using 5′ and 3′ probes. The neo cassette was removed by a single mating to a FRT deleter strain, leaving behind the single LoxP site. Mice were bred back to C57BL/6 for 10 generations.

DNA isolation and genomic DNA PCR

For standard genotyping, ~5-mm portions of tail were boiled in 50 mM NaOH until fully dissolved. Then 1 M Tris was added to neutralize the NaOH. Following centrifugation to remove insoluble material, DNA was precipitated from supernatants, following standard ethanol precipitation guidelines. *Vav-Cre* and *Zfp318* genomic DNA PCR was performed via incorporation of [^{32}P] deoxycytidine triphosphate. Amplification products were electrophoresed in polyacrylamide sequencing gels. Products were visualized by exposure to x-ray film at −80°C. Cycling parameters are available upon request. Primer sequences are provided in Supplemental Table I.

RNA isolation, cDNA synthesis, and RT-PCR

Total RNA was isolated from cells using the QIAGEN miRNeasy Mini Kit (Cat. #217004) according to the manufacturer's instructions. Random hexamer primers (Invitrogen, Cat. #58875) were used in combination with SuperScript III Reverse Transcriptase (Invitrogen, Cat. #56575) to synthesize cDNA. Reactions were purified using the Thermo Scientific GeneJET Purification Kit (Cat. #K0702). Quantitative RT-PCR was performed using LightCycler (Roche Diagnostics) technology. When appropriate, products were electrophoresed in 2% agarose gels. All transcript values are shown as mean values ± SEM relative to β-actin. Cycling parameters are available upon request. Primer sequences are provided in Supplemental Table I.

FACS analysis and sorting of hematopoietic cell populations

Upon dissection, the plunger of a 5-ml syringe was used to dissociate thymus and spleen tissues. Cells were strained through a 100-μm filter and collected in 10 ml FACS buffer (1× PBS + 0.1% BSA). Bone marrow was collected from both femurs and tibias. Removing the ends of each bone with a razor blade exposed bone cavities. Marrow was flushed from cavities using a 5/8-inch 25-gauge syringe and FACS buffer. Contents were collected in 8 ml FACS buffer. After centrifugation, erythrocytes were lysed on ice for 10 min using ACK buffer. Following lysis, cells were respun, resuspended in FACS buffer, and counted using a hemocytometer. Cells were stained on ice for 30 min using the appropriate Ab mixture. Samples were washed with FACS buffer, centrifuged, and resuspended in FACS buffer. To discriminate between live and dead cells, DAPI was added at a final concentration of 3 μm. The Abs used with their indicated dilutions are available in Supplemental Table I. Population analysis was performed on the FACSCanto II (BD Biosciences), and results for a given cell type are graphically represented as mean values ± SEM of total live cells or ratios of live cells analyzed per tissue. Cell sorting of select populations was performed on the Aria Cell Sorter (BD Biosciences) at the University of Utah Flow Cytometry Core.

Analysis of whole blood cell populations

Blood was collected in heparinized capillaries via the retro-orbital route. Complete blood counts were obtained using a Hemavet 950 FS (Drew Scientific). Results for a given parameter are listed in Supplemental Table II and are represented as mean values ± SEM.

RNA-sequencing analysis

A total of 5×10^5 splenic CD19$^+$ B cells were FACS sorted from three WT and three *Zfp318* cKO mice. Total RNA was isolated as described above. A total of 50 ng total RNA was used for RNA-sequencing (RNA-Seq) library preparation, using the Illumina TruSeq RNA Sample Preparation kit with the polyA enrichment step omitted. Libraries were subjected to HiSeq2000 50 Cycle Single Read Sequencing. Greater than 20×10^6 reads per sample were obtained and aligned to the mm10 (Ensembl build 75) transcriptome index, using Novoalign. Aligned reads were further processed for splicing and expression variance with the UsEquation 8.7.4 software package. Data tracks were visualized with the University of California–Santa Cruz genome browser.

Statistical analysis

For FACS, RT-PCR, and complete blood count data, two-tailed unpaired Student *t* tests were applied for all relevant statistical comparisons, using GraphPad Prism software. For RNA-Seq analysis, two-tailed Student *t* tests using two-sample equal variance were performed with Microsoft Excel. Statistical cutoffs are noted in the figure legends.

Results

Analysis of Zfp318 expression, the generation of a Zfp318-deficient animal, and analysis of B cell development in the absence of Zfp318

Our previous screen of maturing and mature B cells for the expression of Zfp318 used gene grid array analysis of pooled age- and tissue-specific B cells (6). To expand and specify the time frame of *Zfp318* expression during B cell development, we FACS sorted and isolated pro, pre, and newly formed (NF) B cells from the bone marrow, and T1, T2, MZ, and FO B cells from the spleen (Supplemental Fig. 1). RNA was extracted and analyzed for *Zfp318*-specific transcripts. As shown in Fig. 1A, the presence of the *Zfp318* transcript parallels the maturity of the cell, similar to our previous observation. Of interest, although the FO cells showed the highest level of expression, the MZ cells had dramatically less *Zfp318* transcript, similar to levels seen in the NF marrow population.

To create a conditional Zfp318-deficient animal, we generated a targeting construct that possessed a LoxP site upstream of the transcriptional start site and a second LoxP site ~7000 bp 3′ (Fig. 1B). Deletion of the sequences between the two LoxP sites would thus remove the promoter sequences, the initiating ATG, and the first two coding exons of the gene. This construct was used to create a germline-targeted animal, which was then bred to the *Vav-Cre* deleter line (maintained as a heterozygote). Genotyping of this animal (Fig. 1C) for the WT and flox'd/knockin alleles was done using PCR primers specific for the products and DNA isolated from either the tail or the bone marrow of heterozygote (*WT/fl*) or homozygous *Zfp318*-targeted animals (*fl/fl*) with or without the *Vav-Cre* deleter transgene. With use of the P1 and P2 PCR primers, the 175-bp fragment of WT DNA is evident, as is the same sequence containing the inserted LoxP site in the tail of the heterozygote and KO. However, that sequence is entirely lost in the marrow of the KO animal possessing the *Vav-Cre* construct, indicating a very efficient deletion of those sequences in the tissue expressing the *Vav-Cre* transgene. The loss of *Zfp318* expression was confirmed and quantified in the spleen of the cKO compared with that of WT (Fig. 1D), using the primers described in Supplemental Table I (4913/4914).

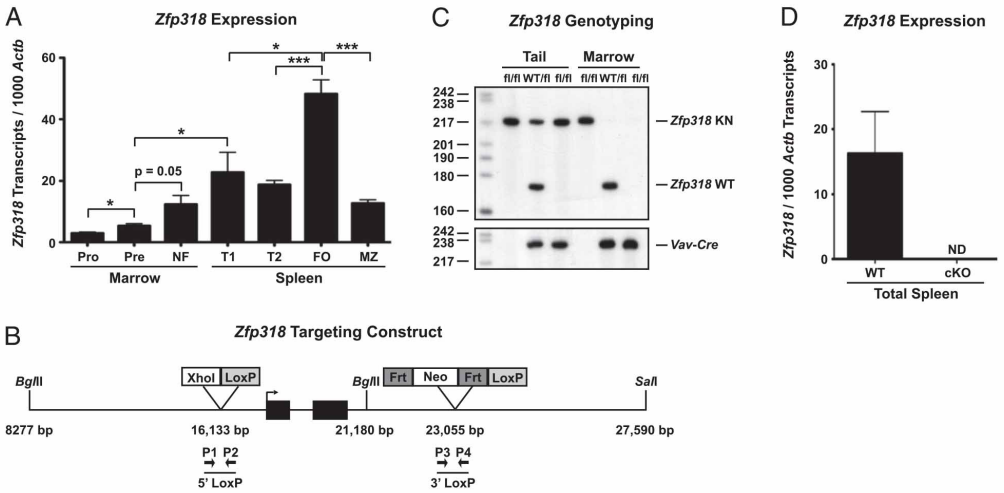

FIGURE 1. *Zfp318* is highly expressed in mature follicular B cells and is conditionally deleted via *Vav-Cre*. (**A**) RT-PCR of cDNA derived from the indicated B cell subsets. Four biological replicates were assayed for each subset. $*p < 0.05$, $***p < 0.001$. (**B**) Schematic diagram of the $Zfp318^{Fl/Fl}$ conditional allele. Cre-mediated recombination of *LoxP* sites results in the deletion of the *Zfp318* proximal promoter as well as exons 1 and 2 (black boxes). (**C**) Representative genotyping of animals possessing targeted alleles (*fl/fl*) or heterozygous alleles (*WT/fl*) in the presence or absence of the *Vav-Cre* deleter construct. Analysis of genomic DNA isolated from the tail or bone marrow shown using primer set P1/P2 (Supplemental Table I). The $Zfp318^{fl/fl}$ (*Zfp318* KN) allele is deleted only in cells isolated from the bone marrow, demonstrating the hematopoietic specificity of gene deletion. (**D**) Loss of *Zfp318* transcripts was validated using cDNA derived from WT and cKO total spleen tissues. Three biological replicates were performed per genotype. For (A) and (D), *Zfp318* transcripts were normalized to *Actb*, and data are represented as the mean ± SEM. ND, not detected.

The development of B cells in the cKO animal was analyzed. The percentage of $CD19^+$ cells and quantification of total cells of the marrow (Fig. 2A) were assessed using markers to define the pro, pre, NF, and mature, recirculating B cells ($CD22^+AA4.1^-$) in 4-wk-old animals. No significant difference was noted between the WT and cKO marrow samples. A similar analysis was carried out using the T1, T2, MZ, and FO populations of the spleen (Fig. 2B). Again, the cKO animals closely tracked with WT animals, except for a slight but significant depression in T2 B cells in the cKO animals. Hemavet analysis of peripheral blood also showed no

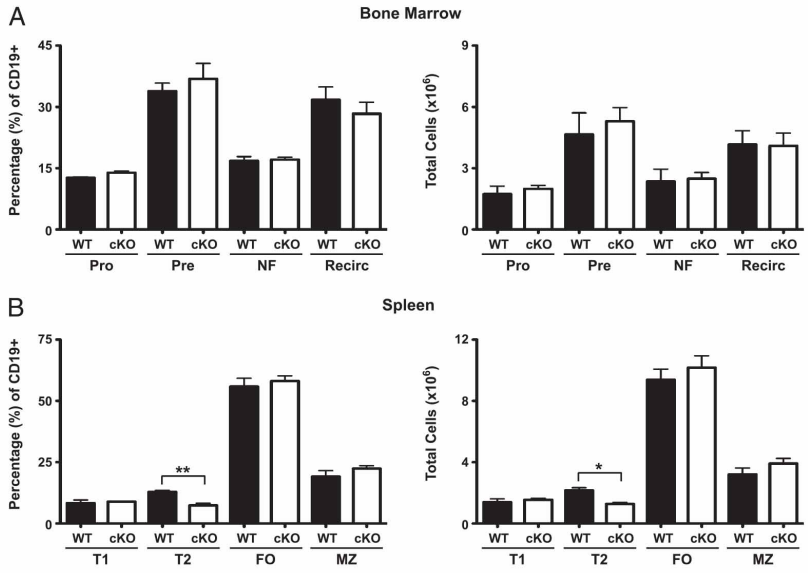

FIGURE 2. FACS analysis of B cell development in the *Zfp318* cKO animal. (**A**) Bone marrow and (**B**) spleen tissues from WT and cDKO animals were assessed by FACS for the disruption of B cell development as a result of *Zfp318* deletion. Three to four animals per group were analyzed. In (A) and (B), data represent mean percentage (*left*) or absolute cell count (*right*) ± SEM for an indicated cell population. $*p < 0.05$, $**p < 0.01$. Recirc, mature recirculating.

significant difference between WT and the *Zfp318* cKO animal (Supplemental Table II).

The absence of Zfp318 results in the loss of IgD

The previous analyses indicated that the development of mature B cells in the cKO animal was very similar to that of WT, but did not determine if the lack of Zfp318 altered the expression of B cell gene products. As a primary screen, we analyzed the cKO splenic B cells for the expression of mature marker proteins such as CD35, CD21, B220, and CD19 and found expression levels of these proteins to be indistinguishable from those of WT (Fig. 3A–C). When assaying for the expression of IgM and IgD, the two Igs expressed by mature naive B cells, we were surprised to find the level of IgM elevated in the cKO animals compared with WT. As shown in Fig. 3D, cells from the cKO animal (gray filled plot) expressed significantly higher levels of IgM than did either WT or the *Zfp318* cKO heterozygote animal in the T2 and FO populations. The analysis of IgD expression demonstrated the complete lack of IgD surface protein on cells of T1, T2, MZ, and FO populations compared with WT and heterozygote animals (Fig. 3E). The differences in expression levels of IgM and IgD were quantified by analysis of mean fluorescence intensity (MFI) in the WT and cKO populations (Fig. 3F). The elevated level of expression of IgM in the cKO cells was significantly different from that of WT in the T2, FO, and MZ populations, whereas the loss of IgD in the T1, T2, FO, and MZ populations was significantly different in the cKO samples.

Both IgM and IgD are encoded from a single heterogeneous nuclear RNA (hnRNA) transcript via alternative splicing of the VDJ sequences to those exons encoding the C region domains. To

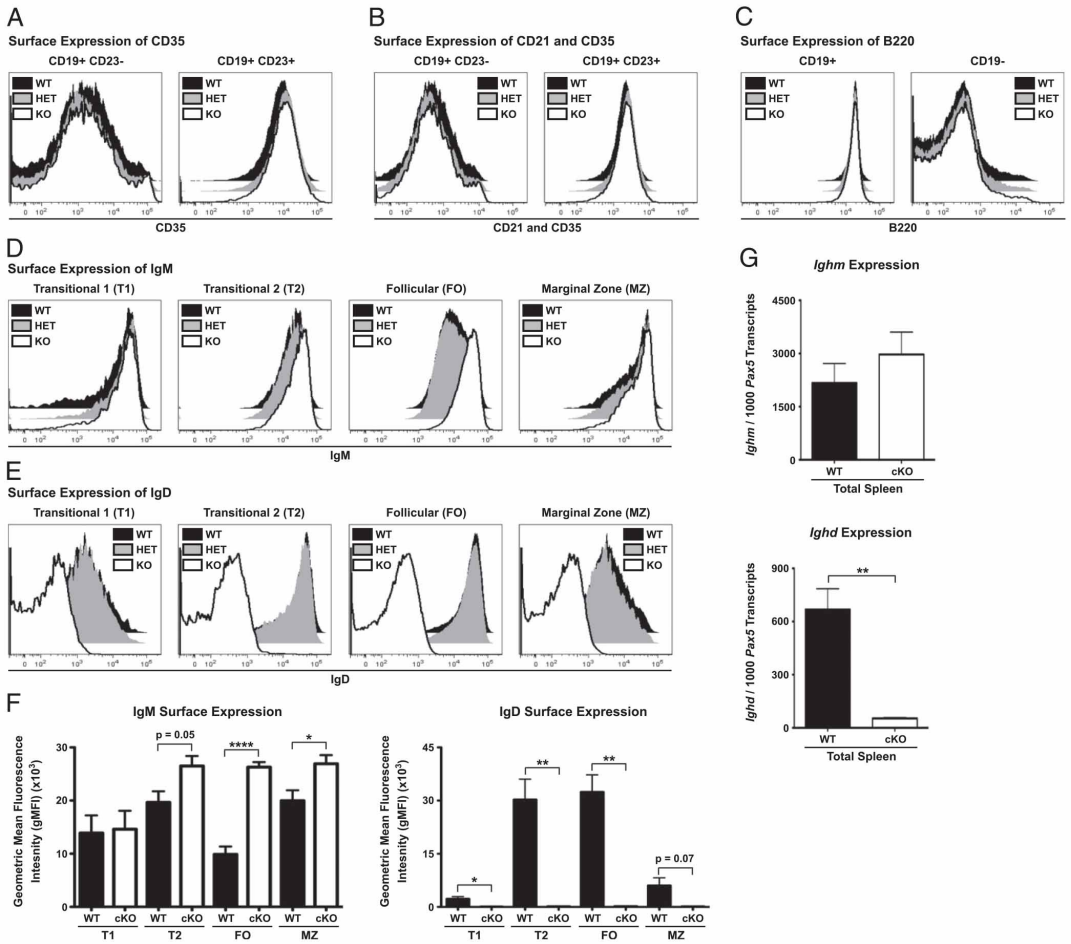

FIGURE 3. Deletion of *Zfp318* abrogates surface expression of IgD on B cells. (**A**–**C**) Representative MFI histograms for WT, heterozygous (HET), and cKO animals. (A) CD35 and (B) CD21 and CD35 are equally expressed on the surface of splenic $CD19^+$ $CD23^{+/-}$ B cells from all genotypes. (C) B220 is properly expressed by splenic $CD19^+$ B cells and is still repressed by $CD19^-$ non–B cell spleen populations. (**D** and **E**) Representative MFI histograms for WT, heterozygous (HET), and cKO splenic B cell populations. Upon deletion of *Zfp318*, (D) IgM surface expression is upregulated and (E) IgD surface expression is abrogated. (**F**) Quantification of geometric MFIs of B cell populations analyzed in (D) and (E). (**G**) RT-PCR analysis of total spleen cDNA from WT and cKO animals. Three animals per genotype were analyzed. *Ighm* (*top panel*) and *Ighd* (*bottom panel*) transcripts were normalized to *Pax5* to compensate for any variance in total B cell contribution. Expression of *Ighd* was reduced >90% in the cKO spleen. For (F) and (G), $*p < 0.05$, $**p < 0.01$, $****p < 0.0001$.

determine if these differences in surface expression of IgD and IgM on the surface of *Zfp318*-deficient B cells were reflected in transcripts specific for the IgM and IgD products, quantitative RT-PCR was performed using RNA obtained from total spleen (WT and cKO) and analyzed using primers specific for the IgM (*Ighm*) and IgD (*Ighd*) constant regions. As shown in Fig. 3G, the level of IgM transcripts trended higher in the cKO animal, whereas those encoding IgD in the cKO animal were reduced >90% compared

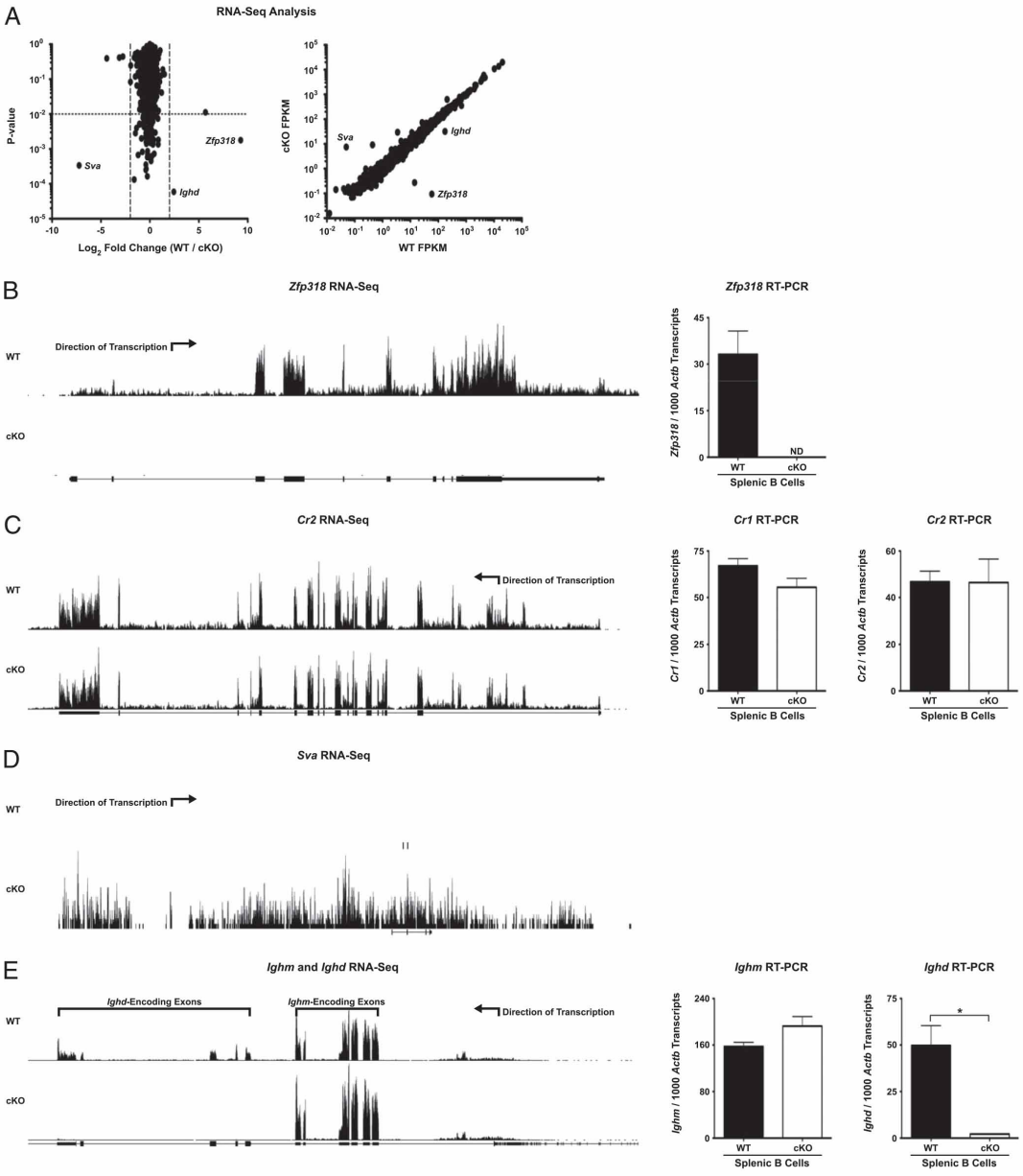

FIGURE 4. RNA-Seq analysis of CD19$^+$ splenic B cells from WT and *Zfp318*-deficient animals. (**A**) Transcriptome analysis of WT and cKO splenic CD19$^+$ B cells. Three replicates per genotype were sequenced and analyzed (Supplemental Table III). On the *left*, $\log_2$ fold change per gene between WT and cKO samples is plotted against the *p* value. On the *right*, WT and cKO FPKM are plotted for all genes analyzed. Genes were considered significantly altered with a $\log_2$ fold change > 2 and a *p* value < 0.01. (**B**–**E**) Representative custom tracks (*left*) and RT-PCR validation (*right*) for selected genes of interest. (B) *Zfp318* expression is lost in the knockout samples. (C) The alternatively spliced *Cr2* locus demonstrates equivalent expression in WT and cKO CD19$^+$ B cells. (D) The genomic region encompassing *Sva* shows global transcript enrichment. (E) Expression of the *Ighm/Ighd* locus is significantly impaired in the cKO specific to the regions for the IgD-encoding exons (*Ighd*) (>95% reduction). $^*p < 0.05$.

with WT. These data, in total, suggest that the absence of the Zfp318 protein does not alter the *transcriptional activity* of the locus encoding the IgM and IgD proteins, but does alter the relative proportion of transcripts destined to encode the IgM and IgD proteins.

The absence of Zfp318 blocks IgD production by transcriptional termination at the end of the IgM-encoding exons

The loss of IgD-encoding transcripts (and IgD protein) in the absence of Zfp318 suggested this protein alters transcript quantities. To determine if this effect was unique to that of IgD, we performed RNA-Seq using RNA obtained from purified $CD19^+$ splenic B cells from three WT and three cKO animals (Supplemental Table III). Analysis of those data indicated that only three gene products showed significantly altered expression in the cKO animals: the *Zfp318* gene itself; the region of the *Ighm/Ighd* locus encoding the IgD protein; and *Sva*, a gene on mouse chromosome 6 that encodes a "seminal vesicle Ag" unique to mice (Fig. 4A). RNA-Seq data from three genes are shown (Fig. 4B–E), using one representative WT and cKO sample. As expected, *Zfp318* transcripts are absent in the cDKO (Fig. 4B), the *Cr2* gene products (which produce the Cr1 and Cr2 proteins via alternative splicing) are identical between the two samples (Fig. 4C), and the *Ighm* and *Ighd* loci show IgM-specific transcripts in both WT and cKO, but absence of IgD-specific transcripts in the cKO animal (Fig. 4E). Therefore, in these B cell populations, Zfp318 uniquely influences only *Ighd* and *Sva* expression.

The loss of IgD-encoding transcripts in the cKO B cells could be due to at least two mechanisms: blocking the alternative splicing of the IgM- and IgD-encoding transcripts, or blocking the hnRNA transcription of the *Ighm* locus to the sequences encoding the IgD protein. The *Ighm/Ighd* locus contains at least three distinct transcriptional stop sites, including one just 3′ of the exons encoding secreted IgM, a second site allowing for the production of membrane bound IgM, and a third site 3′ of the last exon encoding the mature, membrane-bound IgD protein (16–19). To encode both IgM and IgD via alternative splicing of hnRNA, the transcriptional stop sites linked to the IgM-encoding exons must be ignored by the Pol II RNA polymerase complex. A close analysis of the RNA-Seq data obtained from the *Ighm/Ighd* locus revealed a dramatic loss of virtually all RNA transcripts 3′ of the IgM-encoding exons (Fig. 5A), suggesting that production of hnRNA containing the IgD-encoding sequences was significantly reduced in the absence of Zfp318.

The production of *Ighm/Ighd* hnRNA in the cKO animal was further quantified by RT-PCR analysis of intronic sequences from IgM-encoding and IgD-encoding regions of the locus. Two primer sets (Fig. 5A) were used to screen total RNA via RT-PCR. The first primer set (primer set A) included an IgM-specific intronic sequence and a turnaround within the last exon of the IgM region,

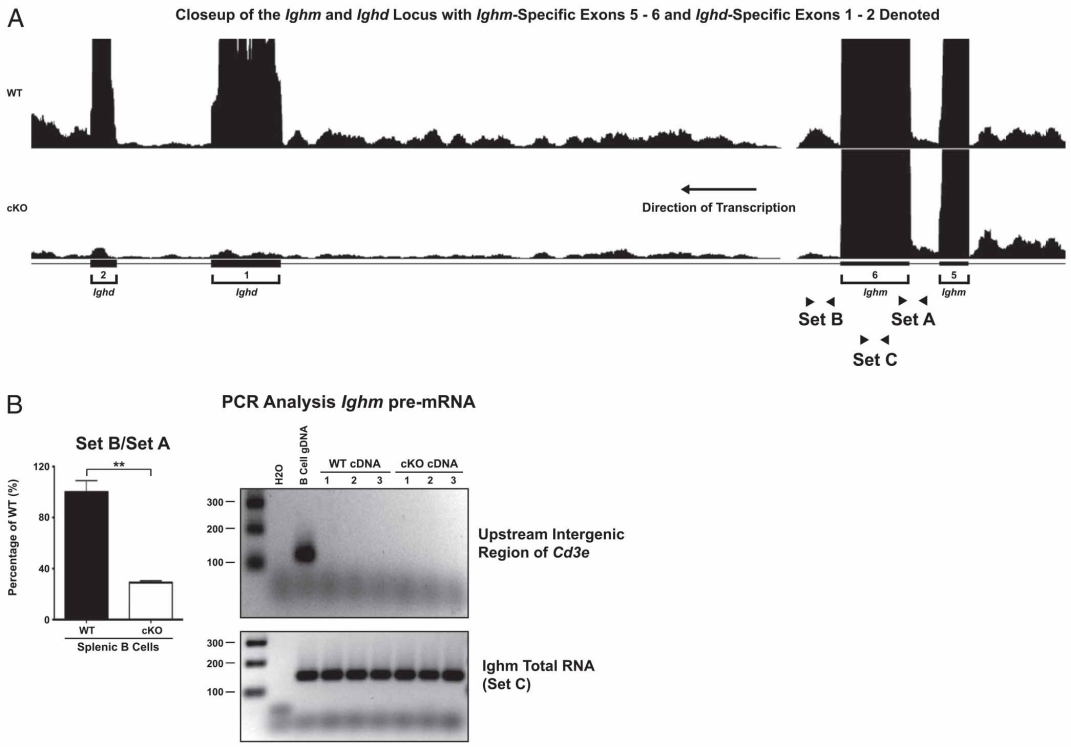

FIGURE 5. Deletion of *Zfp318* blocks transcription downstream of the terminal *Ighm*-specific exon. (**A**) Representative RNA-Seq custom tracks from WT and cKO $CD19^+$ B cells illustrating *Ighm*-specific exons 5–6, the intervening intronic region, and *Ighd*-specific exons 1–2. Primer sets used to quantify transcription throughout the *Ighm* locus are indicated. (**B**) LightCycler-based RT-PCR quantification of transcription downstream of *Ighm*-specific exon 6. *Left*, For each sample, Ct-derived transcript ratios of Set B/Set A were generated. The mean WT value was used to derive the "percentage of WT" for each individual sample (e.g., WT-1/WT-mean or cKO-1/WT-mean). $^{**}p < 0.01$. *Right*, Amplification products from a *Cd3ε* upstream noncoding intergenic region (*top*) and from a region internal to IgM-specific exon 6 (Set C) (*bottom*).

whereas the second set of primers (primer set B) was 3′ of the *Ighm* transcriptional stop site to generate membrane-bound IgM. The relative products from these two sets of primers were quantified (Fig. 5B) by establishing a ratio of the IgD-intronic sequence (primer set B) versus the IgM-intronic sequence (primer set A). Clearly, there is a marked change in ratio of these intronic sequences comparing the WT with the cKO samples (70% reduction in the cKO). RT-PCR analyses of RNA samples can be clouded by the presence of genomic DNA. To control for this, triplicate WT and cKO RNA samples (and genomic DNA as control) were analyzed using primers specific for a region of the *Cd3ε* gene that is not transcribed, and using an oligo set within the final coding exon of the IgM protein (primer set C) (Fig. 5A). The cDNA samples obtained from the WT and cKO RNA samples did not demonstrate amplification of the *Cd3ε*-associated sequences but did show equal quantities of the *Ighm* gene product (Fig. 5B), indicating that amplification of genomic sequences from the IgM- and IgD-encoding regions of the *Ighm* locus was from hnRNA, not genomic DNA.

Discussion

Naive FO cells express both IgM and IgD, whereas MZ cells preferentially express IgM (Fig. 6 B, C). Expression of *Ighd* in naive maturing B cells closely parallels that of *Zfp318* (Fig. 6A, C from Fig. 1A). Upon activation, FO B cells depress IgD expression and, with additional stimulation and T cell help, class switch to additional Ab isotypes. The historical view of IgM versus IgD production has been based upon an alternative splicing model in which the same VDJ coding sequences are alternatively spliced to exons encoding the constant regions of IgM or IgD. Clearly this requires an hnRNA that encompasses the entire *Ighm/Ighd* locus.

Currently, very little is known about what regulates the differential expression of transcripts coding for IgM and IgD via alternative splicing of a common VDJ region to the IgM- or IgD-encoding exons. Indeed, the best parallel to this system may be in the analysis of the U1A-mediated regulation of membrane versus secreted IgM. Similar to Zfp318, U1A expression levels are regulated throughout B cell development/differentiation, with high expression being required for the repression of secretory IgM (20). U1A acts to block the expression of secretory IgM by impairing the binding and, hence, downstream function of the polyA cleavage complex, which includes CPSF (cleavage and polyadenylation specificity factor), Cstf, and polyA polymerase (20–23). U1A mediates this suppression by interacting with multiple nonconsensus U1A binding sites (AUGC-core) both upstream and downstream of the AAUAAA polyA signal. Owing to the nature of these binding sites, a mass action effect of U1A is required to achieve full repression. A similar scenario may be true for the function of Zfp318, as high *Zfp318* gene expression levels correlate with high *Ighd* levels in various B cell populations (Fig. 6). Similar to the secretory IgM polyA site, three AUGC sites are clustered ~500 bp upstream of the membrane IgM polyA signal. Whether these binding sites are functional for Zfp318 recognition remains to be determined. However, Zfp318 does possess multiple U1-RNA zinc finger domains; thus, it is tempting to speculate that Zfp318 regulates *Ighm/Ighd* gene transcription by binding to these AUGC sites. An alternative possibility is that Zfp318 may interact with a yet-to-be-determined binding site(s) and serves to stabilize

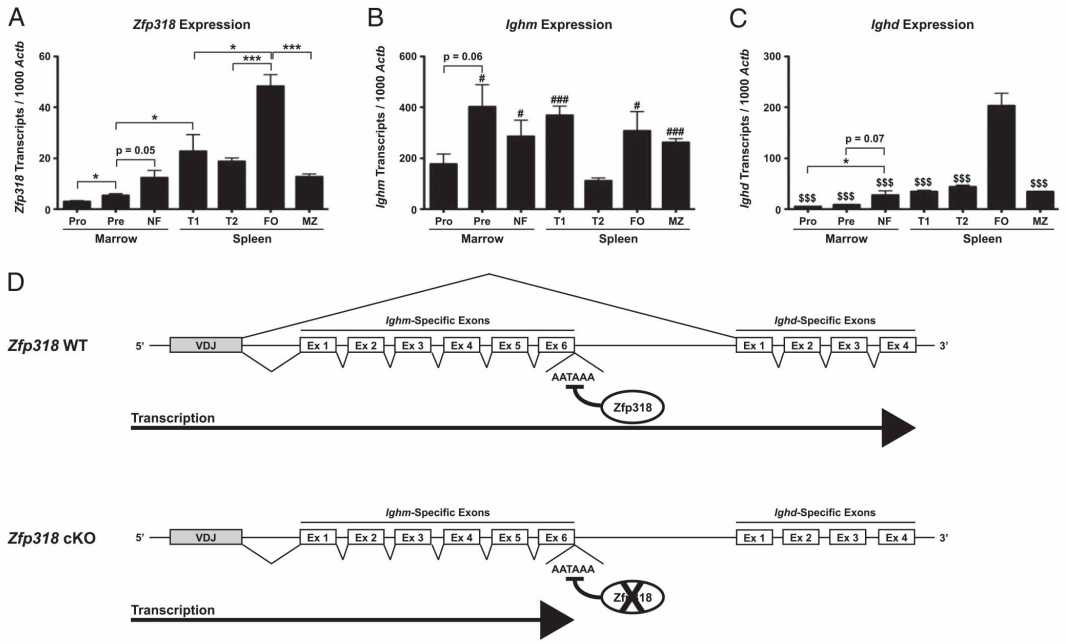

FIGURE 6. Model of Zfp318 transcriptional regulation throughout the *Ighm* locus. (**A**–**C**) Quantification of (A) *Zfp318*, (B) *Ighm*, and (C) *Ighd* coding transcripts within the indicated B cell subsets. (A) was reproduced from Fig. 1A. $*p < 0.05$, $***p < 0.001$. In (B), # represents comparisons between the indicated cell type and the T2 population, with $\#p < 0.05$ and $\#\#\#p < 0.001$. In (C), $ represents comparisons between the indicated cell type and the FO population, with $\$\$\$ p < 0.001$. (**D**) Stylized depiction of transcription throughout the *Ighm/Ighd* locus (not drawn to scale). In the presence of Zfp318 (*top*), transcriptional termination is blocked, and transcription continues past the terminal *Ighm*-specific exon. This allows for splicing to *Ighd*-specific exons and generation of a mature IgD protein. Upon the loss of Zfp318 (*bottom*), transcription is terminated at the final *Ighm*-specific exon. As a result, the downstream *Ighd*-specific exons cannot be transcribed or spliced into a mature transcript.

the binding of U1A, leading to a more stable repression of polyA usage. This idea is partially supported by data in Fig. 5, showing the 70% loss of transcription downstream of the membrane IgM polyA signal rather than a complete block upon *Zfp318* deletion.

Our analysis of Zfp318-deficient B cells shows that the absence of IgD expression is linked to the preferential usage of a transcriptional stop site located within the final *Ighm* exon, thus blocking synthesis of the full *Ighm/Ighd* hnRNA, which is required for the production of IgD (Fig. 6D) (16, 18). This finding implicates the Zfp318 protein as functioning to block recognition of the IgM-specific transcriptional stop site, allowing for the RNA Pol II complex to proceed down the chromosome into the IgD-encoding region. This finding suggests that Zfp318, which possesses two putative nucleic acid–binding zinc finger domains (7), recognizes the IgM-specific transcriptional stop site and inhibits transcription termination at that site, possibly by inhibiting RNA pausing and transcription termination via the CPSF protein complexes or those required for cleavage (24–26). It also suggests that the regulation of *Zfp318* is intimately tied to B cell differentiation (MZ B cells express low levels of both *Zfp318* and IgD, whereas FO cells express much higher levels of both gene products) and that FO B cell activation, which results in the loss of IgD (but expression of IgM), may also regulate the expression of *Zfp318*.

We know of no other instance in mammalian cells in which a transcription stop site is blocked, in a similar fashion to what we see for the *Ighm* locus, to allow for the production of a longer hnRNA molecule and increased genetic capacity. The IgM-encoding region of *Ighm* also possesses a transcription stop site that generates the smaller, secreted form of the protein that must also be ignored by the Pol II complex in the naive B cell. This site is not blocked by Zfp318; if it were, we might have expected only secreted IgM in the absence of Zfp318. However, whether this second site is blocked by another protein functioning in an analogous fashion to Zfp318 is not known.

The expression of *Zfp318* parallels that of other transcriptional regulators during the maturation and development of B cells. One such regulator, Mef2c, also demonstrates enhanced expression in FO cells compared with MZ cells. Our previously published analysis of Mef2c-deficient B cells demonstrated a dramatic reduction in expression of *Zfp318* (27). This reduction in *Zfp318* expression, however, was not to the same magnitude as a *Zfp318* gene deficiency. Indeed, B cells lacking Mef2c still express IgD (28), suggesting that sufficient Zfp318 was present to allow for *Ighd* transcription.

The analyses of our *Zfp318* deficiency via *Vav-Cre* phenocopies the results described by Enders et al. (15), although a relative depression of T2 B cells of the spleen was not noted in their report. Enders et al. further suggested that Zfp318 served to regulate IgD production by controlling the alternative splicing of the hnRNA of the *Ighm/Ighd* locus, although no data were presented to support this model (15). Our conclusions regarding the proposed function of Zfp318 differ from those presented by Enders et al. because of our RNA-Seq data, which point to the regulation of transcription termination as the event that subsequently allows for the production of IgD via alternative splicing. Thus it is the primary production of the *Ighm/Ighd* hnRNA that is the key step regulated by Zfp318, not the alternative splicing choice of the VDJ sequence to either the IgM- or the IgD-encoding exons.

Acknowledgments

We thank the University of Utah Core facilities (FACS, RNA-Seq, Transgenic and Knockout Mouse, and Data Analysis), specifically Dr. Susan Tomowski, Dr. David Nix, and Dr. Tim Mosbruger, for assistance; Dr. Dean Tantin for the use of Hemavet; and members of the Weis laboratories for critique of this work and many useful suggestions.

Disclosures

The authors have no financial conflicts of interest.

References

1. Su, T. T., and D. J. Rawlings. 2002. Transitional B lymphocyte subsets operate as distinct checkpoints in murine splenic B cell development. *J. Immunol.* 168: 2101–2110.
2. Busslinger, M. 2004. Transcriptional control of early B cell development. *Annu. Rev. Immunol.* 22: 55–79.
3. Mandel, E. M., and R. Grosschedl. 2010. Transcription control of early B cell differentiation. *Curr. Opin. Immunol.* 22: 161–167.
4. Matthias, P., and A. G. Rolink. 2005. Transcriptional networks in developing and mature B cells. *Nat. Rev. Immunol.* 5: 497–508.
5. Hardy, R. R., P. W. Kincade, and K. Dorshkind. 2007. The protean nature of cells in the B lymphocyte lineage. *Immunity* 26: 703–714.
6. Debnath, I., K. M. Roundy, D. M. Dunn, R. B. Weiss, J. J. Weis, and J. H. Weis. 2008. Defining a transcriptional fingerprint of murine splenic B-cell development. *Genes Immun.* 9: 706–720.
7. Ishizuka, M., H. Ohshima, N. Tamura, T. Nakada, A. Inoue, S. Hirose, and H. Hagiwara. 2003. Molecular cloning and characteristics of a novel zinc finger protein and its splice variant whose transcripts are expressed during spermatogenesis. *Biochem. Biophys. Res. Commun.* 301: 1079–1085.
8. Inoue, A., A. Ishiji, S. Kasagi, M. Ishizuka, S. Hirose, T. Baba, and H. Hagiwara. 2000. The transcript for a novel protein with a zinc finger motif is expressed at specific stages of mouse spermatogenesis. *Biochem. Biophys. Res. Commun.* 273: 398–403.
9. Tao, R. H., H. Kawate, K. Ohnaka, M. Ishizuka, H. Hagiwara, and R. Takayanagi. 2006. Opposite effects of alternative TZF spliced variants on androgen receptor. *Biochem. Biophys. Res. Commun.* 341: 515–521.
10. Wilson, C. A., S. A. Mrose, and D. W. Thomas. 1995. Enhanced production of B lymphocytes after castration. *Blood* 85: 1535–1539.
11. Erben, R. G., J. Eberle, and M. Stangassinger. 2001. B lymphopoiesis is upregulated after orchiectomy and is correlated with estradiol but not testosterone serum levels in aged male rats. *Horm. Metab. Res.* 33: 491–498.
12. Altuwaijri, S., K. H. Chuang, K. P. Lai, J. J. Lai, H. Y. Lin, F. M. Young, A. Bottaro, M. Y. Tsai, W. P. Zeng, H. C. Chang, et al. 2009. Susceptibility to autoimmunity and B cell resistance to apoptosis in mice lacking androgen receptor in B cells. *Mol. Endocrinol.* 23: 444–453.
13. Treiber, T., E. M. Mandel, S. Pott, I. Györy, S. Firner, E. T. Liu, and R. Grosschedl. 2010. Early B cell factor 1 regulates B cell gene networks by activation, repression, and transcription- independent poising of chromatin. *Immunity* 32: 714–725.
14. Yuan, D., P. L. Witte, J. Tan, J. Hawley, and T. Dang. 1996. Regulation of IgM and IgD heavy chain gene expression: effect of abrogation of intergenic transcriptional termination. *J. Immunol.* 157: 2073–2081.
15. Enders, A., A. Short, L. A. Miosge, H. Bergmann, Y. Sontani, E. M. Bertram, B. Whittle, B. Balakishnan, K. Yoshida, G. Sjollema, et al. 2014. Zinc-finger protein ZFP318 is essential for expression of IgD, the alternatively spliced Igh product made by mature B lymphocytes. *Proc. Natl. Acad. Sci. USA* 111: 4513–4518.
16. Danner, D., and P. Leder. 1985. Role of an RNA cleavage/poly(A) addition site in the production of membrane-bound and secreted IgM mRNA. *Proc. Natl. Acad. Sci. USA* 82: 8658–8662.
17. Early, P., J. Rogers, M. Davis, K. Calame, M. Bond, R. Wall, and L. Hood. 1980. Two mRNAs can be produced from a single immunoglobulin mu gene by alternative RNA processing pathways. *Cell* 20: 313–319.
18. Rogers, J., P. Early, C. Carter, K. Calame, M. Bond, L. Hood, and R. Wall. 1980. Two mRNAs with different 3′ ends encode membrane-bound and secreted forms of immunoglobulin mu chain. *Cell* 20: 303–312.
19. Alt, F. W., A. L. Bothwell, M. Knapp, E. Siden, E. Mather, M. Koshland, and D. Baltimore. 1980. Synthesis of secreted and membrane-bound immunoglobulin mu heavy chains is directed by mRNAs that differ at their 3′ ends. *Cell* 20: 293–301.
20. Ma, J., S. I. Gunderson, and C. Phillips. 2006. Non-snRNP U1A levels decrease during mammalian B-cell differentiation and release the IgM secretory poly(A) site from repression. *RNA* 12: 122–132.
21. Phillips, C., N. Pachikara, and S. I. Gunderson. 2004. U1A inhibits cleavage at the immunoglobulin M heavy-chain secretory poly(A) site by binding between the two downstream GU-rich regions. *Mol. Cell. Biol.* 24: 6162–6171.
22. Phillips, C., and S. Gunderson. 2003. Sequences adjacent to the 5′ splice site control U1A binding upstream of the IgM heavy chain secretory poly(A) site. *J. Biol. Chem.* 278: 22102–22111.
23. Phillips, C., S. Jung, and S. I. Gunderson. 2001. Regulation of nuclear poly(A) addition controls the expression of immunoglobulin M secretory mRNA. *EMBO J.* 20: 6443–6452.
24. Richard, P., and J. L. Manley. 2009. Transcription termination by nuclear RNA polymerases. *Genes Dev.* 23: 1247–1269.
25. Glover-Cutter, K., S. Kim, J. Espinosa, and D. L. Bentley. 2008. RNA polymerase II pauses and associates with pre-mRNA processing factors at both ends of genes. *Nat. Struct. Mol. Biol.* 15: 71–78.
26. Nag, A., K. Narsinh, and H. G. Martinson. 2007. The poly(A)-dependent transcriptional pause is mediated by CPSF acting on the body of the polymerase. *Nat. Struct. Mol. Biol.* 14: 662–669.
27. Debnath, I., K. M. Roundy, P. D. Pioli, J. J. Weis, and J. H. Weis. 2013. Bone marrow-induced Mef2c deficiency delays B-cell development and alters the expression of key B-cell regulatory proteins. *Int. Immunol.* 25: 99–115.
28. Khiem, D., J. G. Cyster, J. J. Schwarz, and B. L. Black. 2008. A p38 MAPK-MEF2C pathway regulates B-cell proliferation. *Proc. Natl. Acad. Sci. USA* 105: 17067–17072.